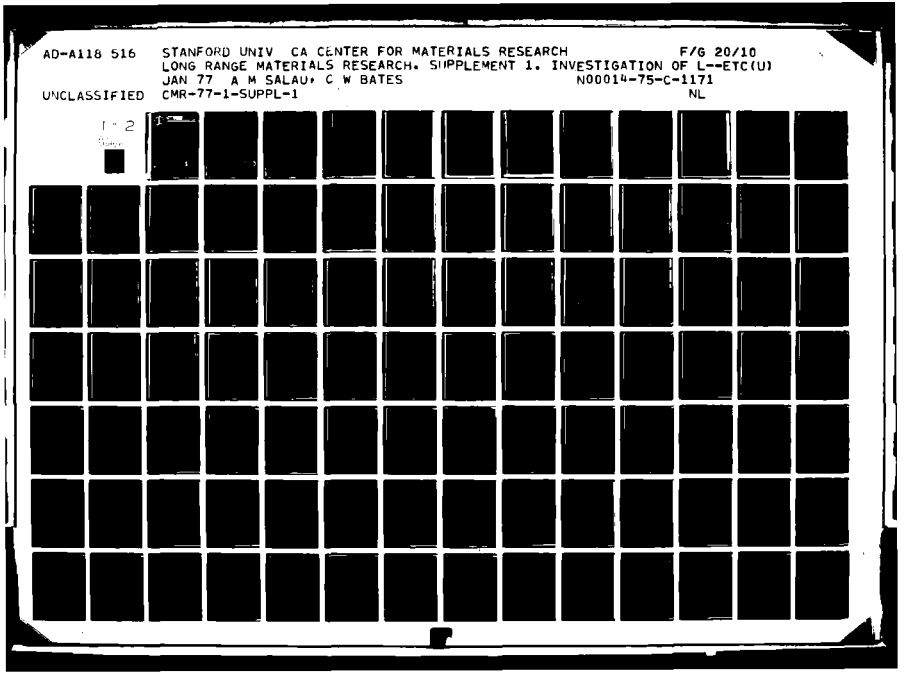
AD-A118 516
STANFORD UNIV CA CENTER FOR MATERIALS RESEARCH F/G 20/10
LONG RANGE MATERIALS RESEARCH. SUPPLEMENT 1. INVESTIGATION OF L--ETC(U)
JAN 77 A M SALAU, C W BATES N00014-75-C-1171
UNCLASSIFIED CMR-77-1-SUPPL-1 NL
1 - 2

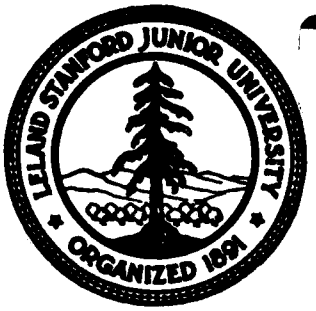

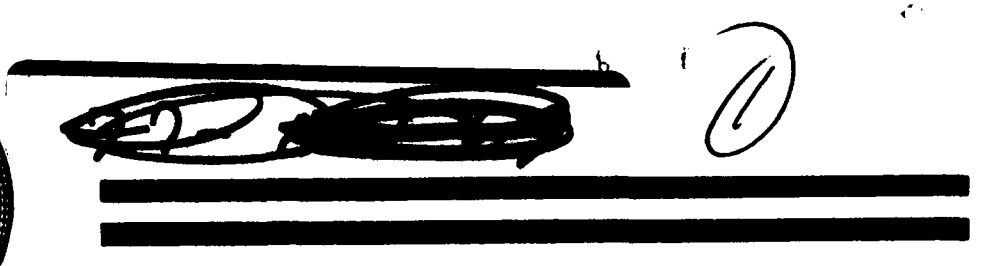

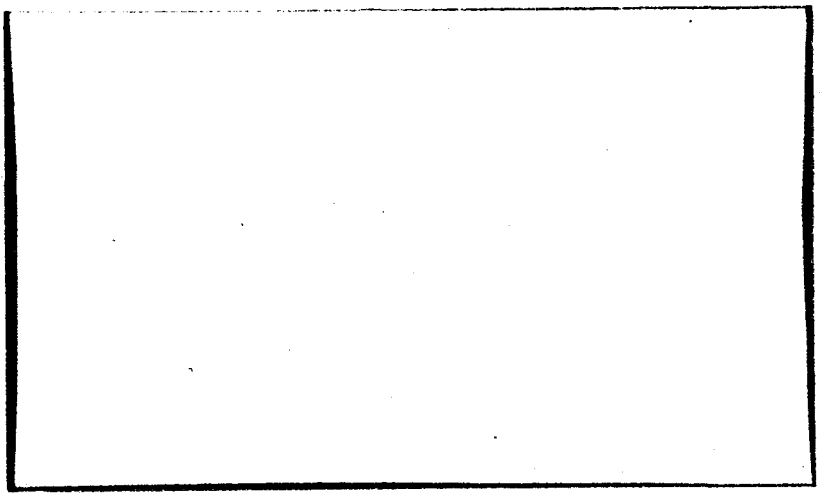

CENTER FOR MATERIALS RESEARCH

STANFORD UNIVERSITY • STANFORD, CALIFORNIA

INVESTIGATION OF LUMINESCENCE FROM TRAPPED EXCITONS IN CsI

by

Akinola Mauritala Salau
and
Clayton W. Bates, Jr.

Supplement 1 to Annual Technical Report CMR-77-1

Long Range Materials Research
Contract N00014-75-C-1171

Sponsored by
Defense Advanced Projects Agency

January 1977

INVESTIGATION OF LUMINESCENCE FROM TRAPPED EXCITONS IN CsI

by

Akinola Mauritala Salau
Department of Applied Physics
Stanford University
Stanford, California 94305

and

Clayton W. Bates, Jr.
Departments of Materials Science and Engineering
and Electrical Engineering
Stanford University
Stanford, California 94305

CHAPTER I

INTRODUCTION

It is well known that normally pure alkali halide crystals (AHC) show the so-called intrinsic luminescence at low temperatures when excited by both ionizing radiations (like x, β, or γ-rays) and non-ionizing ultra-violet radiations.[1-6] Excitations are usually limited to the absorption bands of the intrinsic exciton (electron-hole pair bound together by their Coulombic interactions) as well as to band-to-band transitions. The mechanism responsible for this low-temperature intrinsic luminescence has been studied in the light of experiments on

(i) both polarized and unpolarized absorption, emission and excitation spectra measurements,[7,8] and

(ii) electron spin resonance (ESR) measurements.[9]

Their results show that the observed intrinsic luminescence at low temperatures in alkali halide crystals is due to the radiative recombinations of the excited states of the system of a self-trapped hole (V_K-center, after Kanzig) plus an electron; that is $(V_K + e)^*$, in other words, the excited state of a halogen molecular ion $(X_2^{2-})^*$, oriented along the <110> direction in alkali halide crystals with the sodium chloride structure and along the <100> direction in alkali halide crystals with the cesium chloride structure. This model has been extensively used to explain the observed intrinsic luminescence at low temperatures in alkali halide crystals.[7-11] However, it should be noted that the mechanism responsible for the intrinsic luminescence

in alkali halide crystals with the NaCl structure is well understood while that of alkali halide crystals with CsCl structure is not well understood.

Consequently, the purpose of the study presented in this work was to learn more about the luminescent mechanism in CsI , (CsCl structure), which when activated with Na is a very efficient scintillation material, an ideal X-ray detector and an excellent particle detector.[12-15] It was hoped that these studies might provide new information concerning the validity of the radiative recombinations of $(V_K + e)^*$ states as being an important source of intrinsic luminescence in CsI . Another objective of this work was to have a more complete understanding of the nature of the mechanisms responsible for the luminescence (intrinsic or extrinsic) observed in alkali halide crystals of the CsCl structure, (taking CsI as a case study), at low and room temperatures.

In the course of this work, our combined optical and electron paramagnetic resonance studies at low and room temperatures tenatively suggests the association of the observed luminescence in CsI to excitons trapped (or bound) at negative ion vacancies and/or excitons trapped at F-center (electron in a negative ion vacancy). This is contrary to the general contention that intrinsic luminescence at low temperature results from radiative recombination of $(V_K + e)^*$.[7-10] Another interesting effect we observed was the room temperature luminescence after the sample has been cooled (RTAC) to low temperatures. This RTAC luminescence is discussed in detail in Chapter IV.

Besides the pure sample, thermally quenched and plastically deformed CsI were also studied in this work. We observed that the optical

properties of the strained pure CsI are similar to those of sodium activated CsI .

Chapter II contains a brief review of the work that has been done so far on the photoluminescent study of alkali halide crystals especially the alkali iodides and the cesium halides in which groups CsI falls. Table I shows the optical properties of alkali iodides and cesium halides. Various models used to explain the observed intrinsic and extrinsic luminescence in these crystals are discussed.

The photoluminescent experiment as well as the experimental technique used in this work are briefly described in Chapter III. Chapter IV contains the presentation and interpretation of the photoluminescent study of pure and strained CsI using non-ionizing ultra-violet radiations under different thermal and mechanical treatments.

In Chapter V, we discuss electron paramagnetic resonance and color center studies of CsI . Chapter VI contains a model we proposed for the luminescence phenomena in pure CsI while Chapter VII deals with the conclusion of these studies and recommendations for future work.

	SYSTEM	STRUCTURE TYPE	LATTICE CONSTANTS (Å)	NEAREST NEIGHBOR DISTANCE (Å)	DIELECTRIC CONSTANTS $K_0 = n^2$	$K^{(a)}$	W_A (nm)[b] RT	W_A (nm)[b] LNT	W_A (nm)[b] LHeT	W_E (nm)[c] LNT	W_E (nm)[c] LHeT	W_E (nm)[c] RTAC	TRAPPED CENTER ABSORPTION BANDS α	β	F	M	V_k
LiI	Cubic	NaCl	6.0	3.0	3.80	11.03	1.84	1.82 297+	--		366[c] 403		* 227	* 221	* 530	--	--
NaI	Cubic	NaCl	6.46	3.23	2.91	6.60	229	223 216+	221		295[c]		* 243	* 234	* 590	--	400[c]
KI	Cubic	NaCl	7.05	3.52	2.69	4.94	220	214 213+	211	300 370	302[c] 371	--	238	226	663	1008	404[c]
RbI	Cubic	NaCl	7.33	3.66	2.63	5.00	222	218	216 217+	318 404	318[c] 425	--	240	229	725	--	405[c]
CsI*	Cubic	CsCl	4.56	3.95	3.03	5.65	220	215 213+	213	320 350 430	300 320 350 430	350 440	237 235+	225 226+	750	1181	406
CsBr	Cubic	CsCl	4.29	3.71	2.78	6.51	187	180 180+	182			--	* 200	* 193	632	1042	
CsCl	Cubic	CsCl	4.11	3.56	2.60	7.20	162	156 155+	158			--	* 174	* 167	571	1976	

* This work
(a) Fowler: Physics of Color Centers
(b) Schulman and Compton: Color Centers in Solids
(c) Murray
W_A 1st exciton absorption band, W_E intrinsic emission bands, + calculated 1st exciton absorption band using Eq. (2.1)

CHAPTER II

REVIEW OF PREVIOUS WORK ON THE PHOTOLUMINESCENCE OF ALKALI HALIDES

A. INTRODUCTION

For the past few decades, work has been done by many authors[1-8,16-19] in studying the luminescent properties of alkali halides by measuring absorption, emission and excitation spectra of these materials. Both experimental results and theoretical calculations on the optical properties of the alkali iodides are presented in Table II.1. The first part (B-C) of the review on the work that has been done on the luminescent properties of alkali halides will deal with absorption measurements while the second part (D) deals with emission and excitation measurements and part (E) deals with the electron spin resonance measurements.

B. ABSORPTION MEASUREMENTS

In this section, we shall first discuss the work that has been done so far on the absorption spectra of excitons while the second part deals with absorption spectra due to defects induced by exposing the alkali halides to radiations of threshold energy of about 5 eV.[20,21]

1. Exciton Absorption Bands

The exciton absorption spectra of alkali halides have been widely studied in the ultra-violet region of the electromagnetic spectrum by many authors.[22-24] Pohl et al.[22] did the pioneering work on the ultra-violet absorption spectra of alkali halides at room and nitrogen temperatures. Hilsch and Pohl gives the positions of the first exciton

absorption for the iodides and bromides by an empirical formula

$$h\nu_{max} = \alpha \frac{e^2}{4\pi\epsilon_0 r} + E - I \qquad (1.1)$$

where α is Madelung constant, r, the interionic distance, ϵ_0 the high frequency dielectric constant, E the electron affinity of the halogen and I the ionization potential of the alkali atom. The comparison between the observed and calculated absorption peaks by Martienssen[23] is shown in Table I.1.

Later on, Teegarden and Baldini,[24] Eby[23] and a host of others not only repeated Pohls work but also extended the measurements to liquid helium temperatures (L He T). They observed halogen atom doublet splittings which in most cases did not agree with the predicted minimum splitting,[25] given by

$$\Delta E \geq \sqrt{8/9}\ \lambda = \begin{cases} 0.047 \text{ eV} \rightarrow \text{Fluorides} \\ 0.103 \text{ eV} \rightarrow \text{Chlorides} \\ 0.432 \text{ eV} \rightarrow \text{Bromides} \\ 0.889 \text{ eV} \rightarrow \text{Iodides} \end{cases}$$

where λ is the halogen atom ground state doublet splitting obtainable from atomic data. Even the halogen atom doublet splitting observed in the chlorides or bromides has not been successfully observed in the iodides probably because of the large splitting and strong configuration interactions.

The exciton absorption bands observed in alkali halides are explained by using the Transfer and excitation models.[26] As the name implies, the transfer model involves the transfer of an electron from a halogen

ion to the nearest neighboring alkali ions, while the excitation model requires the excitation to be sufficiently localized in a unit cell as to make it resemble an excited state of a free atom. However, Knox and Inchauspe[25] showed the identity of both models from group theoretical considerations in predicting the multiplicity of the exciton absorption peaks expected in alkali halides at room and low temperatures; though the equivalence of the transfer and excitation models does not extend to predictions regarding the positions and strength of the exciton absorption bands. The models do not apply too well to CsBr and CsI because they exhibit strong configuration interactions between their low-lying excited states. These authors predicted nine bands in the low-energy structure associated with the halogen doublet, arising from transitions to the $P^5\gamma_1$ configuration, and a triplet and quartet from transitions to $P^5\gamma_3$ and $P^5\gamma_5$ configurations respectively. On either model, Overhauser[27] predicted five exciton lines for the alkali halides with the NaCl-structure due to the combination of a doublet and a triplet while for alkali halides with CsCl-structures, he predicted six exciton bands due to a combination of a doublet and a quartet. He further suggested that the effect of configurations interaction should be taken into account in considering the splitting due to the halogen atom doublet in CsCl structure alkali halides.

Using the transfer model, Teegarden and Baldini were able to explain the observed exciton absorption spectra of all the alkali halides measured at 10° K to be due to transitions from the P^6 shell of the halide ion (leaving a P^5 hole on the halide ion) to effective-mass states based on S- and d-like conduction bands.

Besides the well resolved exciton absorption bands there exist shoulders (on the short wavelength side of the first exciton absorption band) which are attributed by Taft and Phillips[28] to the onset of band-to-band transitions. However it should be noted that because of lattice relaxation, the occurrence of photoconductivity in the shoulder region does not necessarily imply the onset of band-to-band transitions.

C. DEFECT ABSORPTION BANDS

Here we review briefly the experimental and theoretical work that has been done on the study of the ultra-violet absorption spectra due to defects on the long wavelength side of the first exciton absorption band.

Besides the excitonic absorption bands, the long wavelength tail of the fundamental absorption band is modified by the presence of defects or impurities which can act as either electron, hole or exciton traps. Since the main concern here is intrinsic absorption bands, absorption bands due to impurities will not be discussed. The most widely studied both experimentally and theoretically absorption bands on the fundamental absorption region are the so-called α and β absorption bands. The α-band is the absorption band due to excitons trapped at negative ion vacancies while the β-band is the absorption band due to excitons trapped at F-centre (a negative ion vacancy plus an electron).

Delbecq et al.[29] measured the α and β-absorption bands in KI to be located at 238 nm and 226 n, respectively. Later on Klick and

Patterson[30] measured the α and β bands in other alkali halide crystals. The locations of these absorption bands are as tabulated in Table II.1. Mention should be made of the fact that these α - and β - absorption bands are induced in these alkali halide crystals by exposing them to ionizing radiations (X-rays) at room and low temperatures. But in this work we are able to produce the α- and β-absorption bands in CsI by straining by cooling to low temperatures. The position of the α and β absorption bands in CsI agree with calculations and other measurements.

Using the charge transfer model of the exciton, Bassani and Inchauspe[31] computed the shift of the α and β-absorption bands from the first exciton band for the alkali halides. Their calculated values for the positions of these bands agree fairly well with measured values. Figure II.1 shows the model for the creation of an exciton in which the arrow represents the transfer of an electron from the halogen ion to the neighboring alkali ions.

The energy difference as calculated by Bassani and Inchauspe between the first exciton transitions and the trapped exciton transitions is made up of three parts:

(a) the difference in electrostatic energy (ΔE_{es}) due to the Coulomb interaction of the charges in the lattice;

(b) the difference in repulsive energy (ΔE_{rep}) between closed shells of electrons and

(c) the difference in the polarization energy (ΔE_{pol}) due to the dipole moments induced on the ions by the charges present in the lattice; that is

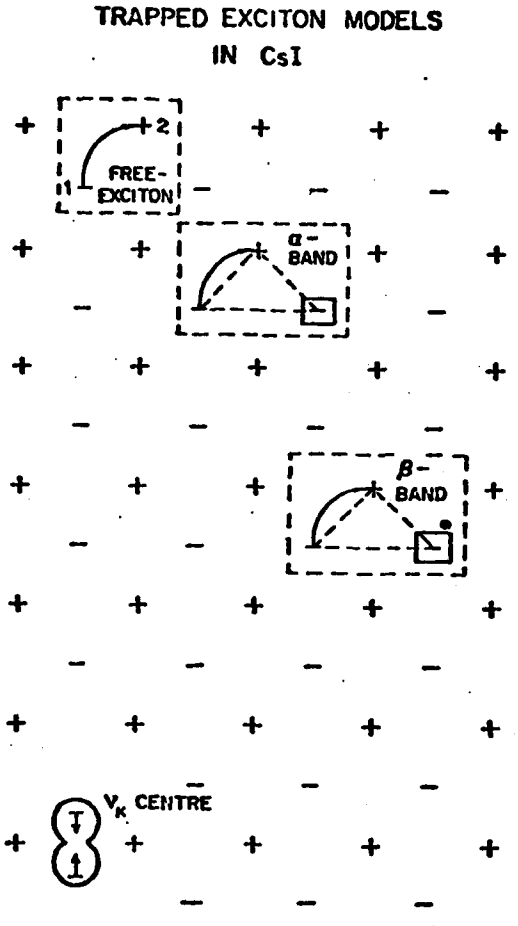

FIG. II.1--Model for the creation of a trapped exciton in CsI.

(a) Schematic representation of an exciton as the transfer of a valence electron from halogen ion 1 to alkali ion 2 in a CsCl-type alkali halides.

(b) Schematic representation of a β-exciton. One electron is transferred from halogen ion 1 to alkali ion 2 in the presence of the F-center 3.

(c) Schematic representation of an α-exciton. One electron is transferred from 1 to 2 in presence of the negative ion vacancy 3.

$$\Delta E = E_{ex} - E_{\alpha,\beta}$$

$$= \Delta E_{es} + \Delta E_{rep} + \Delta E_{pol} \quad . \qquad (2.2)$$

Using Eq. (2.2), these authors found general expression for the location of the α and β bands with respect to the first exciton absorption band in all alkali halide crystals. They observed that the energy difference between the first exciton absorption band and the β-absorption band is given by

$$\Delta E = E_{exc} - E_{\beta}$$

$$= -\frac{\alpha_M}{\partial}\frac{\rho}{r_0}\frac{e^2}{r_0} + \left\{\frac{1}{r_{1i}^4} + \frac{1}{r_{2i}^4} - \frac{2\cos(r_{1i}, r_{2i})}{r_{1i}^2 r_{2i}^2}\right\}$$

$$(M_F - M_-)\frac{e^2}{2r_0} \quad . \qquad (2.3)$$

In Eq. (2.3) the change in electrostatic energy is zero because the electrostatic energies involved in the extraction of the positive and negative ion are the same in the case of the free exciton as in the case of the β-exciton.

Also the energy difference between the first exciton absorption band and the α-absorption band is

$$\Delta E = E_{ex} - E_{\alpha}$$

$$= \left(\frac{1}{r_{23}} - \frac{1}{r_{13}}\right)\frac{e^2}{r_0} - \frac{\alpha_M}{\partial}\frac{e^2}{r_0}\frac{\rho}{r_0} - 0.2714\, M\frac{e^2}{r_0}$$

$$-\left\{ \sum_{\substack{\text{pos} \\ \text{ions}}}{}_{i} \frac{\cos(r_{2i}, r_{3i})}{r_{2i}^2 \; r_{3i}^2} - \sum_{\substack{\text{pos} \\ \text{ions}}}{}_{i} \frac{\cos(r_{1i}, r_{3i})}{r_{1i}^2 \; r_{3i}^2} \right\} M'_{+} \frac{e^2}{r_0}$$

$$-\left\{ \sum_{\substack{\text{neg} \\ \text{ions}}}{}_{i} \frac{\cos(r_{2i}, r_{3i})}{r_{2i}^2 \; r_{3i}^2} - \sum_{\substack{\text{neg} \\ \text{ions}}}{}_{i} \frac{\cos(r_{1i}, r_{3i})}{r_{1i}^2 \; r_{3i}^2} \right\} M'_{-} \frac{e^2}{r_0}$$

(2.4)

where

α_M - Madelung constant

r_0 - interionic distance

ρ - overlap (repulsive) constant

r_{ij} - distance between ions i and j

$\cos(r_{ij}, r_{kl})$ - cosine of angles between $\bar{r}_{ij}$ and $\bar{r}_{kj}$

e - electronic charge

α_+ - cation ionic polarizability

α_- - anion ionic polarizability

α_F - F-center ionic polarizability

$= e^2/4\pi^2 m \nu_F^2$

m - electronic mass

ν_F - frequency corresponding to F-band maximum

α - polarizabilities due to the displacement of the ions

ϵ_∞ - high frequency dielectric constant

ϵ_s - static

E_α - absorption peak energy of α-band

E_β - absorption peak energy of β-band

E_{ex} - absorption peak energy of first exciton band

$$M_- = \frac{2\alpha_-}{\alpha_+ + \alpha_-} \frac{1}{4\pi} \left(1 - \frac{1}{\epsilon_\infty}\right)$$

$$M_F = \frac{2\alpha_F}{\alpha_+ + \alpha_-} \frac{1}{4\pi} \left(1 - \frac{1}{\epsilon_\infty}\right)$$

$$M'_\pm = \frac{\alpha + \alpha_+}{\alpha + \frac{1}{2}(\alpha_+ + \alpha_-)} \frac{1}{4\pi} \left(1 - \frac{1}{\epsilon_s}\right) \quad .$$

It should be noted that r_0 , ρ , M_- , M^*_- , M'_+ depend only on the host lattice while the coefficients of M_- , M'_- , M'_+ denoted by A , B and C respectively depend on the relative positions of ions 1 , 2 , 3 M_- , M'_- and M'_+ are quantities related to the dielectric properties of the components of the lattice and can be quantitatively computed from data given in the book by Mott and Gurney.[32] Also the coefficients of M_- , M'_- and M'_+ which depend on the positions of ions 1 , 2 , 3 are summed over all positive or negative-ion sites except that the sites 1 , 2 , and 3 are omitted as suggested by the primes. The lattice sums involved in the quantities B and C are discussed in Appendix (A) while the quantity A can be obtained directly from Fig. II.1 using elementary geometry. The calculated values of A , B and C are 0.2714 , 1.232 and 0.7015 respectively.[33] The numerical results of the location of α and β-bands for the alkali iodides and CsCl structure alkali halides are presented in Table I and are compared with experimental data where available. This model has been modified and extended by other authors[34-36] to calculate the energy of formation of an exciton localized near cationic or other complex

vacancy pairs. Tsertsvadze[34] has also used this model to calculate the energy of formation of an F-center in all alkali halides.

D. PHOTOLUMINESCENT MEASUREMENTS

The photoluminescent properties of alkali halides are studied by measuring their emission and excitation spectra. In this section, we review the work that has been done on the photoluminescent properties of alkali halides under the subheadings (1) emission and (2) excitation measurements.

1. Emission Measurements

As with absorption measurements of alkali halides, quite a lot of work has also been done on the luminescence properties of alkali halides with NaCl structure[1-8] while relatively little work has been done on alkali halides with CsCl-structure.[16-19] The observed emission spectra can be classified as being intrinsic or extrinsic depending on whether they are excitable by host crystal absorption bands or by impurity absorption bands in the perfect crystal respectively. As a result of these excitations, the two major emission bands observed in alkali halides are located in the ultra-violet and visible regions. In this section we review the responsible mechanism for the two major intrinsic emission components in perfect alkali halides.

In an attempt to understand the mechanism responsible for these (emission bands) luminescence phenomena in alkali halides, these crystals are either activated with monovalent or divalent impurities such as Na^{+}, Tl^{+}, Sr^{++}, Mr^{++}. Electron traps are introduced in the case of

monovalent impurity doping and cation vacancies for divalent impurity doping.[37-40] In other situations, crystals are exposed to ionizing radiations to create color centres.[41-43] Recent studies showed that energies of the order of (5-10) eV were enough to create color centres in alkali halides. However, some authors[19,43] proposed from their optical and electron paramagnetic resonance measurements at low temperatures that defects of stable configurations are difficult to create in CsI even when exposed to severe ionizing radiations.

The intrinsic luminescence which occurs at lower temperatures in alkali halide crystals with the NaCl structure has been attributed by Kabler[7] and also Murray and Keller[8] to the recombination of an electron and V_K-centre (self-trapped hole), this configuration being denoted by $(V_K + e)^*$. This model has been used extensively to explain the intrinsic luminescence excited with either non-ionizing ultra-violet light or with ionizing radiation at lower temperatures. There is limited luminescence data on materials with the CsCl structure.[16-19] Even the existing data is mainly on ultra-violet absorption spectra.[19,23,24] The results of Lamatsch et al.[19] on ultra-violet absorption and luminescence spectra of thin films and bulk crystals of both relatively strain free, defect free and pure CsI can be compared with our results.

At this juncture, a review of the work that has been done on the photoluminescence of norminally pure CsI is presented.

In the so-called norminally pure CsI , some authors[16-19] (Morgenshtern, Masunaga, Towyama etc.) observed the two major components of luminescence the ultra-violet and blue emission. They attributed the ultra-violet

emission at LNT to the radiative recombination of electron-hole pairs, while the second component - blue emission was explained to be due to radiative recombinations of electrons with holes or excitons at structural lattice defects probably of the vacancy type.

One of these authors, Morgenstern,[16] observed emission (luminescence) at room temperature before he cooled (RTBC) the norminally pure CsI sample to liquid nitrogen temperature. Probably traces of impurities which could be an important source of luminescence was not detectable in Morgenstern's norminally pure sample.

Recent studies on the luminescence of pure CsI by Lamatsch et al.[19] at low temperatures showed that the ultra-violet emission band is due to radiative recombination of self-trapped excitons, while the blue-emission band component results from radiative recombination of excitons localized near cationic-divalent vacancy complex. Since our main concern in this work is the study of intrinsic luminescence then we shall not discuss impurity luminescence observed by Lamatsch et al. any further. However, the intrinsic luminescence observed in pure CsI by Lamatsch et al. is excitable within the excitonic region at low temperatures. At LHeT , excitonic excitation gave a 290 nm emission band besides the usual 338 nm emission band. At temperatures above 20°K, the 290 nm emission band disappears, though the 338 nm band presists up to about 120°K above which it disappears. The corresponding life times of the self-trapped excitons responsible for the 290 nm emission and the 338 nm emission are 10^{-7} sec and 10^{-6} sec respectively. The self-trapped excitons responsible for the observed intrinsic luminescence in CsI was proposed by Lamatsch et al. to be composed of electron plus trapped hole configuration.

A third component of luminescence often observed in alkali halide crystals at room (before cooling) and low temperatures arises from excitations in the activator (impurity) or defect absorption bands in these crystals. This extrinsic (impurity induced) luminescence lie in the visible and infra-red regions while the exciting impurity absorption bands lie towards the longer wavelength side of the first exciton absorption band through the infra-red region. This type of luminescence has been extensively studied in activated alkali halide crystals at room and lower temperatures. Since the purpose of this work is to study the intrinsic luminescence due to exposure to non-ionizing UV-radiation, we shall not discuss the observed extrinsic luminescence in alkali halide crystals any further. A detail discussion of the extrinsic luminescence can be found elsewhere.[37-41,44]

2. Excitation Spectra Measurements

In photoluminescent measurements, the excitation spectrum is measured by monitoring the emission intensity at a pre-selected emission wavelength as a function of the excitation photon energy. The peak of the excitation spectrum is then compared with peaks or valleys of the corresponding absorption spectra of the same material and at the same temperature. If the peaks of the absorption and excitation spectra coincide, then the observed emission band is excitable by the absorption band. On the other hand, if the excitation peak lies on the long wavelength side of the absorption peak, the the corresponding luminescence is due to radiative transfer of energy.

Therefore, a combined study of the absorption and excitation spectra can be used to provide information on the responsible mechanism for the observed luminescence in alkali halides or other luminescent materials.

This technique has been used by Teegarden, Weeks, Edgerton and a host of others[5,6,45-46] to elucidate the responsible luminescent mechanism in RbI and KI . Figures II.2 and II.3 show the excitation spectra for the emission bands in RbI and KI . It is interesting to note from these figures that a striking minimum occurs at the peak of the first exciton band. The fact that luminescence does not occur in the peak of the first exciton band in RbI and KI may indicate that excitons are mobile and can diffuse to some quenching centers before degenerating into a trapped hole and associated electron and vice versa. Also Lamatsch et al.[19] measured the excitation spectrum shown in Fig. II.4, for the two ultra-violet emission bands in CsI . The peaks of the excitation spectrum are located at 213 nm and 208 nm on the minimum side of the exciton absorption bands. In Chapter VI, we shall compare our data on excitation spectra with those of Lamatsch et al.[19]

E. ELECTRON SPIN RESONANCE MEASUREMENTS

Electron spin resonance (ESR) is a powerful tool that has been used by many authors[9,47-49] to determine the symmetry or anisotropy of the centers responsible for the luminescence observed in alkali halides. This is accomplished by measuring the magnetic dipole transitions between the spin levels of an unpaired electron (or a system containing several electrons, whose total spin S is nonzero) in these crystals

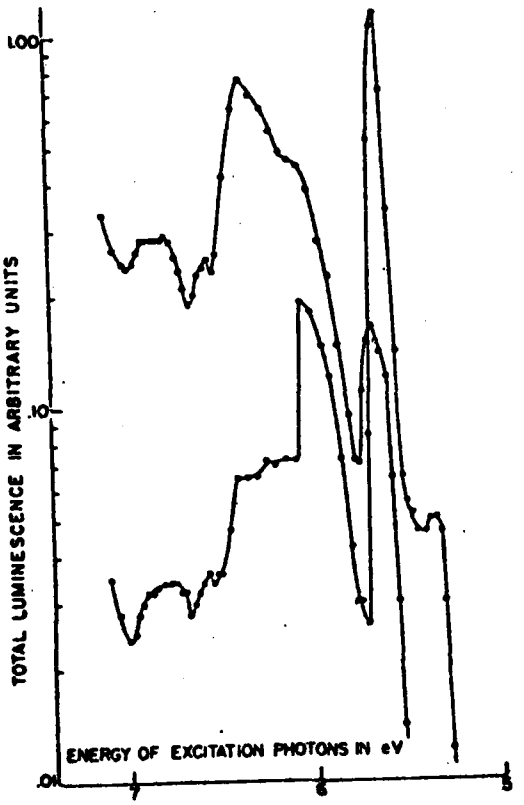

FIG. II.2--Excitation spectra for the two emission bands of RbI observed at 80°K. (After Edgerton, 1962).

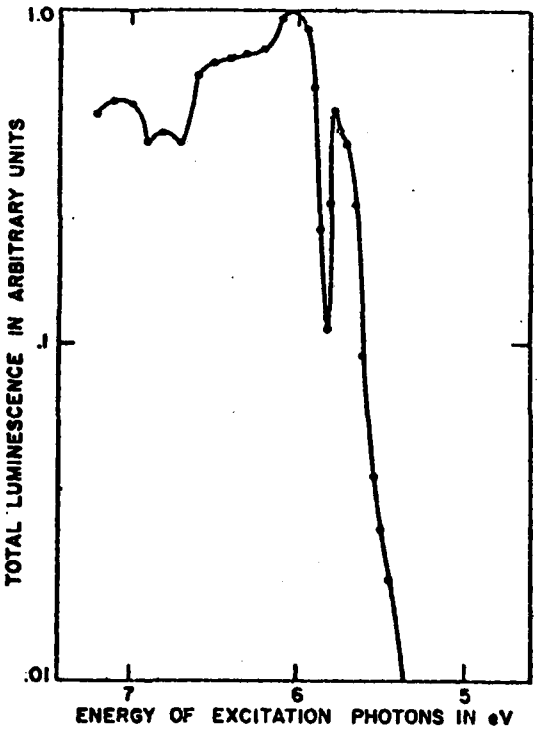

FIG. II.3--Excitation spectrum for both emission bands of KI at 80°K. (After Weeks and Teegarden, 1959).

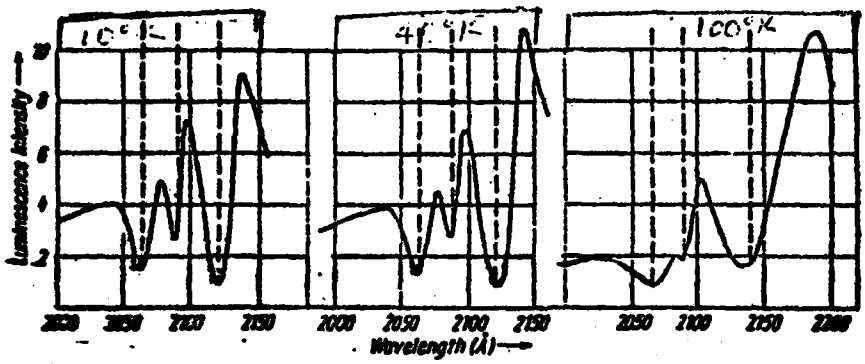

FIG. II.4--Excitation spectra for a bulk crystal of CsI for three temperatures. (After Lamatsch).

in a static magnetic field B_0 . The change of the ESR spectrum with the orientation of the sample in the D.C. magnetic field determines the degree of anisotropy of the paramagnetic center in the sample. If the ESR spectrum does not change with orientation, then the center can be considered to be isotropic (like the so-called F-center) while the center is anisotropic if its ESR spectrum changes with orientation. In alkali halides, the V_K-center (self-trapped hole) is anisotropic. Figures II.5 and II.6 show typical ESR spectra of an F-center and a V_K-center in a KCl crystal.

From the ESR spectra, other information besides the degree of anisotropy that can be obtained include

(a) the number of centers which can be obtained from the area under the ESR spectrum and the number of spins. The ESR technique can also be applied to the measurement of the oscillator strengths in optical absorption bands.

(b) the hyperfine structure (HFS) which provides the most extensive and exact information concerning the atomic and electronic structure of the centers. This information can be obtained from the number and the intensity ratio of the resolved HFS lines, the size of the splitting and the angular dependence of the spectra.

(c) the g-factor gives important information about the structure and energy levels of the centers from small g shifts (from the free electron value 2.0023) and their anisotropy, and

(d) the relaxation times, T_1 and T_2 can give information regarding the nature and strength of the coupling of the

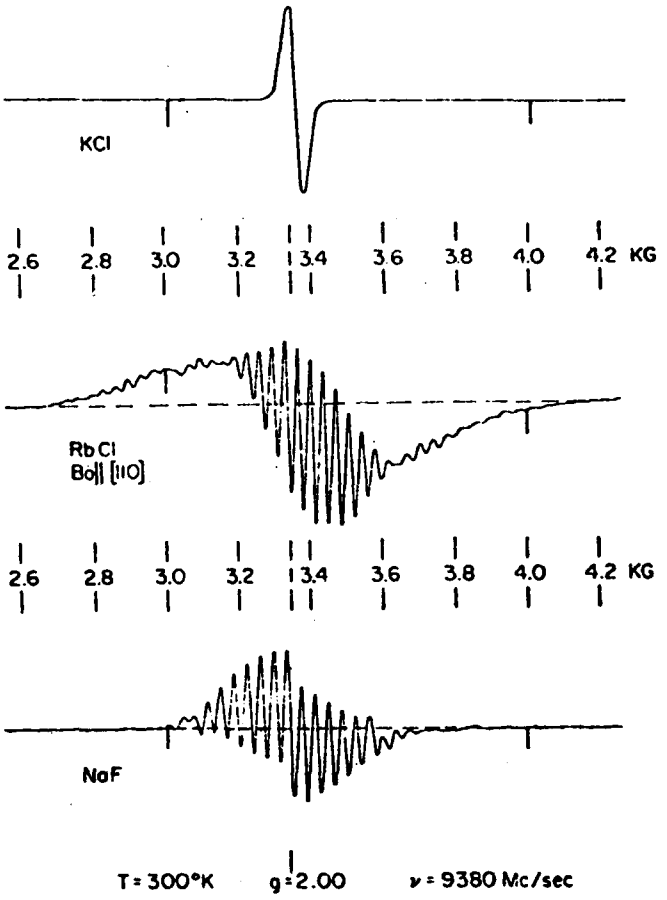

FIG. II.5--ESR spectra of F-centers in KCl , RbCl, and NaF.

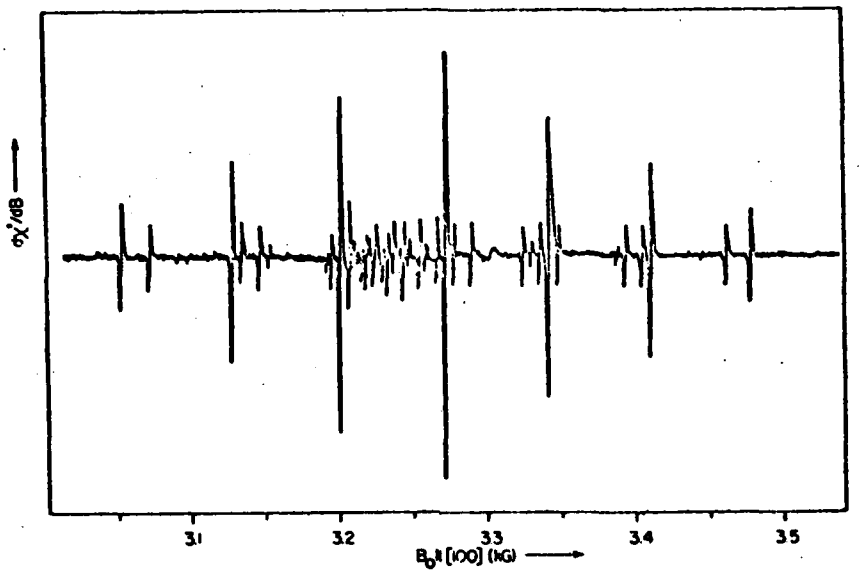

FIG. II.6--The ESR spectrum of V_K centers in KCl. B_0 field along a <100> axis, T = 77°K, ν = 9263 Mc/sec. The hyperfine structure results from the interaction with the nuclei Cl^{35} and Cl^{37} (each with I = 3/2) (Castner and Känzig, 1957).

electron spins with one another and the thermal reservoir of the lattice as well as the structure of this reservoir.

Thus from a combined knowledge of the g-value, the degree of anisotropy and the number of lines and the width of the ESR spectrum, we can often associate a specific configuration with the center under consideration. This method has been used by Hutchison,[41] Kanzig,[9] and others[48-49] to identify trapped electron and holes in alkali halides. We also use this technique in this work to identify the paramagnetic species produced by cooling and exposing CsI to non-ionizing radiations. The ESR work on CsI presented in Chapter V was done, not only because there has been no ESR data on pure CsI which is relatively strain and defect free, but also to support our optical data on CsI which suggests the existence of paramagnetic centers produced by cooling and exposure to non-ionizing radiations.

CHAPTER III

THE PHOTOLUMINESCENT EXPERIMENT AND EXPERIMENTAL TECHNIQUES

A. INTRODUCTION

The details of the photoluminescent and electron spin resonance experiments and associated apparatus have been discussed elsewhere.[5,6,9,45-49] In view of this, only a skeletal synopsis is included here and emphasis will be on sample preparation and apparatus used in the course of this work.

B. THE PHOTOLUMINESCENT EXPERIMENT

In this work photoluminescent properties of pure and strained CsI samples were studied by measuring their absorption, emission and excitation spectra discussed in Chapter II, as the temperature was cycled from room temperature before cooling (RTBC) to low temperatures (LT) and back to room temperature after cooling (RTAC). These samples used in this work were mounted on a copper block with silicone vacuum grease to provide thermal contact between sample and copper. The aim of this work was to learn more about the responsible mechanism for the observed intrinsic luminescence in alkali halides with CsCl-structure taking CsI as a case study. The strained samples of CsI were studied in order to substantiate our association of the RTAC luminescence observed in pure CsI with vacancies produced by cooling and exposure to non-ionizing UV-radiation.

Evaporated thin films of CsI were obtained using superpure powders purchased from the Merck Company while the bulk single crystals were supplied by the Harshaw Chemical Company. The sodium content of the

Harshaw sample was less than one part per million. These bulk single crystals measured (1.27 × 1.27 × 0.2) cm in size. The vapor depositions technique used to evaporate our films has been discussed in detail elsewhere. A Cary 14 spectrophotometer was used for the absorption measurements while Fig. III.1 shows the experimental set-up for the emission and excitation measurements. The light source was a Bausch and Lomb deuterium lamp which had a fairly flat spectrum from 2000 Å to 4000 Å without any sharp lines. The light went through a grating monochromator which had a small driving motor to provide steady scanning speed, and then through a mechanical light chopper. The chopped monochromatic light was incident upon the large face of the samples (the 100 face in the case of single crystals) in the dewar. The emission was measured at right angles to the exciting light in order to avoid the interference from the transmitted and reflected light. Passing through another grating monochromator, the emission was detected by an RCA 8645 photomultiplier tube with an S-20 spectral response. The detected signal was fed into a lock-in amplifier, which picked up the reference frequency from the chopper, and then recorded by a strip chart recorder. A family of absorption, emission and excitation spectra for both thin films (500-2000 Å) and bulk single crystals were measured as a function of excitation wavelength as the temperature was cycled from RTBC to LT and back to RTAC.

In photoluminescent measurements on alkali halides some basic assumptions are generally made. They are:

(a) only direct optical transitions between electronic states are involved,

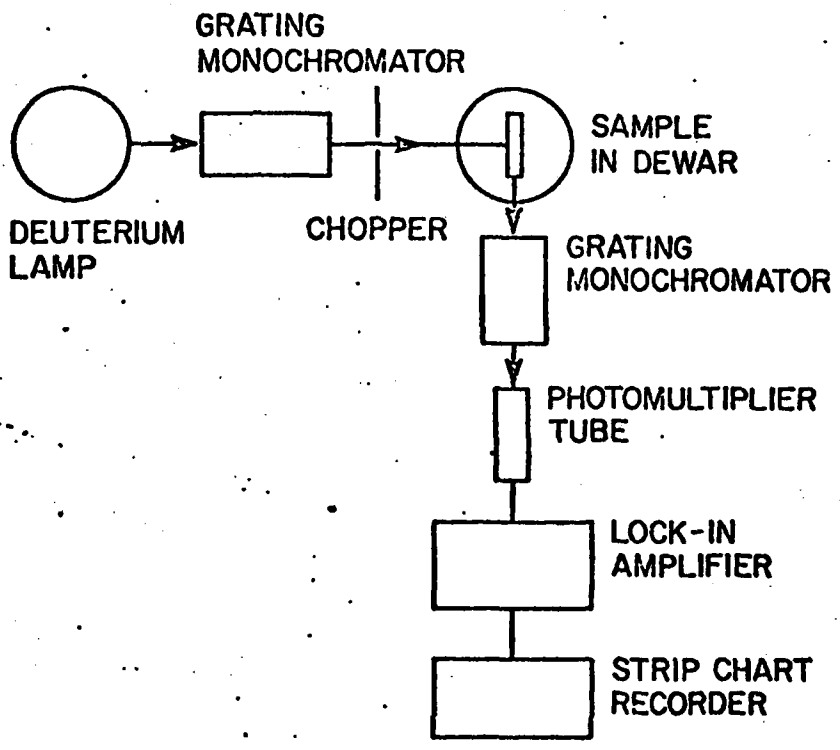

FIG. III.1--Experimental arrangement used to measure emission and excitation spectra.

(b) irradiations of threshold energy of about 5 eV is enough to create excitons, color centers and free electrons and holes.[20,21]

The first assumption stems from the fact that alkali halide crystals have direct band gaps. The case of indirect transitions in alkali halides, to our knowledge, has not been reported. One of the models used to relate optical properties to electronic structure in alkali halides is the Adiabatic or Born-Oppenheimer Approximation[50] which asserts that (a) in optical transitions, the electronic state at each instant is taken to be the same as though the nuclear coordinates were at rest at the positions they have at this instant; and (b) the state of the system can be decoupled into electronic and lattice parts

$$\Psi_{system} = \psi_{electrons} \quad \phi_{lattice} \tag{3.1}$$

where Ψ_{system}, $\psi_{electrons}$ and $\phi_{lattice}$ are wavefunctions. It should be noted that the first assertion under the Adiabatic Approximation requires that the frequency of the electronic motion be much greater than the frequency of lattice vibration[51] or

$$\left(\frac{\hbar\omega}{E_a - E_b}\right) \frac{\Delta x}{(\Delta x)'} << 1 \tag{3.2}$$

where $E_a - E_b$ is the energy separation of the electronic levels; $(\Delta x)'$ is the nuclear displacement and Δx is the amplitude of the lattice vibrations of frequency ω. Under this condition, a slight departure from the validity of the Adiabatic Approximation represents the primary sources of dissipative, non-radiative transitions because

the lattice vibration frequency is now greater than the frequency of the electronic motion. Consequently the electrons will just give off their energy in the form of heat to the system. Another model generally used in the study of the optical transitions in alkali halides is the Frank-Condon Principle[52] which asserts that during optical transitions the nuclear coordinates do not change and which leads to the so-called "vertical transitions". The essential difference between these models is that the Adiabatic Approximation deals with decoupling electronic states from nuclear states while the Frank-Condon Principle deals with the vertical transitions between electronic states.

Within the frame-work of the Adiabatic Approximation, the basic equations which relate the emission probability and absorption cross-section to energy $E_{jk,\alpha\beta}$ for transitions between electronic states j and k are[53]

$$W_{kj}(E) = \left\{\left(\frac{\epsilon_{\ell H}}{\epsilon_0}\right)^2 n\right\} \frac{4\ell^2}{3\hbar^4 c^3} AV_\beta \sum_\alpha |E_{kj,\beta\alpha}|^3 |\vec{r}_{kj,\beta\alpha}|^2 S^{\ell}_{kj,\beta\alpha}(E) \tag{3.3}$$

and

$$\sigma_{jk}(E) = \left\{\left(\frac{\epsilon_{\ell H}}{\epsilon_0}\right)^2 \frac{1}{n}\right\} \frac{4\pi^2 e^2}{3\hbar c} AV_\alpha \sum |E_{jk,\alpha\beta}| |\vec{r}_{jk,\alpha\beta}|^2 S^{a}_{jk,\alpha\beta}(E) \tag{3.4}$$

respectively. The matrix element $\underline{r}_{jk,\alpha\beta}$ is defined as

$$\vec{\underline{r}}_{jk,\alpha\beta} = \int d\vec{\underline{r}} \int d\vec{\underline{x}}\, \psi^*_{j\alpha}(x)\, \phi_{j\vec{x}}(\vec{\underline{r}})\, \vec{\underline{r}}\, \psi_{k\beta}\, \phi_{k\vec{x}}(\vec{r}) \tag{3.5}$$

Here AV_α , AV_β are statistical average over the occupied initial vibrational states α and β ; ϵ_0 , the average electric field within

the medium, $\epsilon_{\ell}\mathcal{H}$ is the effective field at the center, n the refractive index and the shape functions $S^{a}_{jk}(E)$ and $S^{\ell}_{kj}(E)$ are normalized such that

$$\int S^{a}_{jk}(E)\, dE = \int_{k} S^{\ell}_{kj}(E)\, dE = 1 \quad .$$

Other constants have their usual meaning. The ratio $(\epsilon_{\ell}\mathcal{H}/\epsilon_{0})^{2}$ is of the order of 2 in alkali halides. Using the principle of conservation of energy, the shape functions $S^{a}_{jk}(E)$ or $S^{\ell}_{kj}(E)$ can be replaced by delta function $\delta [E_{k\beta} - E_{j\alpha} - E]$, which in effect smears out to give the broad bands (composed of a large number of unresolved lines) observed in absorption and emission spectra in photoluminescent measurements.

Exposing alkali halides to radiations of (~ 5 eV) at room and low temperatures is believed to generate free electrons, holes, excitons (electron-hole pair bound together by their Coulombic interactions) and color centers.

Excitons:

Excitons are detected by optical absorption measurements from which the peak energy of absorption can be related to the energy band gap and effective mass by[10,24,26,54]

$$h\nu_{n} = E_{g} - \frac{\mu e^{4}}{2\hbar^{2}\epsilon^{2}n^{2}} \qquad (3.6)$$

where n is the principal quantum number and the reduced mass μ defined as

$$\frac{1}{\mu} = \frac{1}{m_e^*} + \frac{1}{m_h^*} \qquad (3.6)$$

with m_e^* and m_h^* the electron and hole masses and ϵ is the appropriate dielectric constant. For very small radius (of the order of one interionic spacing) excitons, a value of unity is appropriate for ϵ while for extremely large radius exciton, the static dielectric constant (ϵ_s) should be used. However within these two extremes, as is always the case in alkali halides, the high frequency dielectric constant (ϵ_∞) is appropriate. The bound states and corresponding energy level diagrams of the exciton below the bottom of the conduction band are shown in Fig. III.2 . Figure III.3 shows the absorption spectra of a typical alkali halide over a wide range of energy. The exciton bound states are created between E_x and E_G^o . Above E_G^o , free electron-hole pairs are created and photoconductivity sets in.

The luminescence process thus involves the downward transtions of these excitons from their relaxed excited states to lower or ground states. The combined process of absorption and emission is represented fairly well on a configuration coordinate diagram (CCD) shown in Fig. III.4 . In the Fig. III.4 the ground electronic state m and the excited electronic state k are shown, with the variation in energy of the system with the effective nuclear coordinate R given by the parabolic curves and the long arrows show vertical transition between ground and excited states. From the CCD , information concerning the bandwidths of absorption and emission, the temperature dependence of the luminescence process and the Stoke's shift (energy difference

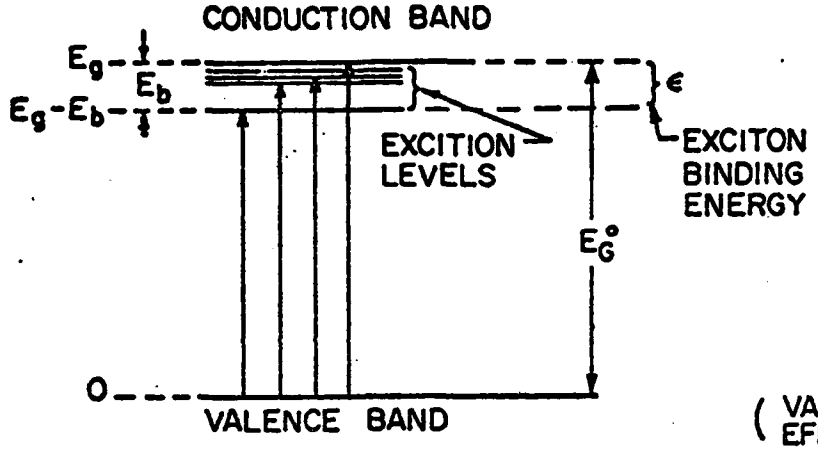

FIG. III.2(a)--Energy levels of an exciton whose center of mass is at rest.

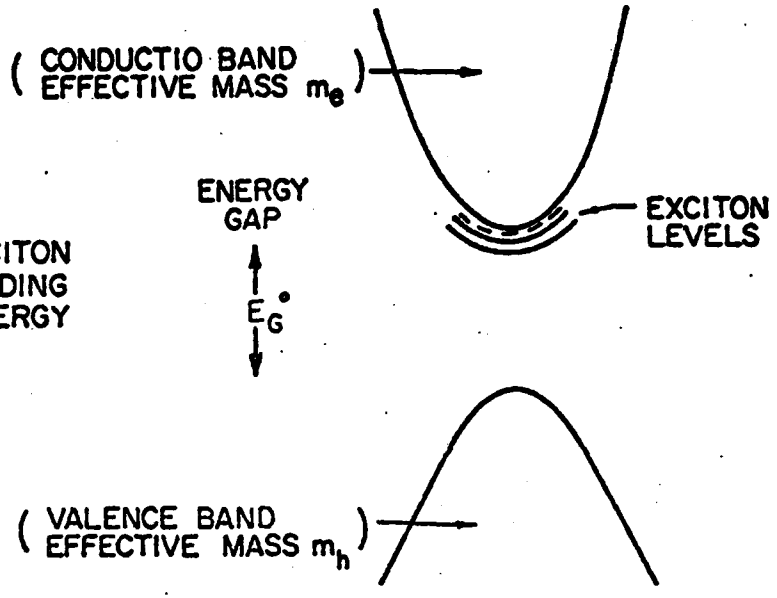

FIG. III.2(b)--Exciton levels in relation to the conduction band edge, for a simple band structure with both conduction and valence band edges at $\vec{K} = 0$.

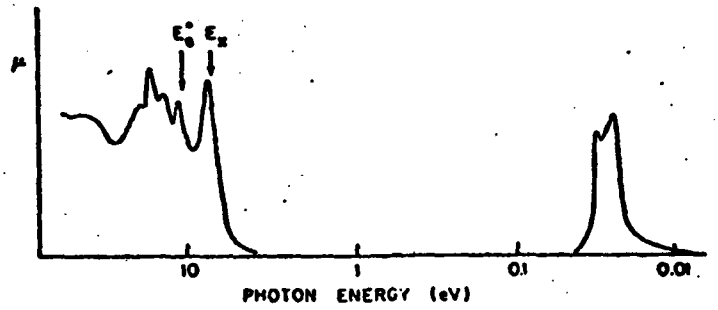

FIG. III.3--Absorption spectrum of a typical alkali halide crystal over a wide range. The mechanisms responsible for the various peaks are discussed in the text.

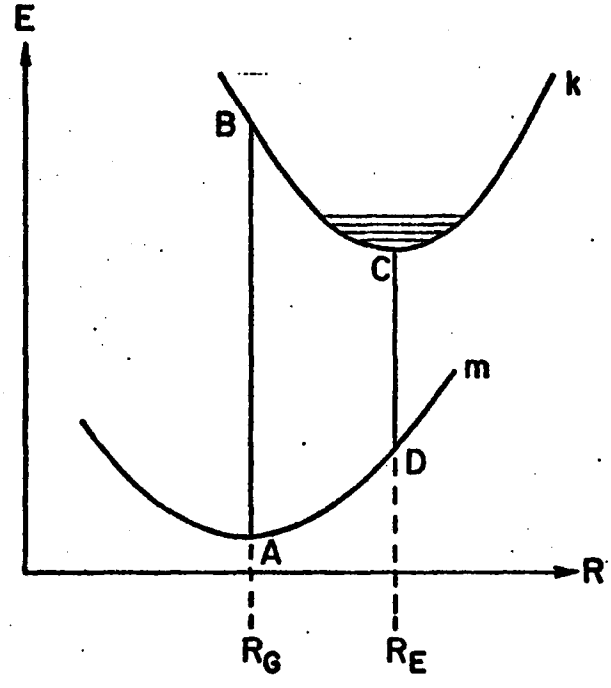

FIG. III.4--Typical configuration coordinate diagram (CCD).

between peak of absorption and emission) can be obtained from this model. An experimental calculation of the CCD has been discussed elsewhere.[53-54]

Color Centers:

These are lattice defects that absorb visible or infra-red light. Examples of which include the F- and F-center aggregates and V-centers. An F-center is an electron trapped at a negative ion vacancy. Other complexes formed from F-center aggregates are the so-called M- and R-centers. The M-center is composed of two F-centers while the R-center is made up of three F-centers clustered together. Another center of interest is the F′-center which is an F-center plus an electron.

Of all the V-centers, the V_K-center or the self-trapped hole have been most widely studied and fairly well understood in alkali halides. Another well known center is the H-center, a self-trapped hole in an interstitial position in the lattice. The V_K- and the F-centers are discussed in Chapter V. A detail discussion of these centers can be found elsewhere.[7,8,9,47-55]

C. EXPERIMENTAL TECHNIQUES

In this section, the equipment and techniques used for the photoluminescent and electron spin resonance measurements will be discussed.

1. High Vacuum System

The high vacuum system used in our photoluminescent measurements consisted of a standard Varian Associates FC12-E high vacuum system

containing two VacSorbs, titanium sublimation pump, 200 *l*/s vac ion pump and a cryopump. This system provided fast pumping speed and extremely low contamination which is more difficult to achieve with oil diffusion pumps. The control unit consists of two gauges, one gauges measures pressure between one atmosphere to about one micron and the other gauges pressure between 10^{-5} - 10^{-9} torr. Figure III.5 shows the entire unit. Typical base pressure of this high vacuum system is 10^{-9} torr.

2. Dewars

Two different types of dewar were used to measure the absorption, emission and excitation spectra of pure CsI as a function of temperature. One is a small liquid nitrogen dewar which can only be used to take measurements from room to liquid nitrogen temperatures. The other one is the liquid helium dewar which can be used to take measurements at regulated temperatures from room to liquid helium temperature and back to room temperature in a continuous fashion. Figures III.6 and III.7 show the schematic diagrams of these dewars.

Liquid helium dewar - Fig. III.7 shows the schematics of the liquid helium dewar, which consists essentially of two major parts:

(a) the sample support tube which consists of the electrical feedthroughs, the heater system, the thermocouples (temperature sensor) and the sample holder on which the samples used in this work were mounted with silicone vacuum grease.

and

(b) the dewar body itself which includes the vacuum jacket, samples chamber, liquid nitrogen and liquid helium reservoirs,

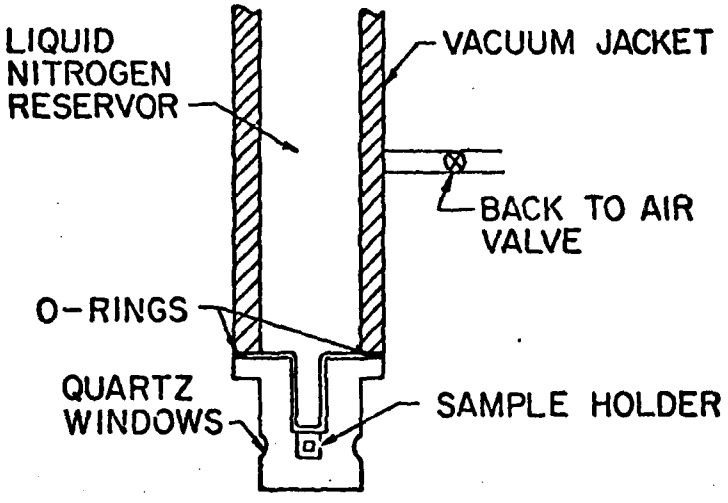

FIG. III.5--Schematic diagram of the Liquid Nitrogen Dewar.

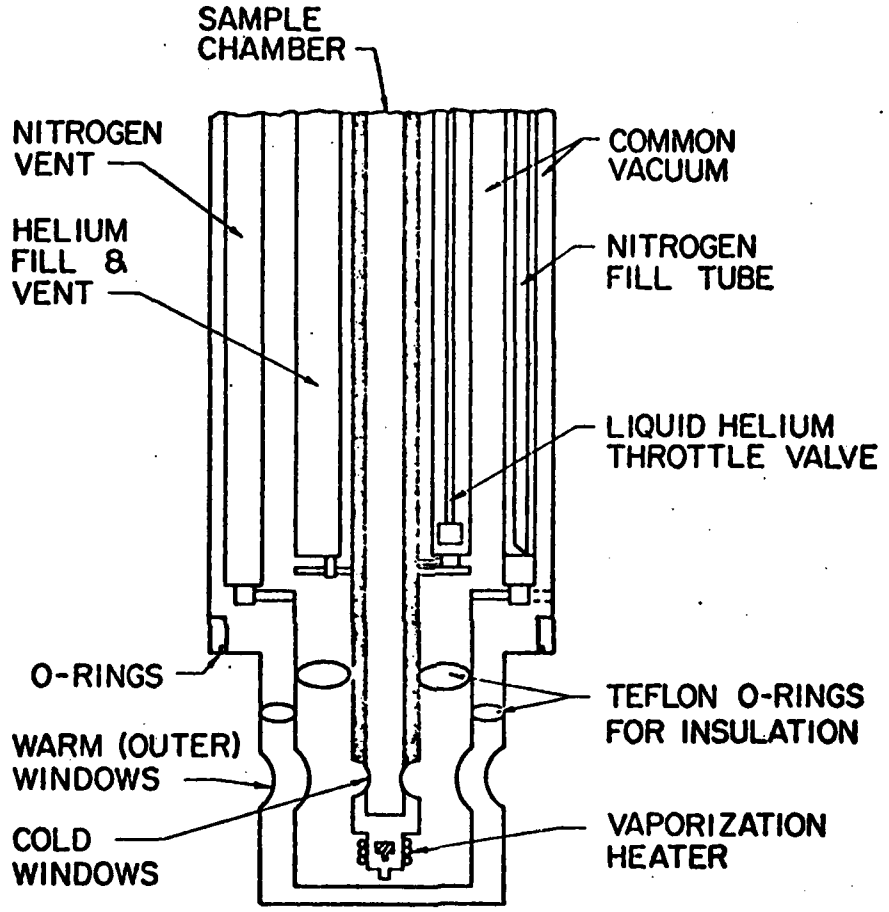

FIG. III.6--Schematic diagram of the Liquid Helium Dewar.

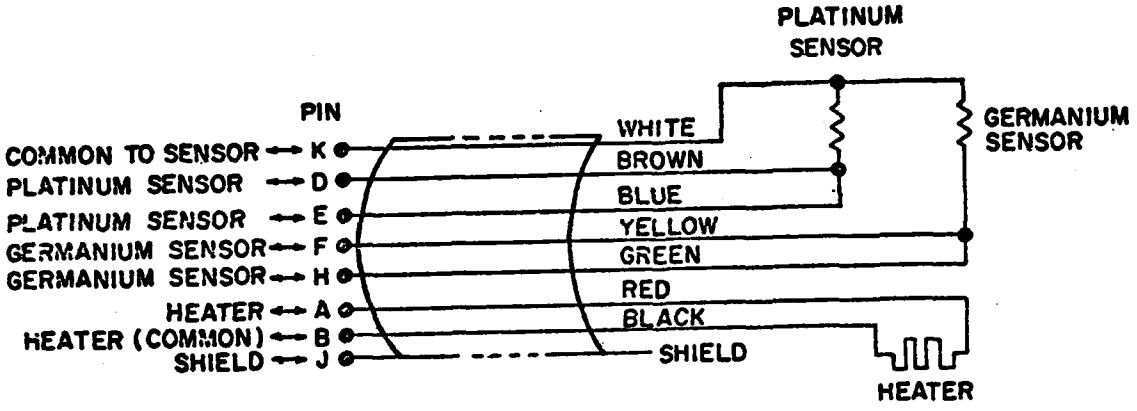

FIG. III.7--Electrical connections of the temperature sensors to the temperature controller.

throttle valve (which regulates the flow of coolant), the nitrogen shield and the tail which consists of the four outer or "warm" windows three of which are made of suprasil quartz and the fourth from beryllium for introducing ionizing radiation onto the sample.

This dewar is a 024/7M variable temperature cryogenic system made by Andonian Cryogenics, Inc. Though the dewar is pretty standard for photoluminescent measurements, we mention a few alterations made during the course of this work.

One of the changes made was on the heating system. The heater wire was changed from stainless steel wire to a manganin wire which can withstand greater power. A special type of low temperature epoxy called stay cast epoxy was used to glue the heater wire to the block the sample holder is screwed into. This epoxy was made from the mixture of about 96% stay cast plus 4% catalyst which can be obtained from the Emerson and Cuming Company. For a very firm hold, and to avoid short-circuits, the heaterwire was embedded in layers of the epoxy painted on the block holding the sample holder.

Another change made was on the seal for the cold windows. The major problem encountered came from leaking cold windows during the use of the liquid helium dewar for measurements at liquid helium temperatures. However, this problem was overcome by the use of a 10 mil thick indium wire instead of the indium gasket that came with the system. Loops of appropriate windows size were made from the 10 mil thick indium wire for sealing purposes. It should be noted that care

should be taken to cool a fixed cold window very slowly to liquid nitrogen temperature before leak checking, otherwise a rapid cooling will freeze up the indium seal and consequently open the window again. The only advantage the indium wire has over the indium gasket is that the indium wire not only allows greater pressure to be applied but also spreads more evenly when sealing the windows.

The last alteration made was on insulation. We observed that we cannot cool the system to liquid helium temperatures if there is contact between the tail of the sample chamber (which consists of the cold windows), the nitrogen shield and the outer tail (which consists of the "warm" windows). To overcome this problem we insulated them from each other by using "O-rings" (made from teflon tapes) between the inner tail and nitrogen shield and between the nitrogen shield and the outer tail. The insulation facilitated easy cooling things being equal in the system.

Liquid Nitrogen Dewar:

This is a very simple dewar. It has a liquid nitrogen reservoir and a sample chamber with four windows made of suprasil quartz, as shown in Fig. III.6.

3. Temperature Sensor

The temperature between room and liquid nitrogen temperatures was sensed by a platinum resistance thermometer while that below liquid nitrogen temperature down to about $1^{\circ}K$ was sensed by a Carbon-glass thermometer. These temperature sensors are commercially obtained from the Lake Shore Cryotronics, Inc. Figure III.8 shows the electrical

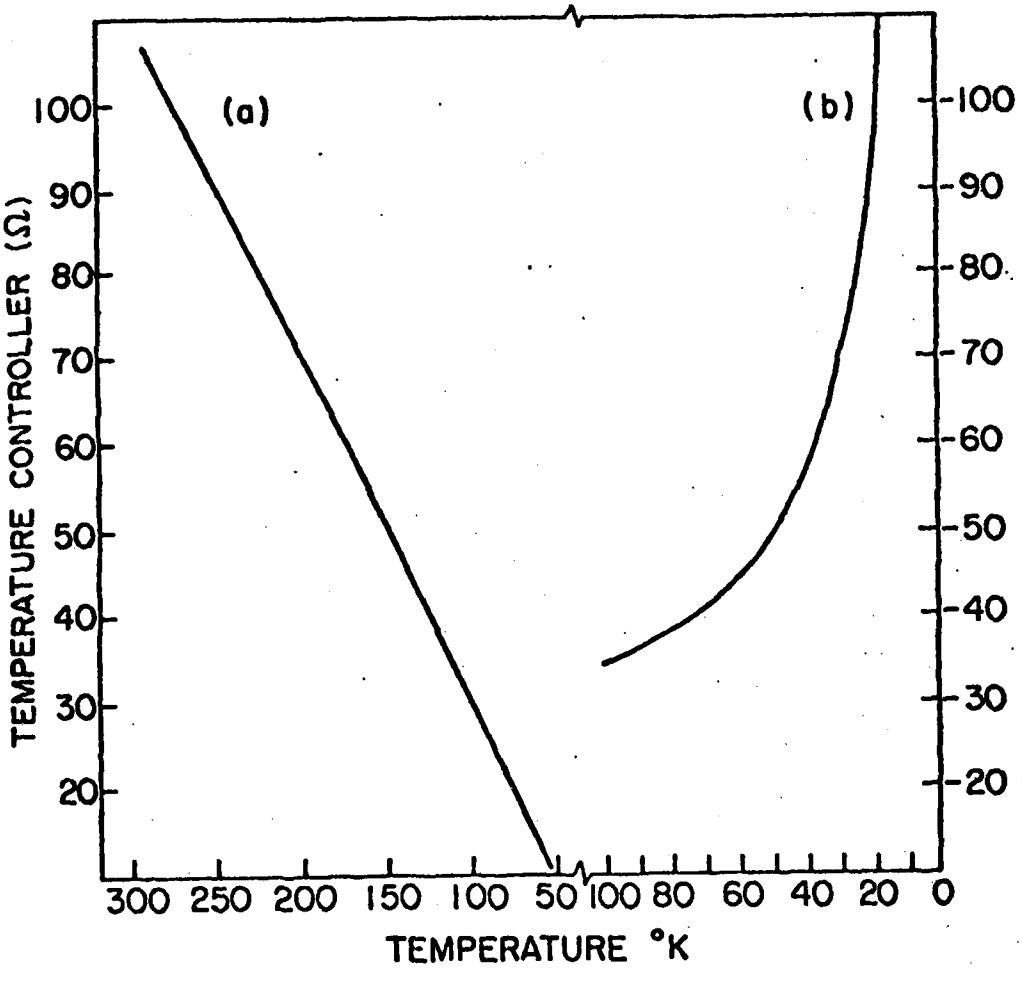

FIG. III.8--Calibration curves of (a) Platinum Resistance and (b) Carbon-Glass Sensors.

connections of these sensors from the electrical feedthroughs on the sample support tube of the liquid helium dewar to the temperature controller TC-103. Figure III.9 shows the caliberation curves for these sensors.

4. Sample Preparation

(a) Preparation of CsI

Pure bulk single crystals of CsI were purchased from the Harshaw Chemical Company. They were cut from ingots that have been well-annealed and zone refined and oriented along the (100) face. The crystals were (1.27 × 1.27 × .2) cm in size. The sodium content was less than one part per million. Before these samples were used for measurements, they are polished with methanol on lens paper.

Thin films:

A vapor deposition technique mentioned previously was used to evaporate the films. These films were evaporated on RT(300°K) and (400°K) suprasil quartz II substrates 1.27 cm × 1.27 cm × 0.1 cm in size, and annealed at this temperature for a period of 12 hours and slowly cooled to RT at a rate of roughly 8.3°K/hour to produce relatively strain and defect free films. More rapid cooling produced strained films which then luminescenced at RTBC. Heating was provided by a stainless steel block with heaters and a chromel-alumel thermo-couple embedded in it upon which the substrates were mounted. The thickness of the films deposited were measured by a Sloan DTM guage

connected to a quartz sensor head in the vacuum chamber. After films were prepared in vacuum, the system was let down to nitrogen atmosphere and the samples were tranferred to the experimental dewar discussed above while continuously blowing dry nitrogen gas on them.

(b) Preparation of strained CsI:

Pure bulk single crystals of CsI were strained both mechanically and thermally. The mechanical strain is achieved by compressing along the (100) plane using an Instrom Mechanical Testing Machine with plastic deformation of 4% ($\frac{\Delta L}{L}$) being typical. Thermal strain is obtainable by heating the bulk single crystals or thin films of pure CsI to a temperature of about 500°C and cooling the sample to room temperature in 3-4 hours.

5. ELECTRON SPIN RESONANCE MEASUREMENTS[56]

The samples used for ESR studies were single crystals all having a rectangular shape of dimensions 15 mm × 4 mm and a thickness of 2 mm. The crystals were purchased from the Harshaw Chemical Company with the pure CsI having an impurity content of < 2 ppm or roughly .001 mole percent and CsI(Tl) of 21 ppm or approximately 0.1 mole percent. The crystals were attached to a quartz sample holder with DUCO cement and rotated about the long axis with a goniometer such that the (100) crystallographic direction could be oriented parallel and perpendicular to the DC magnetic field, H_o . The experimental apparatus consisting of a standard Varian E-112 ESR spectrometer with a standard E-231 multipurpose cavity operating in the TE_{102} mode was used along with

a standard dewar insert and variable temperature unit (E-257) operating between 80°K and 573°K. All spectra were recorded using a field modulation frequency of 100 kHz and a peak-to-peak field modulation amplitude of 20 G. Although the incident microwave power on the cavity was varied, generally, experiments were carried out at incident powers of 200 mW for purposes of sensitivity. Field scans of 1 kG to 4 kG centered about g = 2 (~3.3 kG) were chosen to present the data in the most convenient manner.

ESR experiments at 20°K were done with a Helium flow system employing a home built transfer tube, a silvered extention dewar, and a standard E-231 cavity dewar insert. One end of the transfer tube was immersed in a 25 liter He dewar while an extension dewar was attached to the other end and to the standard dewar with common pinch clamps to glass ball and joint sockets. The total distance from the He dewar to the ESR cavity was about one meter. The temperature at the sample was controlled by regulating the flow rate of He gas over the sample - He dissipated at a rate of about one liter per hour was sufficient to maintain sample temperature of ~ 20°K. The flow rate was controlled by the amount of power dissipated in a 2 watt resistor attached to the immersed end of the transfer tube, the current through the resistor being controlled with a standard 0-20V 0-1.5A Harrison 6201A DC power supply.

Optical irradiation of the sample was done with a Bausch and Lomb high pressure Hg vapor lamp and attachable monochromator. The incident light passed through the optical grid of the standard microwave cavity

(50% transmission) through a suprasil quartz dewar insert and onto the sample. In nearly all cases, sample irradiation was done at 217 nm and 235 nm, the first exciton absorption band and the absorption edge respectively.

CHAPTER IV

PHOTOLUMINESCENT STUDY OF PURE AND STRAINED CsI

A. INTRODUCTION

In this chapter is presented a study of the photoluminescent properties of both strained and pure CsI crystals. In each case, thin films and bulk single crystals of CsI were studied by measuring their absorption, emission and excitation spectra as the temperature was cycled from room to low temperatures and back to room temperature. We denote this cycling as RTBC (room-temperature before cooling) to liquid nitrogen LNT to LHeT (liquid helium temperature) to RTAC (room-temperature after cooling).

This chapter will be divided into three parts, the first of which deals with the general information which is necessary for the understanding of the photoluminescent experiments on CsI . In Section B, the photoluminescent studies on CsI are given and possible interpretations are given for the observed spectra. Similarly in Section C, the photoluminescent studies on plastically deformed or thermally quenched CsI are presented and discussed. The results of the deformed and undeformed crystal were then compared.

B. INTRODUCTION TO CsI[57-59]

The crystallographic structure of CsI is shown in Fig IV.1. The physical, thermal as well as optical properties of CsI are tabulated in Table I.1 along with other alkali iodides and cesium halides. Since

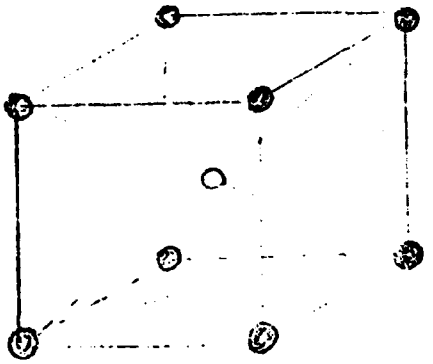

FIG. IV.1--The cesium chloride structure.

CsI crystallizes in the cesium chloride structure, it has a coordination number of eight. That is each ion (Cs^+ or I^-) is surrounded by eight nearest neighbors. So, an electron transferred from the iodine ion is shared between eight nearest neighboring alkali ions. Like all other alkali halides, the highly ionic character of CsI makes it properties profoundly affected by strong Coulomb interactions. CsI has a large binding energy (~ 6.3 eV) and high melting point (~ 621°C) which makes available a wide range of temperatures over which its properties can be studied. The electronic band gap of CsI is 6.37 eV. This large electronic band gap thus also provides a wide transparent spectral region in which the effects of impurities, vacancies, color centers and other defects may be studied.

At normal temperature and pressure, CsI crystallizes in the body centered cubic configuration, with a basis consisting of the anion (iodine ion) at (0, 0, 0) and the cation (alkali ion at $(\frac{1}{2}a, \frac{1}{2}a, \frac{1}{2}a)$, where a is the length of a cube side. However, at a temperature above 420°C, CsI changes phase and crystallizes in the NaCl structure.

Also CsI is a soft material and is so temperature sensitive that strain patterns develop when it is held by hand (probably the effect of strain hardening). CsI should be handled with care because it is slighly hydroscopic and also its solubility is temperature dependent as 44 g of CsI will disolve in 100 g of water at 0°C while at 35.6°C, 106 g will disolve in 100 g of water. Thus the temperature dependence of its solubility not only limits the use at high temperatures but also great caution should be taken in polishing operations using a wet lap. The elastic constants especially that along the (100) direction

(c_{44}), density and dielectric constants of CsI depend strongly on temperature. The anisotropy drops considerably in going from Lithium halides to cesium halides. This sudden drop is probably due to the increase of nearest neighbors in Cs-halides. Even among the Cs-halides, CsI is the least anisotropic. This highly isotropic behavior of CsI is probably responsible for the inability of many experimentalists to induce color centers in this material by using X-rays or other energetic particles except only by electrolysis. However, we observed that cooling and exposing CsI to non-ionizing ultra-violet radiation at low temperatures is enough to create a measurable amount of color centers.

Figure III.3, shows the absorption spectrum of a typical alkali halide crystal, where the peak at ~ 0.03 eV is associated with optical phonons and that at ~ 8 eV is due to electronic excitations. For CsI, the peak associated with electronic excitations starts from ~ 5.64 eV and the transparent region lies between 5.64 eV and 0.03 eV. The dispersion behavior in this transparent region can be characterized by a high-frequency dielectric constant $\epsilon_\infty = n^2$, where n is the refractive index. Figure IV.2, shows the available data on the alkali iodides refractive indices as a function of energy.

As in other alkali halides, the alkali ion (C_s^+) lies considerably lower in energy than the halide ion (I^-) in CsI such that the electronic excitation giving rise to the absorption peak at E_x (5.64 eV) results from the transfer of an electron from the halide-ion p-orbital to an orbital that leaves the crystal in the lowest excited states. The

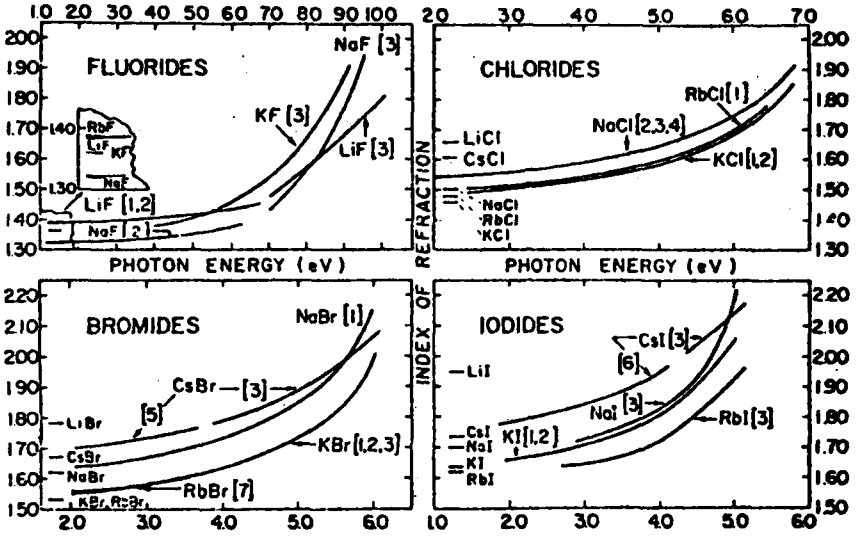

FIG. IV.2--A plot of refractive indices as a function of energy for alkali halides.

lowest excited state orbital is supposed to be totally symmetric about the halogen, thus possessing a Γ_1 - symmetry. Between E_x and E_G^o, bound excitons of large radius are created. For energy greater than E_G^o, photoconductivity sets in.

Consequently, we can view the emission process in CsI (as in other alkali halide crystals) as being due to transition from the relaxed lowest excited states of the crystal to lower or ground states. The configuration coordinate model used to describe the relaxation and emission process in alkali halides is discussed in details elsewhere.[53,60]

It should be noted that alkali halides of the CsCl type have received considerably less attention than the NaCl type crystals in the field of luminescence studies.[12-19] This is probably due to the complexities of these crystals and the difficulty involved in inducing color centers in them by coloration or exposure to ionizing radiations. In fact the only successful attempt to induce color centers in CsI was by electrolysis. The proposed models for the luminescent mechanism in CsI vary from author to author[16-19] and thus much work is necessary to get a clearer picture of what is going on. We therefore undertook our photoluminescent and EPR studies of pure and strained CsI to help elucidate the responsible mechanisms for the intrinisc luminescence observed at room and low temperatures. We discuss our results in the next section and in Chapters V and VI.

Several samples were used for study in each measurements to verify the reproducibility of the results. Additional information concerning the sample preparation can be obtained from Chapter III.

As is often done, the abscissa of the absorption spectrum is measured as the energy of the absorbed photon and the ordinate is measured in optical density (O.D.). The O.D. is related to the absorption coefficient $\alpha(cm^{-1})$ and the sample's thickness $d(cm)$ by

$$O.D. \sim \frac{\alpha d}{2.3} \tag{4.1}$$

which is a dimensionless constant because α is measured in cm^{-1} and d in cm. Similarly, the abscissa of the emission spectra is measured as the energy of the emitted photons and its ordinate as the intensity of the emitted photons. Often the ordinate is measured in the quantum efficiency defined as,

$$= \frac{n^{\underline{o}} \text{ of emitted photons}}{n^{\underline{o}} \text{ of absorbed photons}} = \frac{\text{number of emitted photons}}{\text{number of absorbed photons}}$$

$$= \frac{1}{1 + \frac{S}{A} e^{-\epsilon/kT}} \tag{4.2}$$

where S and ϵ are the frequency factor and the activation energy for the non-radiative transition respectively and A is the spontaneous radiative transition probability.

The photoluminescent data presented throughout this work has been corrected for the spectral response of the system.

C. RESULTS: PHOTOLUMINESCENCE FROM PURE CsI

1. Optical Absorption

Measurements were performed on both thin films and bulk single crystals, the thin films being used for measurement between room and

liquid nitrogen temperatures while the bulk crystals were employed in the 150°K to LHeT range.

The ultra-violet absorption spectra of the thin films (600 Å) of pure CsI are shown in Fig. IV.3. At RT (before and after cooling) absorption peaks are observed at 220 nm (1st exciton band) and 205 nm. These peaks sharpened, with the 220 nm band shifting to 215 nm at LNT as shown in Fig. IV.3. The shift of the first exciton absorption band (220 nm) at RT to 215 nm at LNT is probably due to strain induced by cooling. This effect has been noted by Lynch and Brothers.[16] The bulk single crystals which were $\frac{1}{2}$" × $\frac{1}{2}$" × 2 nm and had the (100) face perpendicular to the radiation in the Cary 14, were used to reveal any structure occurring in the long wavelength tail of the fundamental absorption. The absorption spectra for these crystals in this region are shown in Fig. IV.4 for temperatures of 120°K, 80°K, 60°K and LHeT. At 120°K absorption peaks appear at 225 and 245 nm. The position and relative intensity of the 225 nm peak does not appear to change much with temperature. The peak at 245 nm at 120°K shifts to 240 nm at 80°K, 238 nm at 60°K and 237 nm at LHeT, the relative intensity almost doubling in this sequence.

2. Emission and Excitation

Because of temperature cycling we have for convenience divided our results into data between room (RT) and LNT and RT and LHeT.

(a) Thin films

Figure IV.5 shows the emission spectra which were measured for thin (600 Å) films of pure CsI. As in prior studies,[15] emission

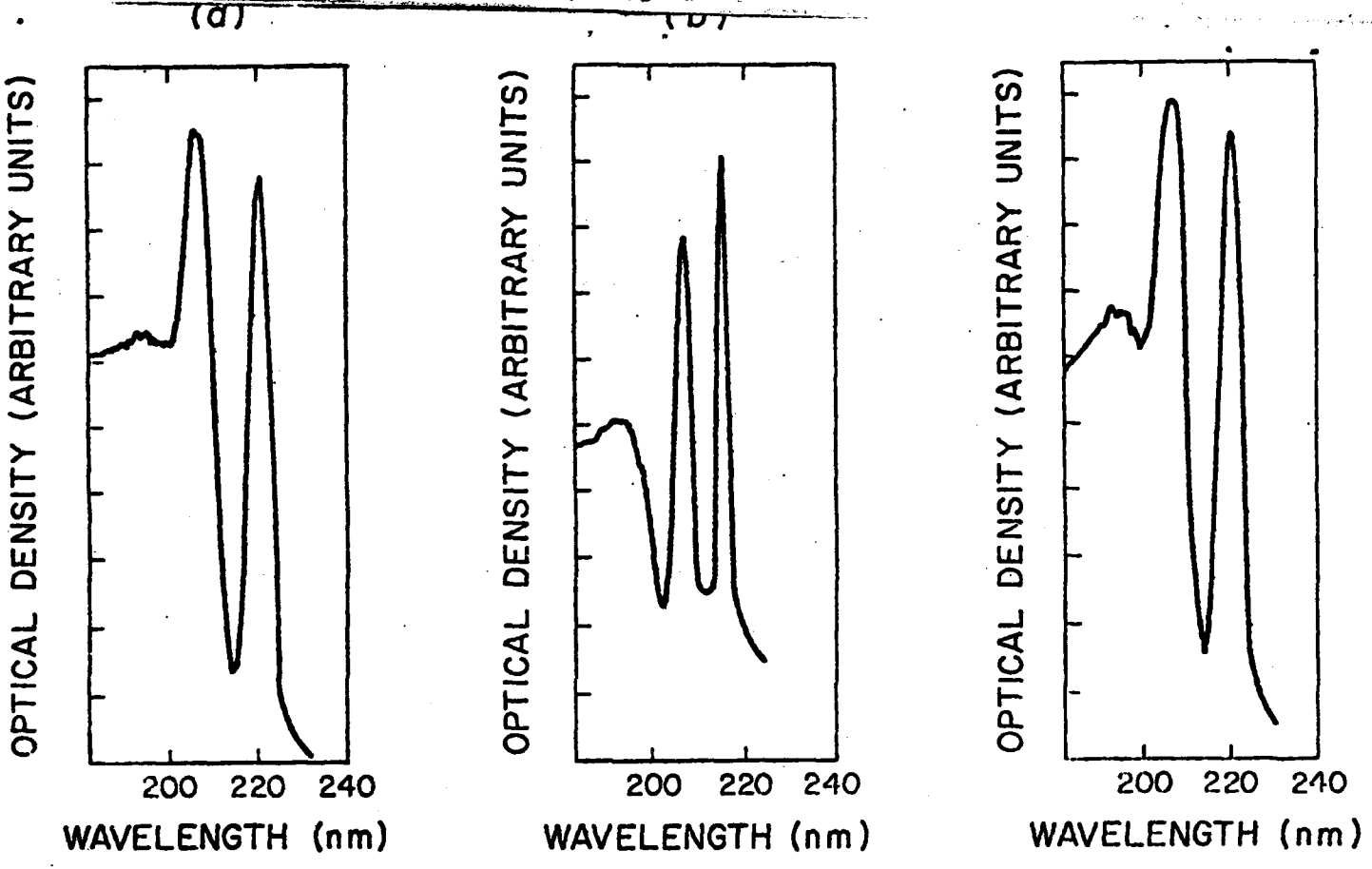

FIG. IV.3--Absorption spectra of thin film at (a) RTBC, (b) LNT and (c) RTAC.

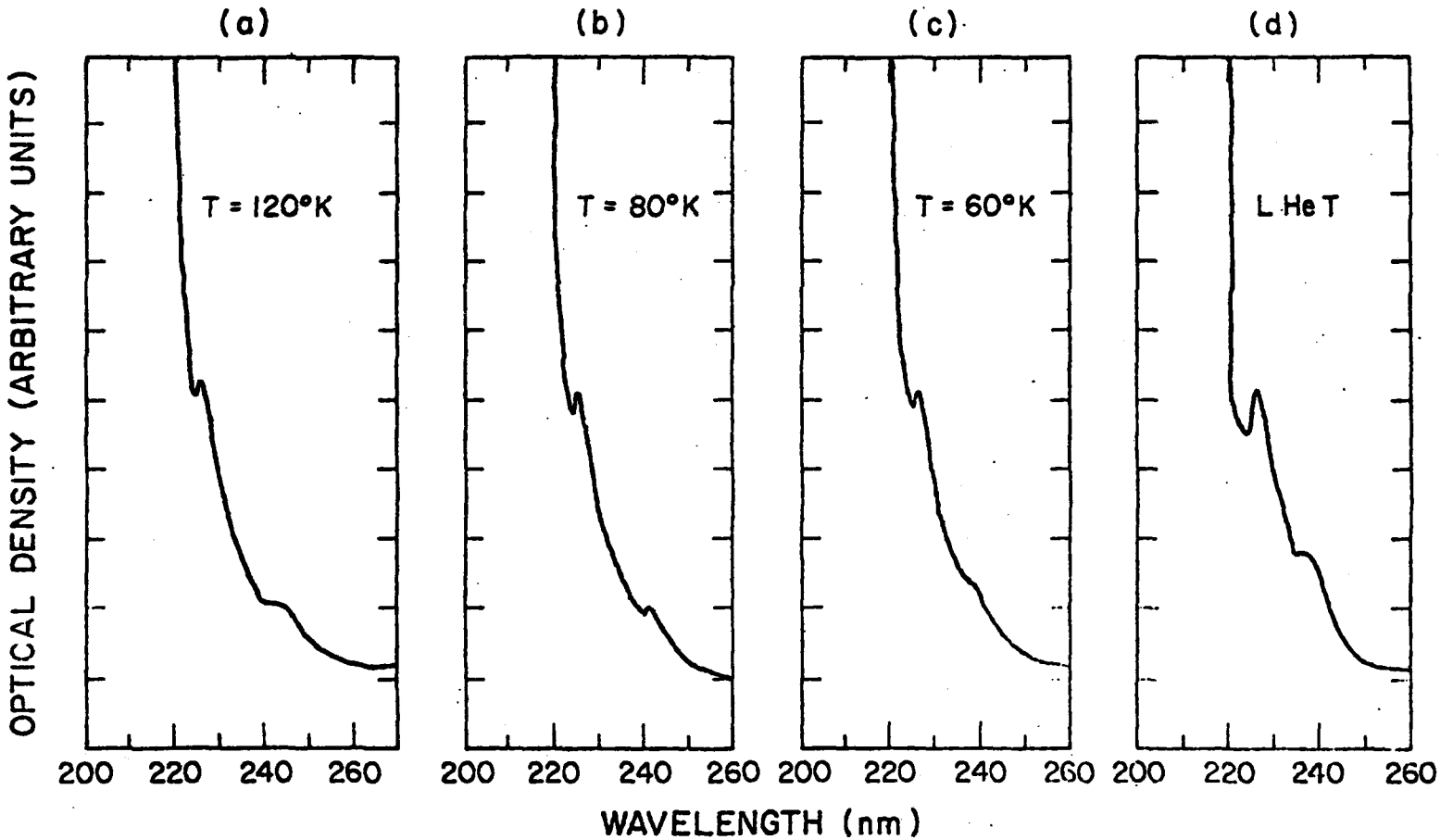

FIG. IV.4--Absorption spectra of bulk single crystal at (a) 120°K, (b) 80°K (c) 60°K and (d) LHeT.

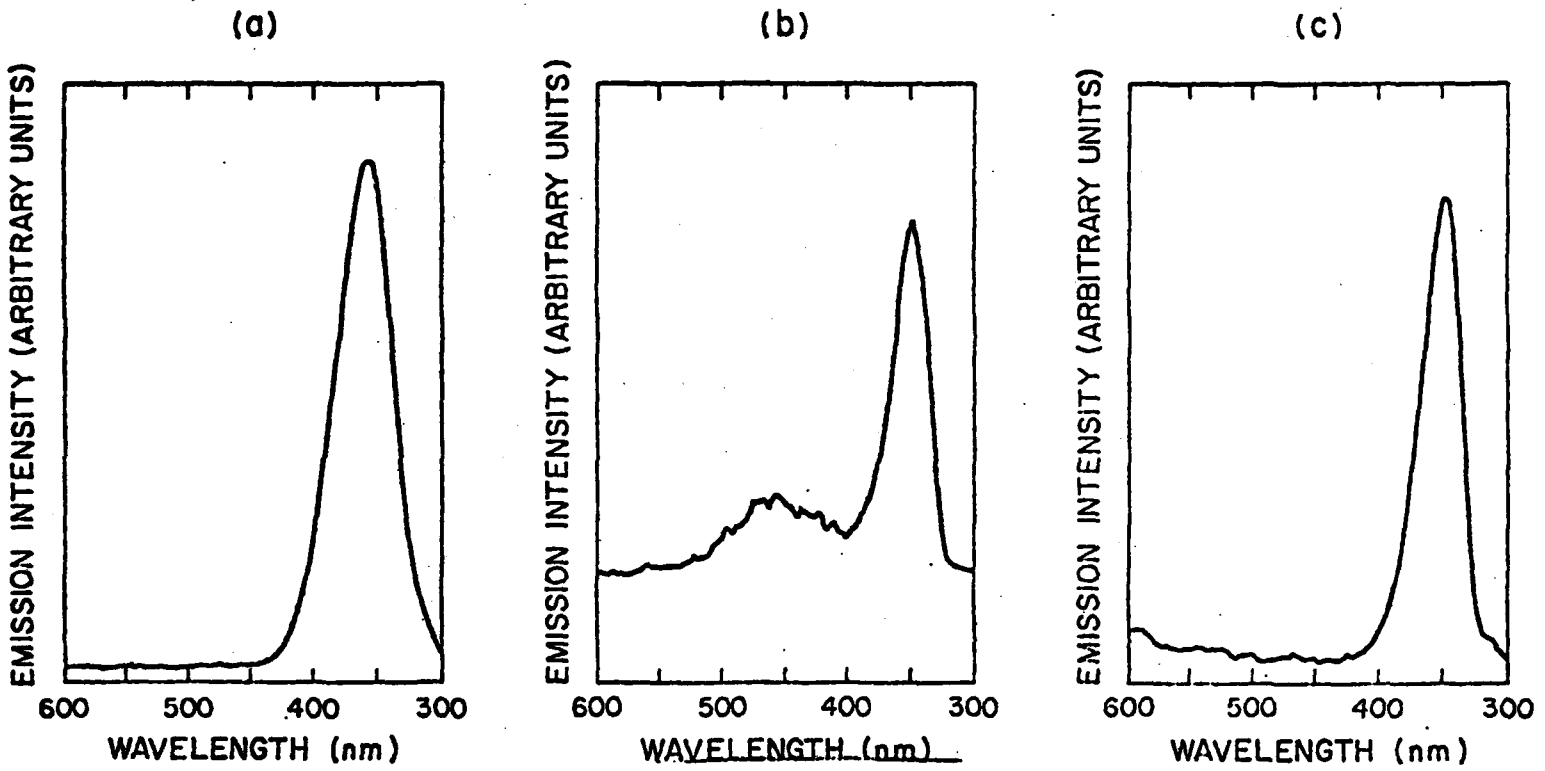

FIG. IV.5--Emission spectra of thin film of CsI at (a) LNT for λ_{ex} = 215 nm, (b) LNT for λ_{ex} = 235 nm and (c) RTAC for λ_{ex} = 235 nm.

was not observed at room temperature before cooling (RTBC) for excitation at the absorption edge or the excitonic region. Excitation in the excitonic region at LNT, however, produced an emission that peaked at 350 nm while excitation in the fundamental absorption edge produced a weak luminescence at 430 nm in addition to that at 350 nm . When the sample was warmed to RT, the crystal exhibited a room temperature after cooling (RTAC) luminescence which peaked at 350 nm .

Figure IV.6 shows excitation spectra for thin films for ultra-violet emission at 350 nm at LNT and RTAC. At LNT, the excitation spectra has a strong peak at 217 nm and a smaller one at 235 nm while the RTAC spectrum has a large peak at 235 nm and a broader one centered at 280 nm .

(b) Bulk single crystals

The bulk single crystals of pure CsI exhibited no emission at RTBC but at LNT, (Fig. IV.7a) gave rise to both the ultra-violet (350 nm) and blue (420-430 nm) emissions for excitonic and fundamental absorption edge excitations respectively. RTAC measurement showed an emission that peaked at 440 nm and 540 nm for absorption edge (235 nm) excitation, as shown in Fig. IV.7(b). Excitation spectra (Fig. IV.8a) of the UV-emission at 350 nm peaked at 220 nm with a relatively small contribution at 235 nm while the blue emission (420-430 nm) has an excitation peak (Fig. IV.8b) at 240-250 nm on the long wavelength tail of the fundamental absorption. Figure IV.8(c) and (d) shows the RTAC excitation spectra for emission at 440 and 540 nm, both having an excitation peak at roughly 237 nm .

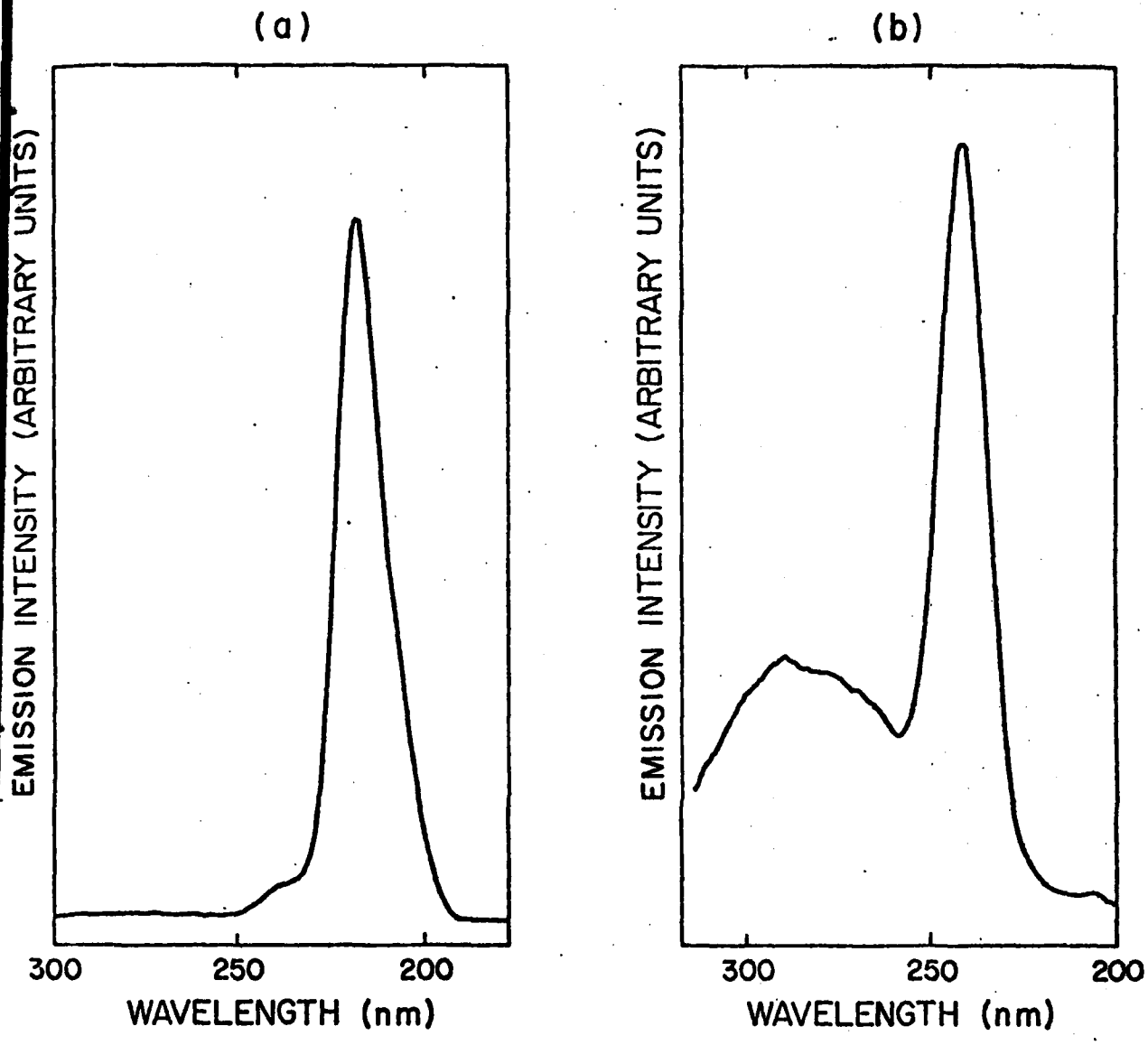

FIG. IV.6--Excitation spectra of thin film of CsI at
(a) LNT for emission at 350 nm
(b) RTAC for emission at 350 nm.

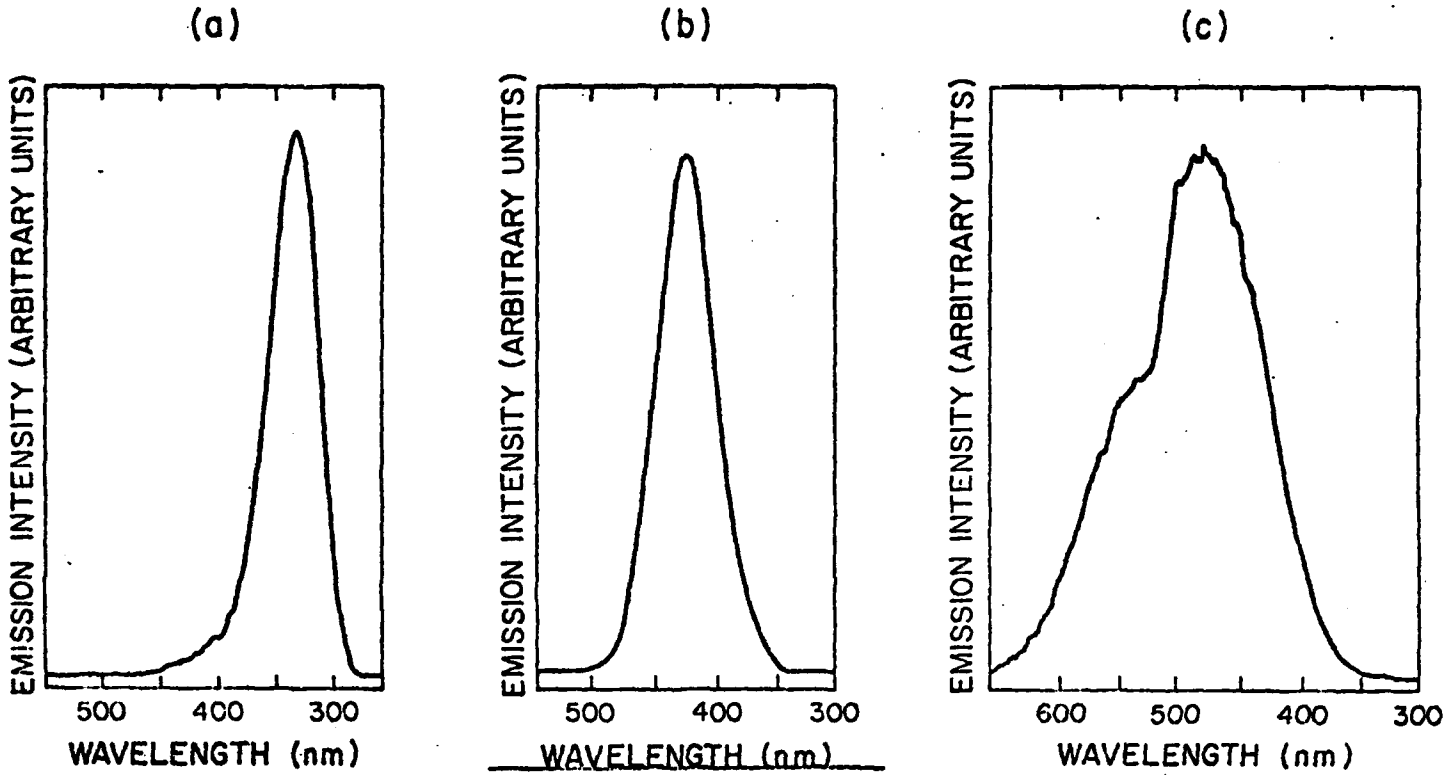

FIG. IV.7--Emission spectra of bulk single crystal of CsI at (a) LNT for excitation at 215 nm (b) LNT for excitation at 235 nm (c) RTAC for excitation at 235 nm.

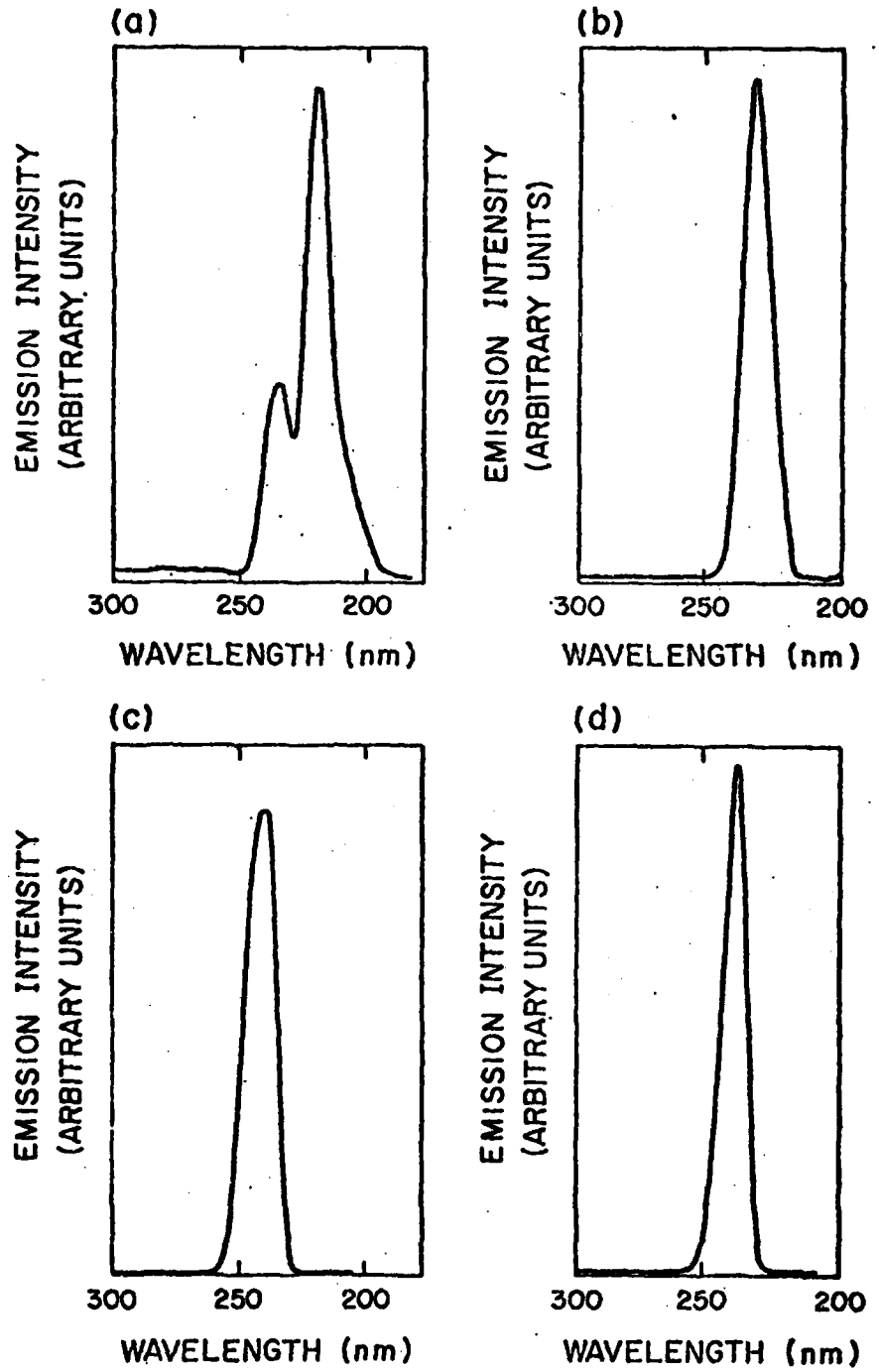

FIG. IV.8--Excitation spectra of bulk single crystal of CsI at
(a) LNT for emission at 350 nm
(b) LNT for emission at 425 nm
(c) RTAC for emission at 470 nm
(d) RTAC for emission at 540 nm.

The absence of luminescence at RTBC for excitation either in the excitonic region or the fundamental absorption edge does not agree with Morgenstern's results[19] who observed emission from his nominally pure CsI samples. From our observations this disagreement might be attributed to the presence in his crystals of trace impurities whose importance as a source of luminescence was not appreciated at the time. Other authors[18,20,21] observed RTBC luminescence in pure CsI but after they had either been plastically deformed or quenched to RT from high temperatures.

The ultra-violet luminescence at 350 nm observed at LNT in both thin films and bulk single crystals of pure CsI for excitonic excitations is in agreement with other studies.[15] That the corresponding excitation spectrum peaks at 217-220 nm in the excitonic region (with humps at (235-237 nm) supports our contention that this luminescence is due to electron-hole radiative recombinations at sites created by cooling and exposure to nonionizing ultra-violet light. Absorption edge excitation (234 nm) at LNT gives strong luminescence at 425 nm for the bulk single crystals and both a weak luminescence at 430 nm and strong one at 350 nm for the thin films. The excitation spectrum of the blue luminescence (425-430 nm) peaks at 237 nm.

When these samples warmed from LNT to RT, they exhibited luminescence for absorption edge excitation which was not observed at RTBC. This RTAC luminescence for the thin films might be tentatively explained as being from radiative electron-hole recombination at sites created by (1) cooling or temperature cycling and (2) exposure to non-ionizing UV-radiation at LNT. Figure IV.9 shows that the intensity of the

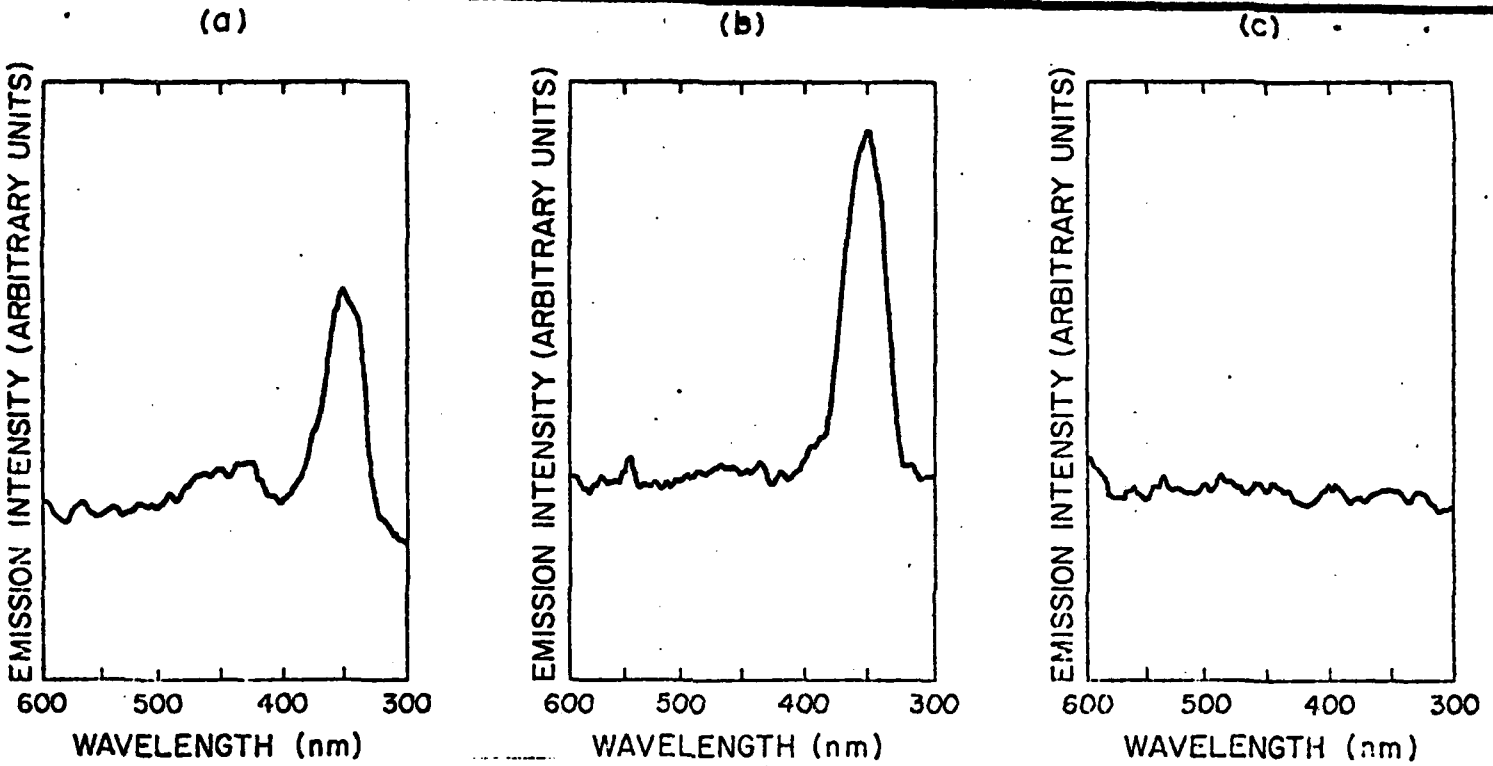

FIG. IV.9--Emission spectra of thin films of CsI under different thermal treatments
(a) RTAC emission of sample without irradiation at LNT
(b) RTAC emission of sample with irradiation at LNT
(c) RTBC emission of sample which previously showed RTAC luminescence and then annealed again.
All excitations at 235 nm.

RTAC luminescence at 350 nm for an unirradiated sample at LNT is less than that of a sample which had been exposed to non-ionizing UV-radiation at LNT. This suggests that the center responsible for the RTAC luminescence is created by temperature cycling (cooling) and apparently further enhanced by irradiation with non-ionizing ultra violet light at LNT. As one explanation, the disappearance of RT luminescence from thin films through annealing might indicate that the center which is responsible for the RTAC luminescence is associated with structural lattice defects (perhaps of the vacancy type) in the crystals.

Using the model developed by Bassani and Inchauspe,[24] we calculated the positions of the α and β - bands in CsI to be respectively located at (235 ± 5 nm) and (224 ± 2 nm). Pauling's theoretical values of ionic polarizability[25] and the position of the F-band given by Lynch et al.[26] have been used. See Appendix I.

The ratio of the position of the β-band relative to the first exciton absorption band and that of the α-band is in agreement with those calculated by Bassani and Inchauspe for some alkali halides crystals.[24]

Therefore, as another explanation, the peaking of the excitation spectra at RTAC of the ultraviolet and both the blue and yellow luminescence at 235 nm (the position of the α-band in CsI) and a small contribution from the 280 nm band suggests that the RTAC luminescence observed in CsI is probably due to radiative recombinations of excitons trapped at halogen-ion vacancies and electron excess-centers which were produced by cooling and exposure to non-ionizing UV-radiation at LNT.

The following discussion concerns measurements between LNT and LHeT and were taken exclusively on bulk single crystals.

The low temperature luminescence of relatively strain and defect free and pure CsI is excitable in both the excitonic and fundamental absorption bands. Excitations in the excitonic region give rise to three emission bands at 300 nm, 350 nm and 430 nm respectively at temperatures below 25°K, the 300 nm band presumably being that measured by Lamatsch et al.[15] At 25°K and above, the 300 nm and the 430 nm emission bands were unmeasurable for excitonic excitations but the 350 nm emission intensity correspondingly increases and stays constant up to 77° (LNT) after which at 90°K the intensity drops considerably to about 10-15% of its value at LNT. At about 150°K and above this 350 nm emission band was unmeasurable for excitonic excitation. The evolution of the emission intensities of the 300 nm, 350 nm and 430 nm for excitonic excitations as a function of temperature is shown in Fig. IV.10(a). Figure IV.10(b) gives the excitation spectra for these emissions at 10°K.

Figure IV.11(a) and (b) shows the evolution of the emission spectra of a bulk single crystal of CsI as a function of temperature for excitations at the α-band (235 nm) and the β-band (225 nm). Between 20°K and 77°K, the emission intensities of the 430 nm and 320 nm bands are relatively constant for β-band excitations as shown in Fig. IV.11(b). For α-band excitation, within this temperature range, the emission intensity of the 430 nm emission band is constant but though the 320 nm emission band has constant emission intensity between 60°K and 77°K and a weaker emission intensity at 35°K, it

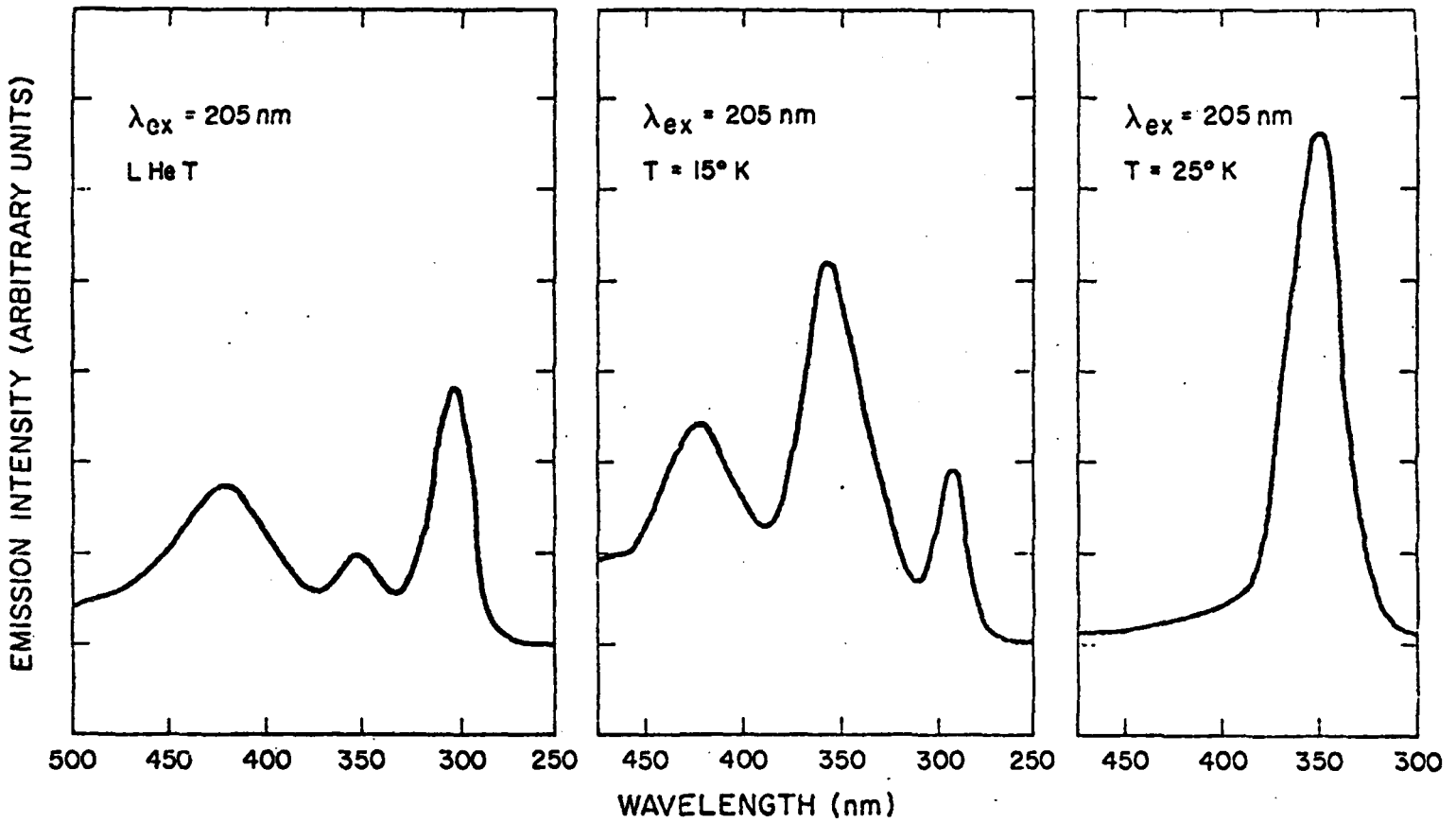

FIG. IV.10(a)--Emission and excitation spectra of bulk single crystal of CsI.
(a) Emission spectra of 300 nm, 350 nm and 430 nm emission for excitonic excitations as a function of temperature.

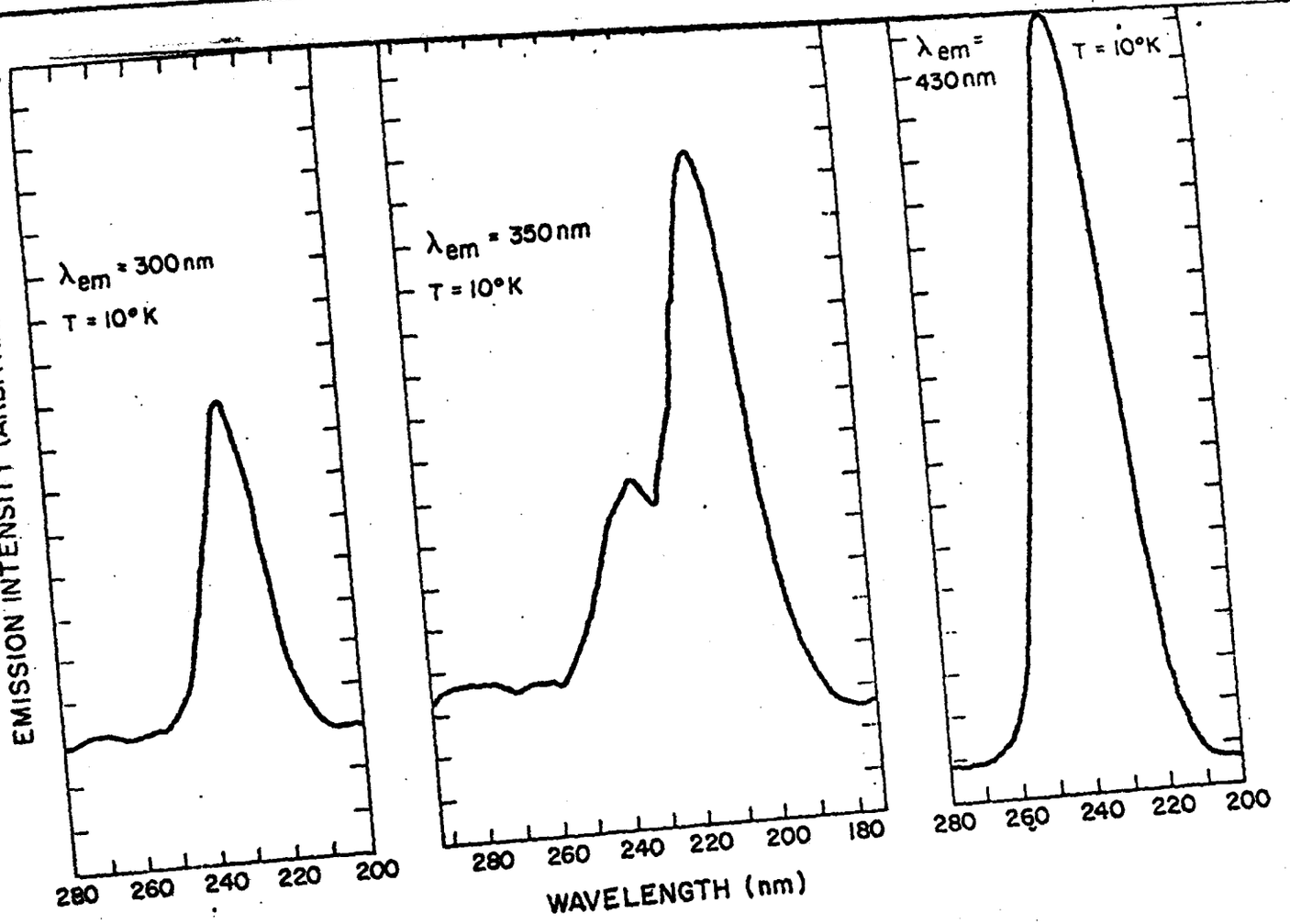

FIG. IV.10(b)--Emission and excitation spectra of bulk single crystal of CsI.
(b) Excitation spectra for these emissions at 10°K.

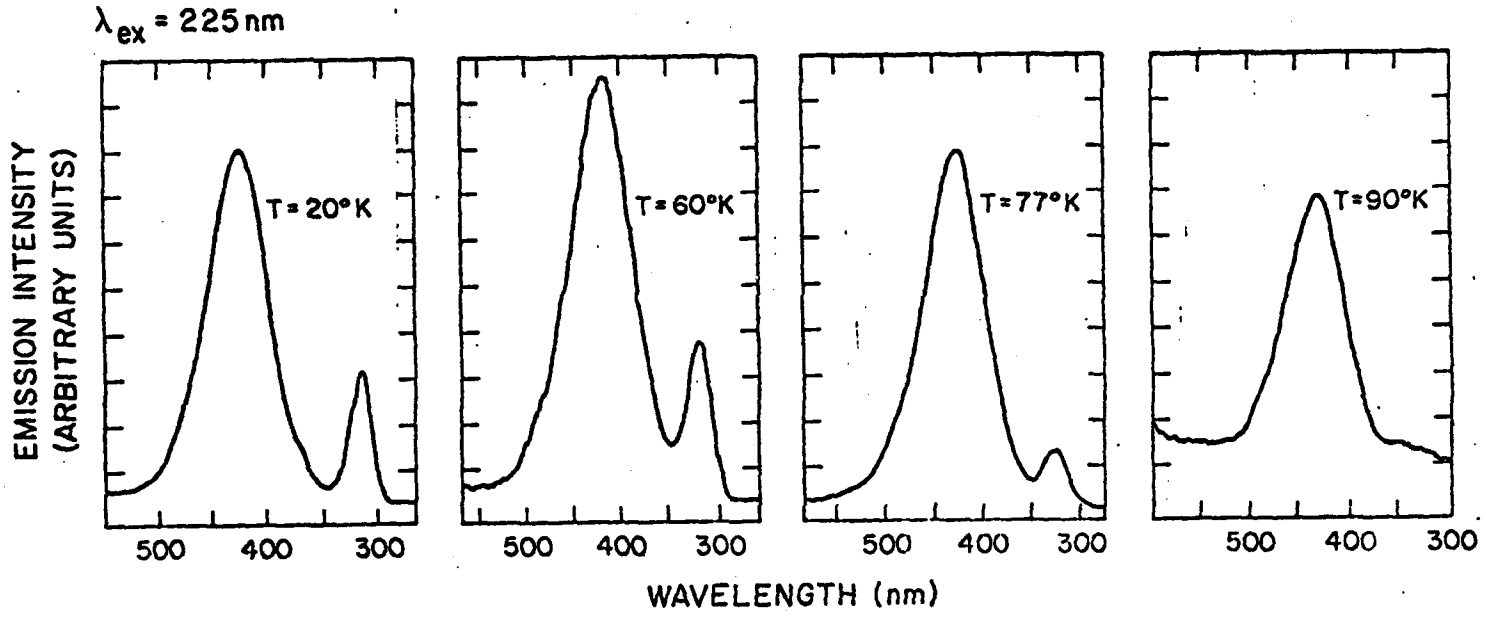

FIG. IV.11(a)--Emission and excitation spectra of bulk single crystals of CsI as a function of temperature.
(a) Emission spectra for α-band excitation.

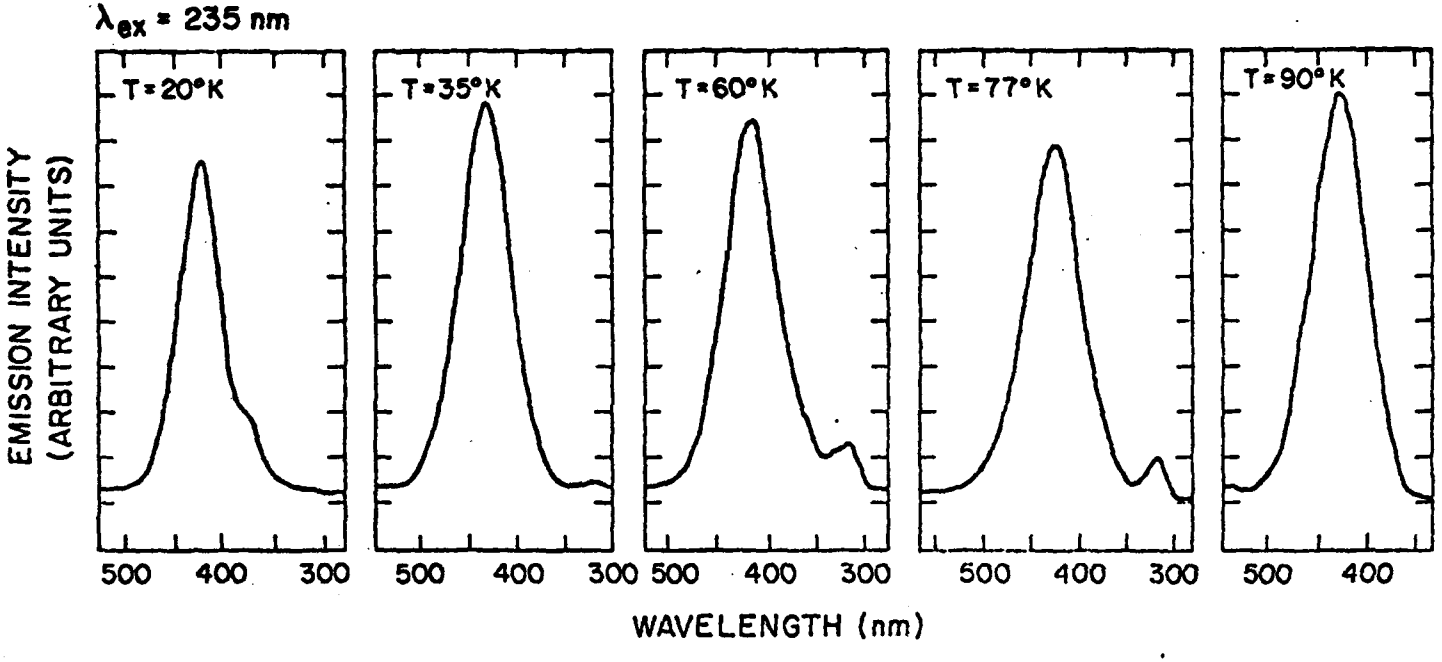

FIG. IV.11(b)--Emission and excitation spectra of bulk single crystals of CsI as a function of temperature.
(b) Emission spectra for β-band excitation.

disappears at 20°K when a new band appears at 380 nm. It is interesting to note that at 90°K, the 320 nm band disappears for excitations in either the α or β-band and the intensity of the 430 nm decreases. Figure IV-11(c) gives the excitation spectra at 20°K.

D. RESULTS: PHOTOLUMINESCENCE FROM STRAINED CsI

1. Optical Absorption

The optical absorption measurements were performed on both thin films and bulk single crystals at room and liquid nitrogen temperatures. Figure IV.12 shows the ultra-violet absorption spectrum of the thin films of strained CsI . The absorption spectra of plastically deformed CsI is also shown in Fig. IV.13.

Thin films: The position of the exciton absorption bands in the strained films are located at 220 nm and 208 nm at RTBC and RTAC while at LNT the 220 nm band shifts to 215 nm and the 208 nm slightly shifted to about 207 nm. This exciton absorption band shift with temperature and strain has been explained by Lynch et al.

The bulk single crystals show shoulders at 225 nm and 237 nm at LNT. There was no structure at RTBC and RTAC.

2. Emission and Excitation

(a) Thin films

Figure IV.14 shows the emission spectra which were measured for thin films (500-2000 Å) of thermally quenched CsI at RTBC and other temperatures. RTBC luminescnece is only excitable at the fundamental

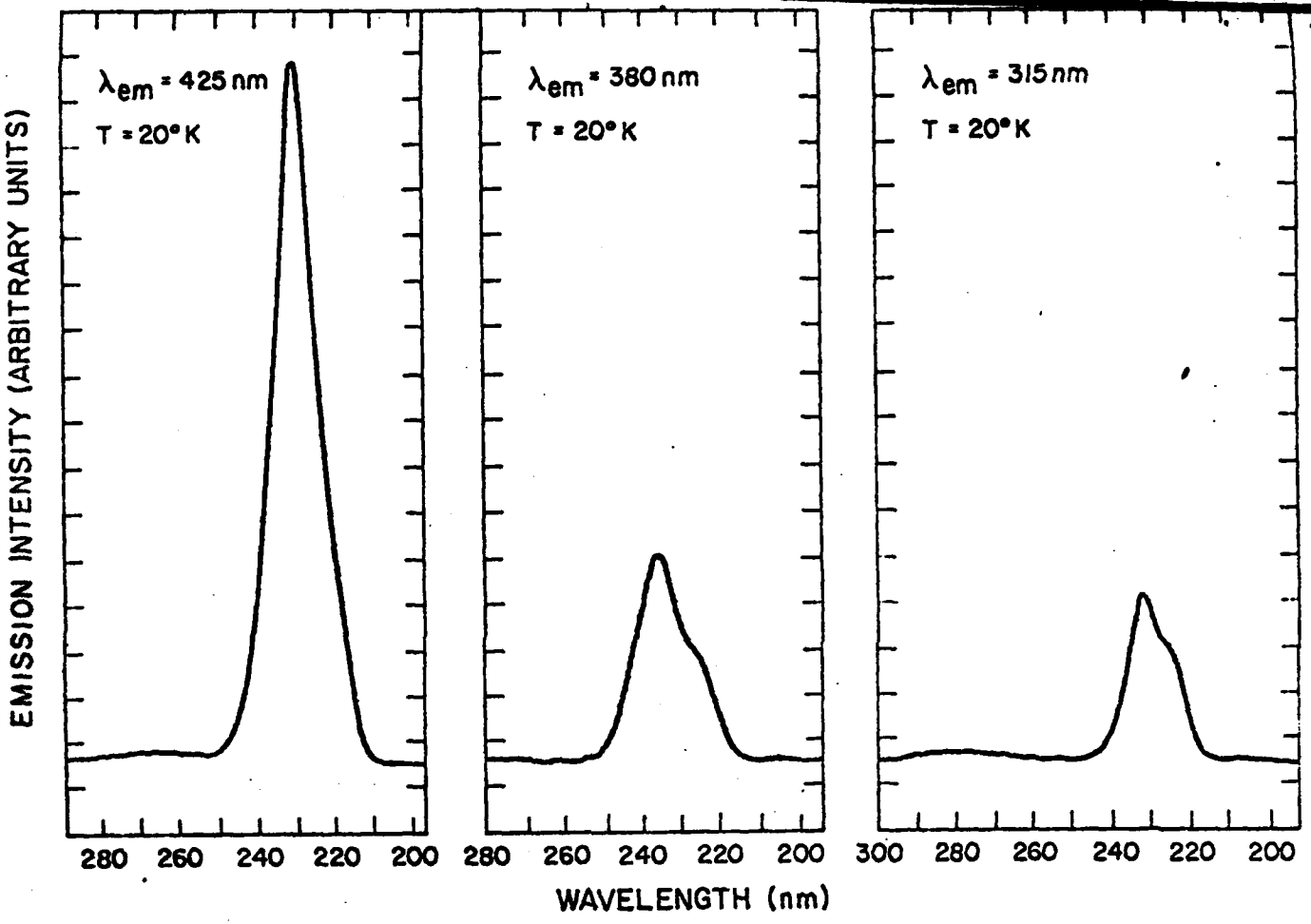

FIG. IV.11(c)--Emission and excitation spectra of bulk single crystals of CsI as a function of temperature.
(c) Excitation spectra at 20°K.

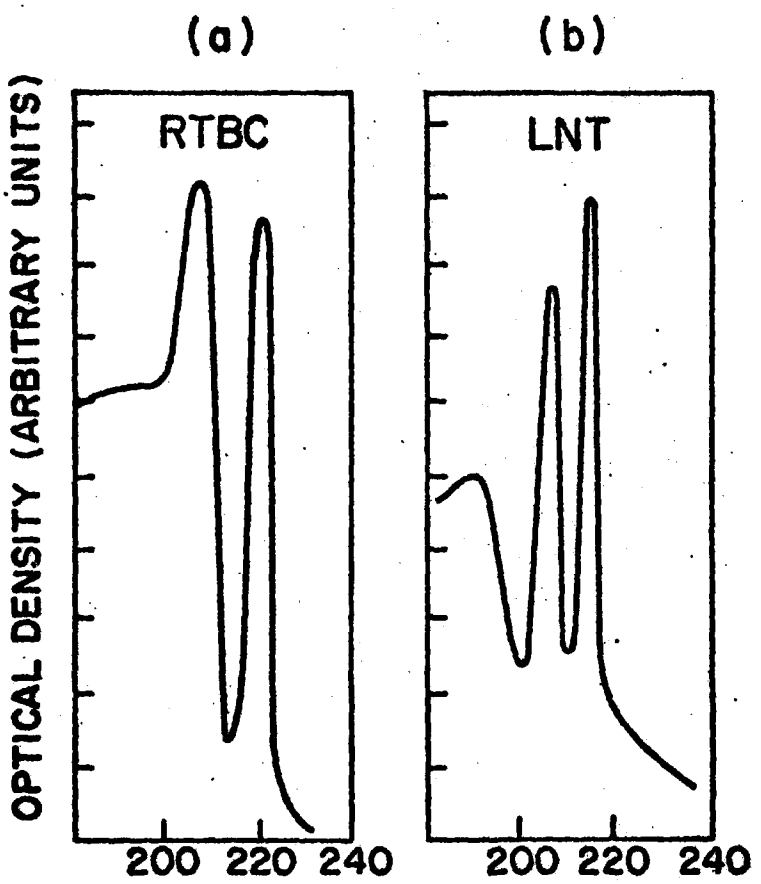

FIG. IV.12--UV-absorption spectra of the thin films of strained CsI

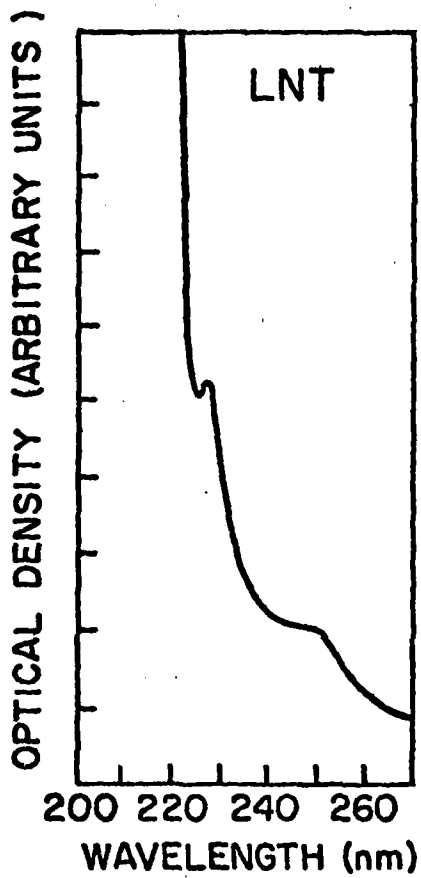

FIG. IV.13--UV-absorption spectrum of plastically deformed CsI .

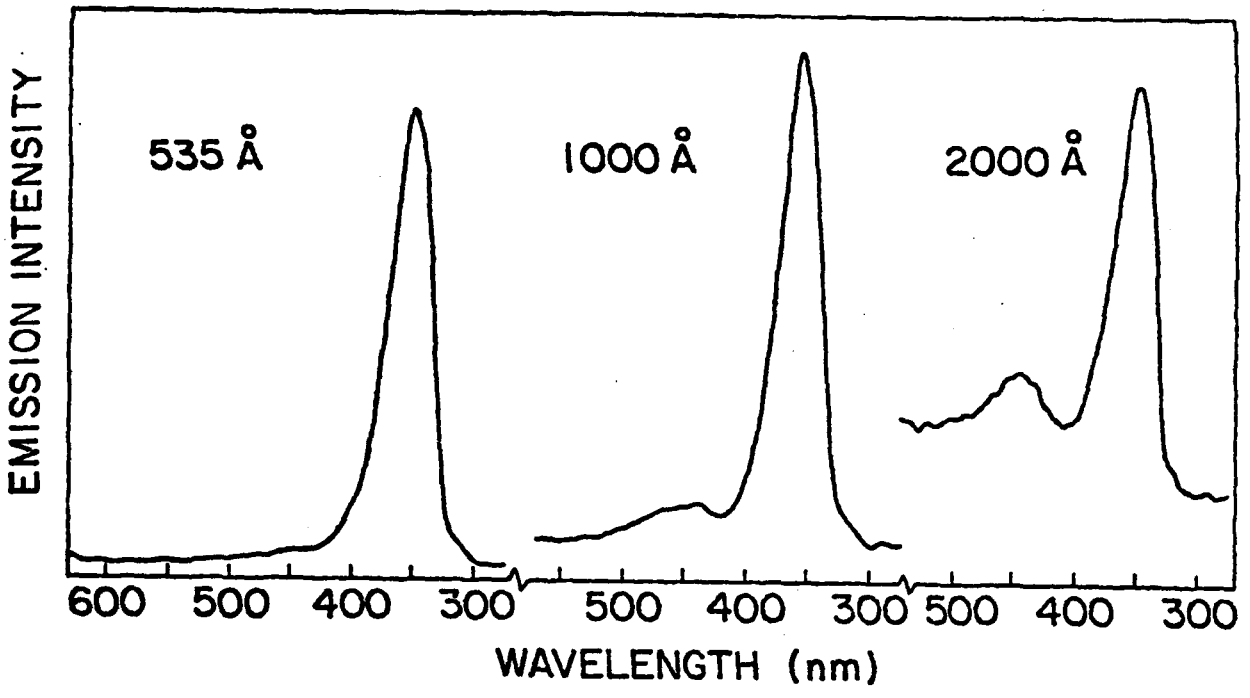

FIG. IV.14(a)--Emission spectra of the thin films of strained CsI at LNT.

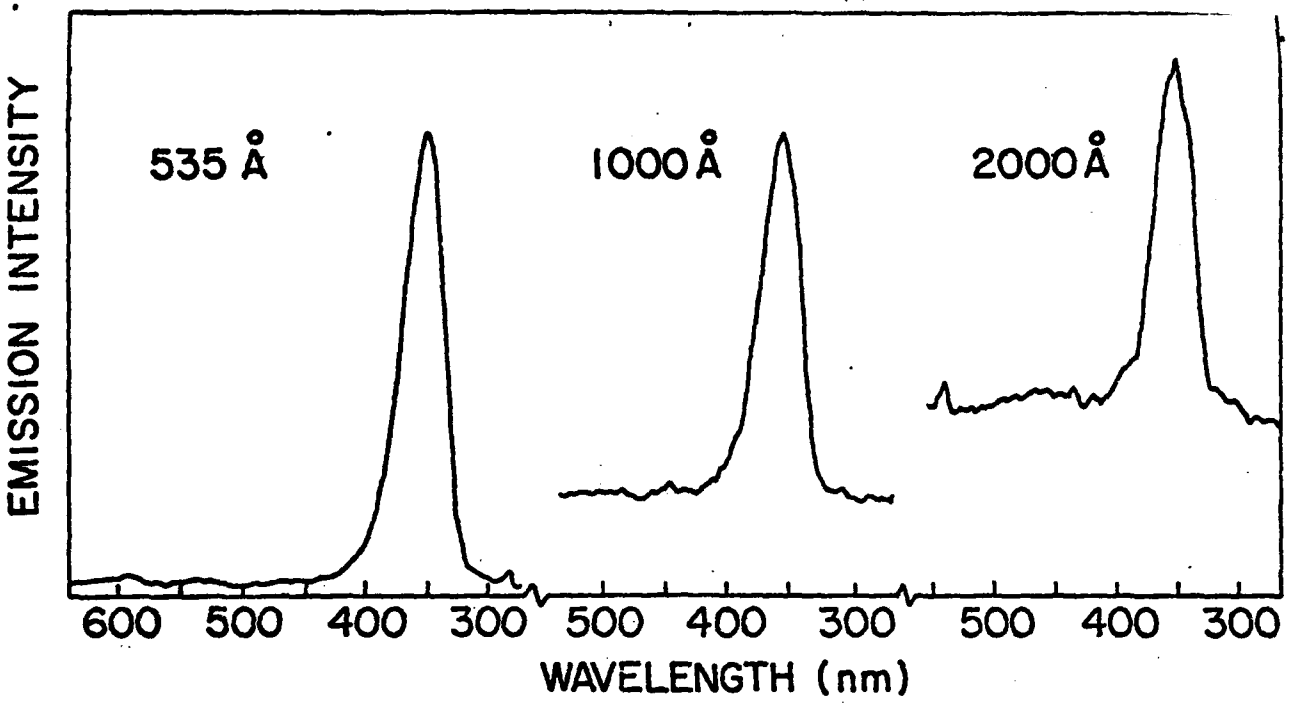

FIG. IV.14(b)--Emission spectra of the thin films of strained CsI at RTBC.

absorption edge, excitonic excitations give no RTBC luminescence. Besides the 350 nm emission, is the broad band luminescence centered at 430 nm though weaker than the 350 nm peak. At LNT and RTAC, luminescence measurements are identical to the pure sample (Section II) except that the strained sample luminescence is more intense.

The excitation spectra for the strained samples shown in Fig. IV.15 are identical to those of the unstrained samples.

(b) Bulk single crystals

Figure IV.16, shows the emission spectra of a plastically deformed CsI with 4% strain for various excitation energies at RTBC. For all excitations, the emission peaks at 440 nm though with varying intensities. At LNT, excitations from the excitonic through the long wave length (200-250 nm) show emission peaks at 320 nm, 350 nm and 430 nm as shown in Figs. IV.17(a) and IV.17(b). As at RTBC, no emission for excitonic excitations occur. The excitation spectra of the observed emission spectra at RTBC, LNT and RTAC are shown in Fig. IV.18.

Discussion:

At room temperature excitation at the so-called α(235 nm) and β-(225 nm) bands did not give rise to emission while excitations within (237.5-250 nm) gave emission bands at 440 nm. This 440 nm emission band at room temperature can be tentatively associated with radiative recombinations of free electrons and holes at structural lattice defects or iodine-ion vacancy created by plastic deformation. This contention

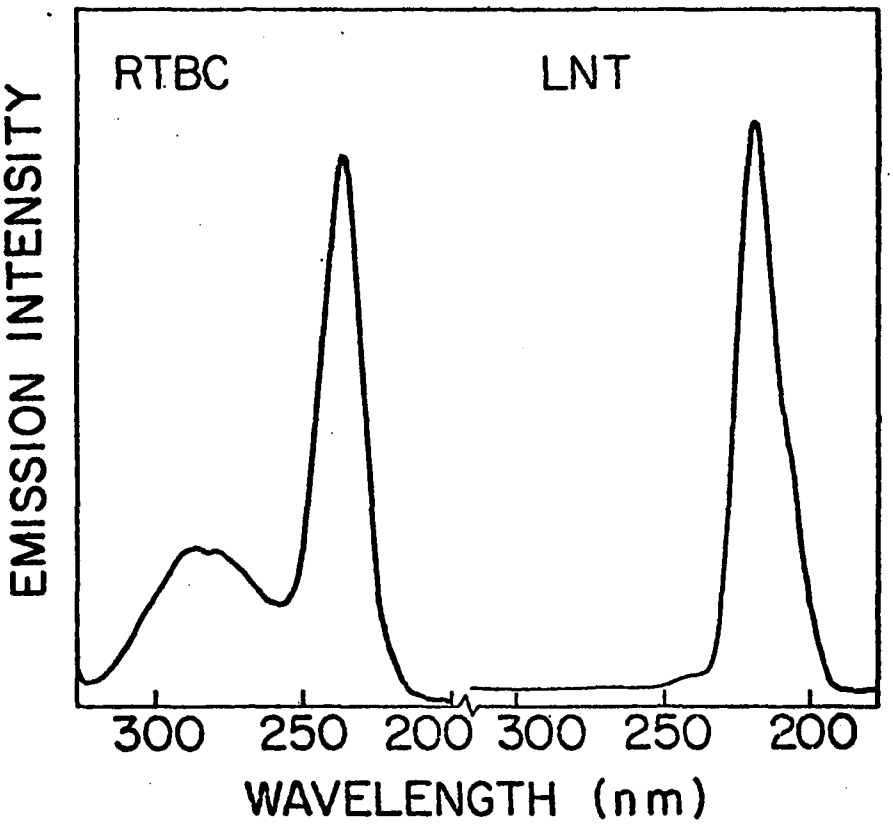

FIG. IV.15--Excitation spectrum for the UV-emission from strained CsI.

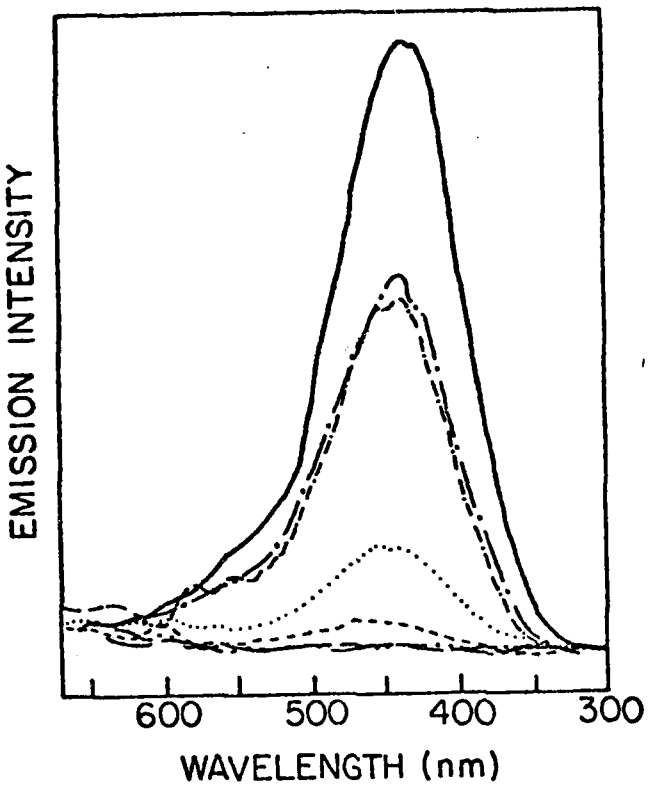

FIG. IV.16--Emission spectra of 4% strained pure CsI as a function of excitation wavelength at RTBC

-·-·-·- Emission spectrum for λ_{ex} = 250 nm
——— Emission spectrum for λ_{ex} = 245 nm
—·—·— Emission spectrum for λ_{ex} = 240 nm
- - - - - - Emission spectrum for λ_{ex} = 235 nm
— — — Emission spectrum for λ_{ex} = 230 nm
—··—·· Emission spectrum for λ_{ex} = 225 nm
····· Emission spectrum for λ_{ex} = 237.5 nm

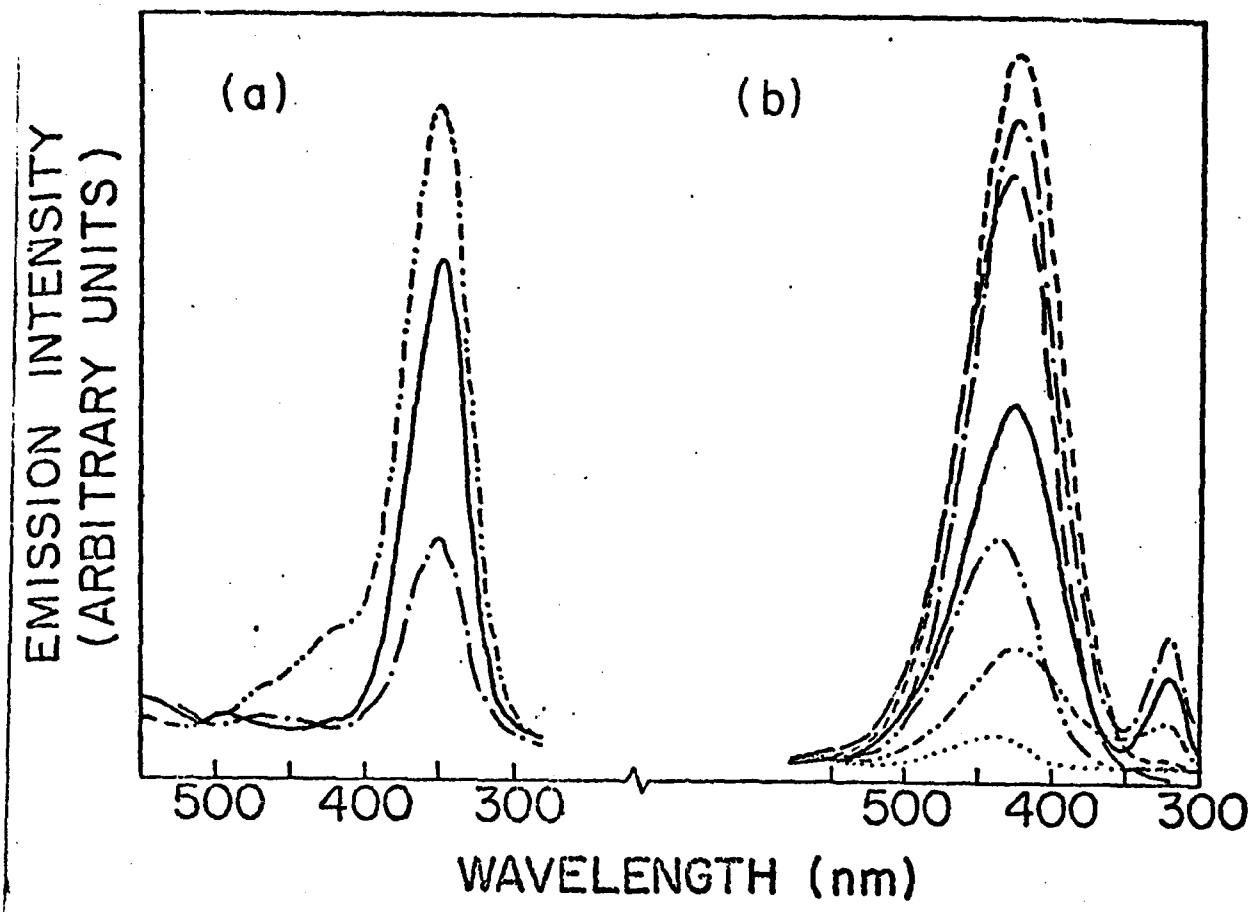

FIG. IV.17--Emission spectra of 4% strained pure CsI as a function of excitation wavelength at LNT.

—·—·— Emission spectrum for λ_{ex} = 215 nm
——— Emission spectrum for λ_{ex} = 210 nm
—·—·— Emission spectrum for λ_{ex} = 205 nm

---------- Emission spectrum for λ_{ex} = 220 nm
——— Emission spectrum for λ_{ex} = 225 nm
—·—·— Emission spectrum for λ_{ex} = 230 nm
— — — — Emission spectrum for λ_{ex} = 235 nm
— — — Emission spectrum for λ_{ex} = 240 nm
—·—··— Emission spectrum for λ_{ex} = 245 nm
..... Emission spectrum for λ_{ex} = 250 nm

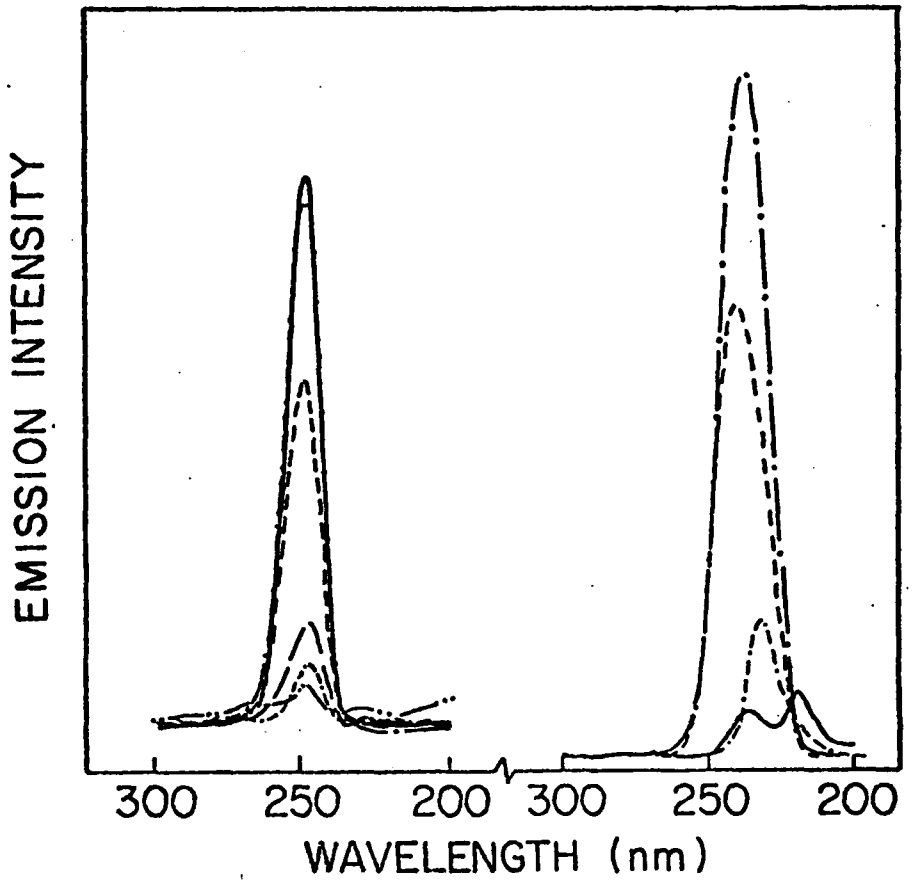

FIG. IV.18--Excitation spectra for emission in 4% strained pure CsI at (left) RTBC and (right) LNT.

RTBC

- – · – – · – – Excitation spectrum for 350 nm emission
- ———— Excitation spectrum for 440 nm emission
- — · — · — Excitation spectrum for 450 nm emission
- – – – – – – Excitation spectrum for 480 nm emission
- — — — — — Excitation spectrum for 550 nm emission
- — ·· — ·· — Excitation spectrum for 600 nm emission

LNT

- – – · – – · – – Excitation spectrum for 320 nm emission
- ———— Excitation spectrum for 350 nm emission
- — · — · — Excitation spectrum for 430 nm emission
- – – – – – – Excitation spectrum for 450 nm emission

is supported by the fact that at LNT, the 440 nm band is efficiently excited in the so-called α-band and a relatively weaker emission at 440 nm due to the β-band also. The long wavelength excitation produced weaker emission bands. Thus the 440 nm emission band at LNT is probably due to radiative recombinations of excitons bound to negative ion vacancies created by plastic deformation.

Besides the 440 nm emission band at LNT, excitation in the range (220-230 nm) gave an ultra-violet emission band at 320 nm. The excitation spectrum of the 320 nm emission band peaks at 230 nm where it is efficiently excited. This ultra-violet emission band is probably due to radiative transitions of excitons in metastable states. It is interesting to note that excitation in the α-band (235 nm) did not give rise to this emission band at 320 nm which suggests that the emission is not due to radiative recombinations of excitons bound to negative-ion (iodine-ion) vacancies, but due to transitions from some energy levels lying between those of the β- and α-levels.

As usual, the 350 nm emission band is excitable and has its excitation spectrum peaking within the excitonic region, which suggests the associations of this emission band with radiative recombination of electron-hole pairs at low temperatures.

However, we observed an interesting effect - the sudden drop in intensities of the 440 nm and 320 nm as we varied the excitation wavelength. At RTBC where only the 440 nm band is observable, its intensity suddenly dropped by a factor of 10 in going from 240 nm excitation to 235 nm excitation. Figure IV.16 shows this sudden transition. From Fig. IV.16, curve 7 shows emission for excitation at 237.5 nm which

is about 1/5 of the intensity of that due to 240 nm excitation. This flash-like (or step-like) dependence of the emission intensity on the exciting wavelength at RTBC is probably due to the fact that the 445 nm emission results from radiative recombinations of free electron-hole pairs (created by absorption of light in the long wavelength tail of the fundamental absorption band) which are loosely bound to the iodine-ion vacancies rather than from excitons tightly bound to iodine-ion vacancies at low temperatures. At LNT, Fig. IV.17 we observed the same flash-like dependence of emission intensity on the exciting wavelength which in this case is probably due to tightly (rather than loosely) bound excitons to the iodine-ion vacancies, because the emission band is most efficiently excited at the α-band (235 nm) and its intensity dropped by an order of magnitude in the range (235 ± 15 nm). Figure IV.19 shows the plot of the emission intensity of the 440 nm emission versus the exciting wavelength.

We therefore believe that the 245 nm band which gave rise to the single emission band at 445 nm observed at RTBC is the α-band whose shift from its low temperature value of 235 nm is probably due to plastic deformation. Also the three emission bands at 440 nm, 350 nm and 320 nm observed at LNT arise from three different centers! The 440 nm emission is due to radiative recombination of excitons bound to the iodine-ion vacancies while the 350 nm emission is due to radiative recombinations of electron-hole pairs and the 320 nm emission band is probably due to radiative recombinations of excitons in metastable states. Consequently the room temperature luminescence is probably

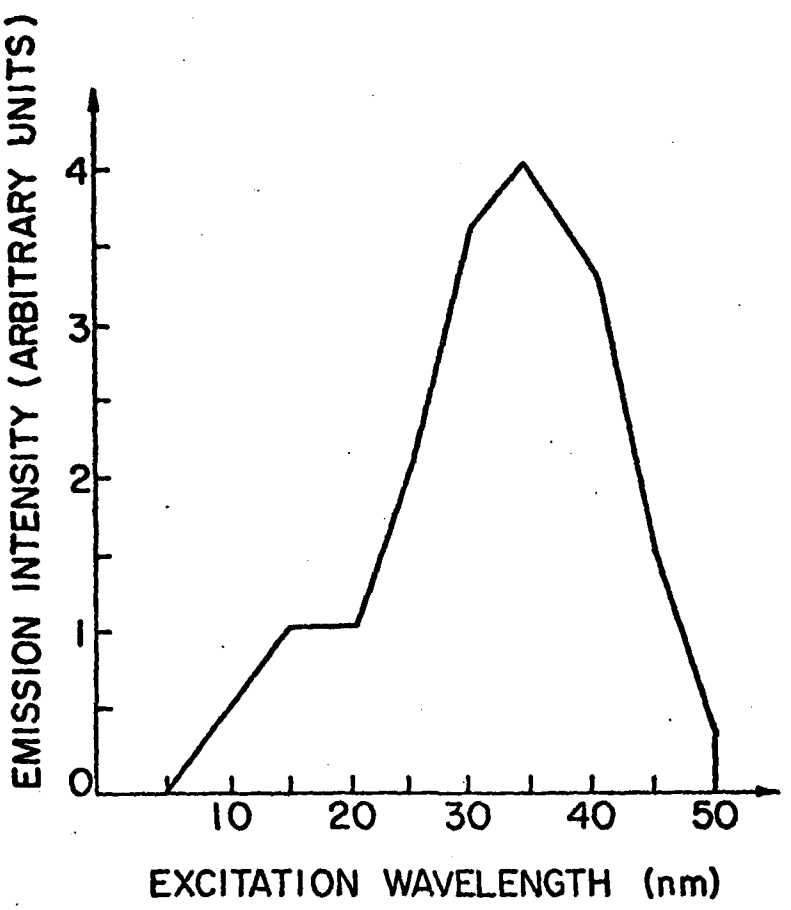

FIG. IV.19--Emission intensity of the 440 nm band versus the exciting wavelength.

due to transfer of energy from the centers responsible for the 350 nm and 320 nm emission by non-radiative transitions at high temperatures.

Except at RTBC, when the plastically deformed CsI luminescence, an effect which was not observed in the pure material of CsI at RTBC, all other luminescent properties are almost identical at low temperatures. The essential difference between the pure and strained CsI is that the blue luminescence observed at LNT is located at 440 nm instead of 430 nm in the pure sample and that strained samples showed more intense emission. The fact that the strained sample gave emission at RTBC at 440 nm, also the peak of the RTAC emission observed in pure sample of CsI supports the contention that cooling plastically deforms CsI . Figures IV.16 and IV.8(b) compare this situation.

CHAPTER V

COLOR CENTER AND ELECTRON SPIN RESONANCE STUDIES OF PURE CsI

A. INTRODUCTION

In this chapter, the data on the infra-red absorption (color centers) and electron spin resonance studies of pure CsI are presented and discussed. In the first section, general information on the study of the color centers in alkali halides with emphasis on CsI is discussed and the observed data on CsI analyzed. The second section however, contains the discussion of the electron spin resonance data on pure and thallium activated CsI .

B. COLOR CENTER STUDIES OF PURE CsI

Introduction:

The production of optical absorption bands in the otherwise transparent crystals of the alkali halides dates as far back as 1894, when Goldstein not only darkened alkali halide crystals but also exposed them to cathode rays to create color centers. The defects thus produced in alkali halides absorb visible or infra-red light, hence the name "Color Center". Since the pioneering work of Goldstein, color centers have been a subject of investigation by many workers.[62-64,66]

The end product of exposing alkali halides to radiations of threshold energy of about 5 eV are the F- and V-centers.[20,21] Excitons, free electrons and holes can also be created during this process.

Other methods of producing these centres include (a) additive coloration by heating in alkali metal vapors; (b) coloration by electrolysis, that is by passing a current between electrodes in contact with the crystal at high temperatures (c) by plastic deformation either at room or lower temperatures and probably by thermal quenching. All these methods have proven to be successful when used to induce color centers into alkali halides except CsI . The only successful attempt to induce color center in CsI was by electrolysis.[62,64] However, we are able to induce color centers in CsI by cooling and exposing it to non-ionizing ultra-violet radiation at room and low temperature. Probably, some authors were unable to produce color centers in CsI because of its elastic properties and crystal structures. From the study of the elastic properties of all alkali halides, some authors were able to show that CsI is the most isotropic (that is least anisotropic) of all alkali halides. Probably this highly isotropic nature of CsI makes it difficult to induce color centers in it even under severe ionizing radiations. Another reason why it has been difficult to induce color centers in CsI is because of its crystal structure which allows only ions of maximum size of 1.04 Å to fit in interstitial positions in this crystal. So because of this limiting factor exposing CsI to ionizing radiations which involve atomic or ionic motion in the lattice will be unable to produce color centers as the ions moved have no place to fit in because of their size that is greater than 1.04 Å and its isotropy. The case of coloring CsI by electrolysis at 460°C is understable since at high temperature (420°C) CsI

changes phase from the body centered to the face centered cubic, a structure which is very simple to color or ionize.

The optical properties of both F and V-centers have been widely studied by many authors.[47-55] The location of the absorption band of F-centers in alkali halides with the NaCl-structure is given by the Mollwo-Ivey empirical formula[65]

$$\lambda_F = 703\ d^{1.84}\ \text{Å}$$

where d is the lattice constant. Recently Dawson and Pooley fitted the observed positions of the F-absorption bands in alkali halides by the empirical formula

$$E_F = (60.5 \pm 9.8)\ a^{-1.81 \pm 0.10}\ \text{eV}$$

for alkali halides with the NaCl-structure and

$$E_F = (190 \pm 41)\ b^{-2.28 + .10}\ \text{eV}$$

for alkali halides with the CsCl-structure. Here a is the lattice constant along the [100] direction and b is also the [100] lattice constant multiplied by $\sqrt{3}$, thus giving an equivalent NaCl unit cell size for equal interionic distances.

Besides the F-bands, there are other absorption bands towards the shorter wavelength side of the F-band called the K and L-bands proposed to be due to excited states of the F-band. Other absorption bands on the long wavelength side of the F-band are called the M- and R-bands proposed to be made of complexes from the combination of two and three F-centers, respectively.[65,67] Another band of interest

s the F′-band, which is an F-center plus an electron. A detailed discussion of these color centers can be found elsewhere.

Of all the V-centers (trapped holes), only the self-trapped hole or V_K-center (Castner and Kanzig) has been widely studied both experimentally[7-9] and theoretically.[10] This center is well understood and its absorption band lies between 400 - 406 nm in the alkali iodides. Most of the low temperature intrinsic luminescence observed in alkali halides with the NaCl-structure has been attributed to the radiative recombination of an electron with a V_K-center, which is the well known "self-trapped exciton" model. At temperatures above 120°K, V_K-center becomes mobile and diffuse throughout the crystal until captured by electron excess centers. The symmetry and the anisotropic behavior of V_K-centers can be studied by taking polarized luminescence and electron spin resonance measurements respectively.

Experimental Procedure:

The experimental procedure used in the course of this work has been discussed in Chapter III except additional irradiation studies which involved exposing CsI sample to non-ionizing ultra-violet radiation for several hours at both room and low temperatures. This irradiation process was accomplished by exposing CsI to non-ionizing UV-radiation from a deuterium lamp along the (010) face of the sample for several hours at room and low temperatures.

Three types of measurements were taken when:

(a) The sample was exposed to UV-light at RTBC for about one hour or longer. Absorption measurements were taken at RTBC, LNI and RTAC. The UV light was on all the time.

(b) Absorption measurements were taken for a sample that was not irradiated at RTBC but at LNT and RTAC.

(c) Absorption measurements were taken on a sample that had been irradiated for about 4 hours at LNT but with the UV-light source off during measurements.

The results of these additional irradiation studies aimed at producing color centers in CsI using non-ionizing ultra-violet radiation are presented and discussed below. Figures V.1 through V. show the absorption spectra in the sequence stated above.

Results:

Figure V.1(a)-(d) show the infra-red absorption spectra of CsI at RTBC, LNT and RTAC when exposed to non-ionizing UV-radiation at all temperatures. The well resolved band centered at about 1120 nm (X-band) can not be assigned to the so-called M-band in CsI because other authors observed this M-band at 1185 nm in their colored CsI crystals. The shift is probably due to the crystal's treatment. However, when the sample is allowed to warm up (with the UV-light still on) the so-called X-band disappears and a weak band centered at 830 nm appears as shown in Fig. V.1(b). But when this sample is cooled to LNT again, infra-red absorption measurements showed the X-band and a strong 820 nm band at LNT as shown in Fig. V.1(c). Upon warming again, the X-band disappears and the 830 nm band still persists but weak. After about 15 minutes of cooling and irradiation, the hugh structure that centered around 1100 nm is reduced in intensity by a factor of 3 but other bands appear at 870 nm, 810 nm and 740 nm as shown in Fig. V.1(d). It is interesting to note that

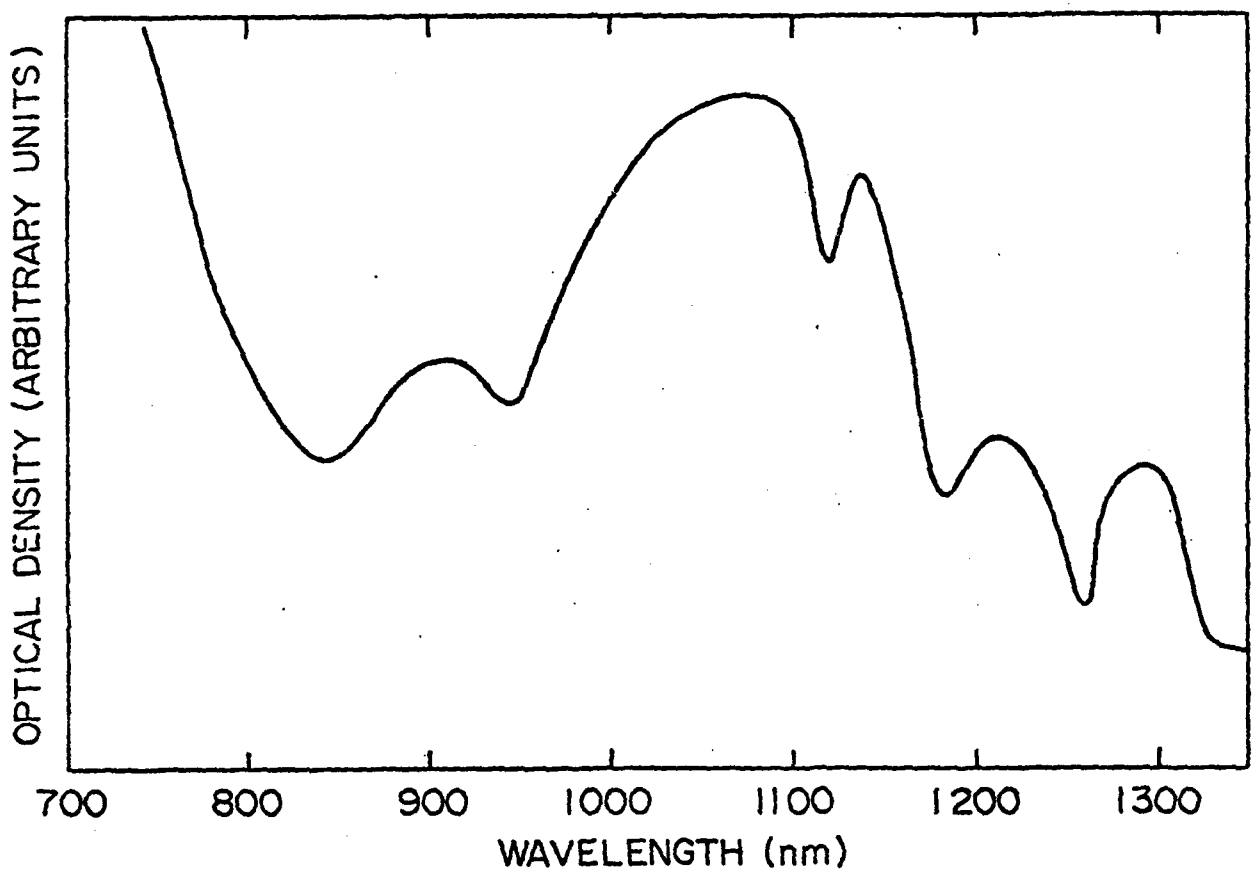

FIG. V.1(a)--Infra-red absorption spectra of pure CsI , when exposed to UV-light along the (010) direction. (a) at LNT.

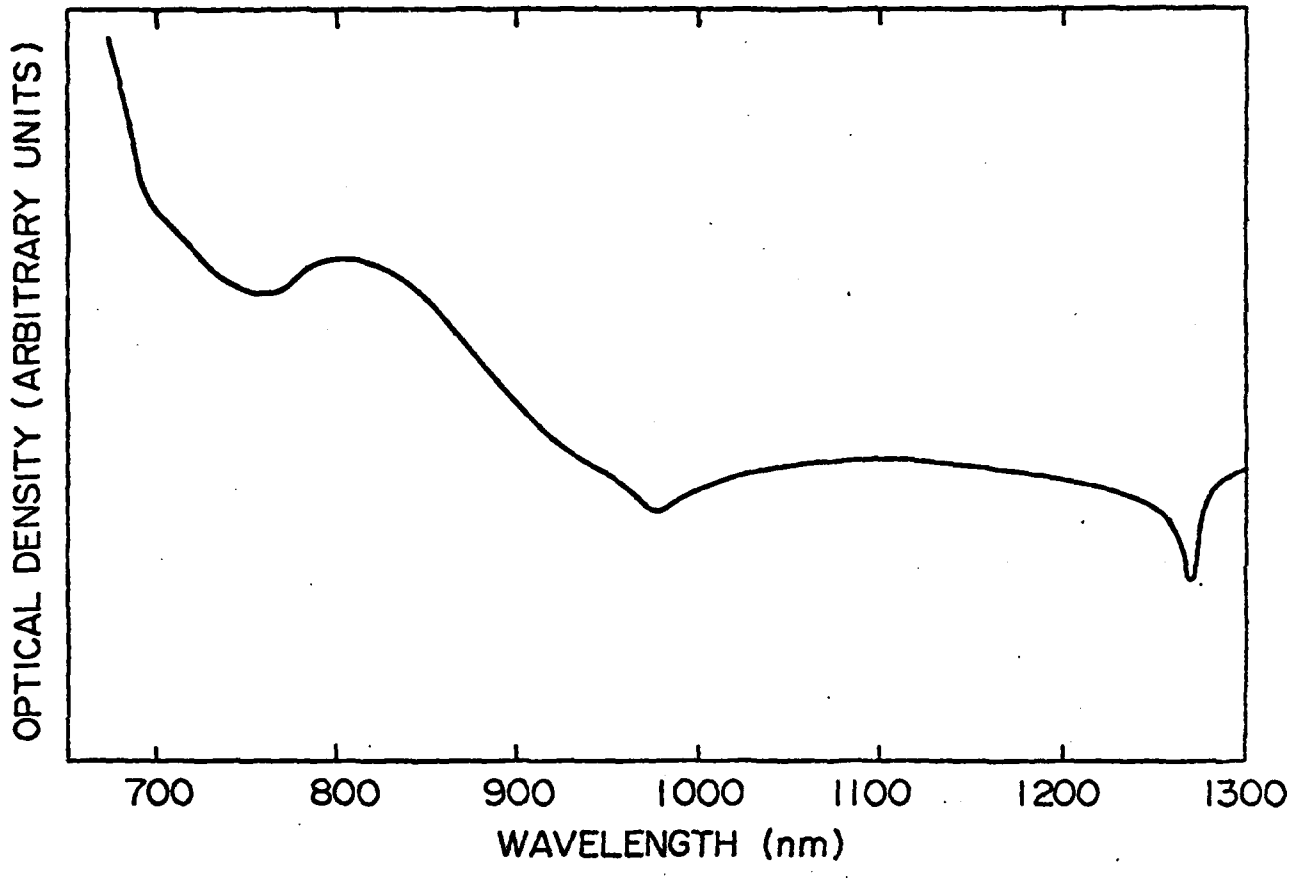

FIG. V.1(b)--Infra-red absorption spectra of pure CsI when exposed to UV-light along the (010) direction. (b) at RTAC.

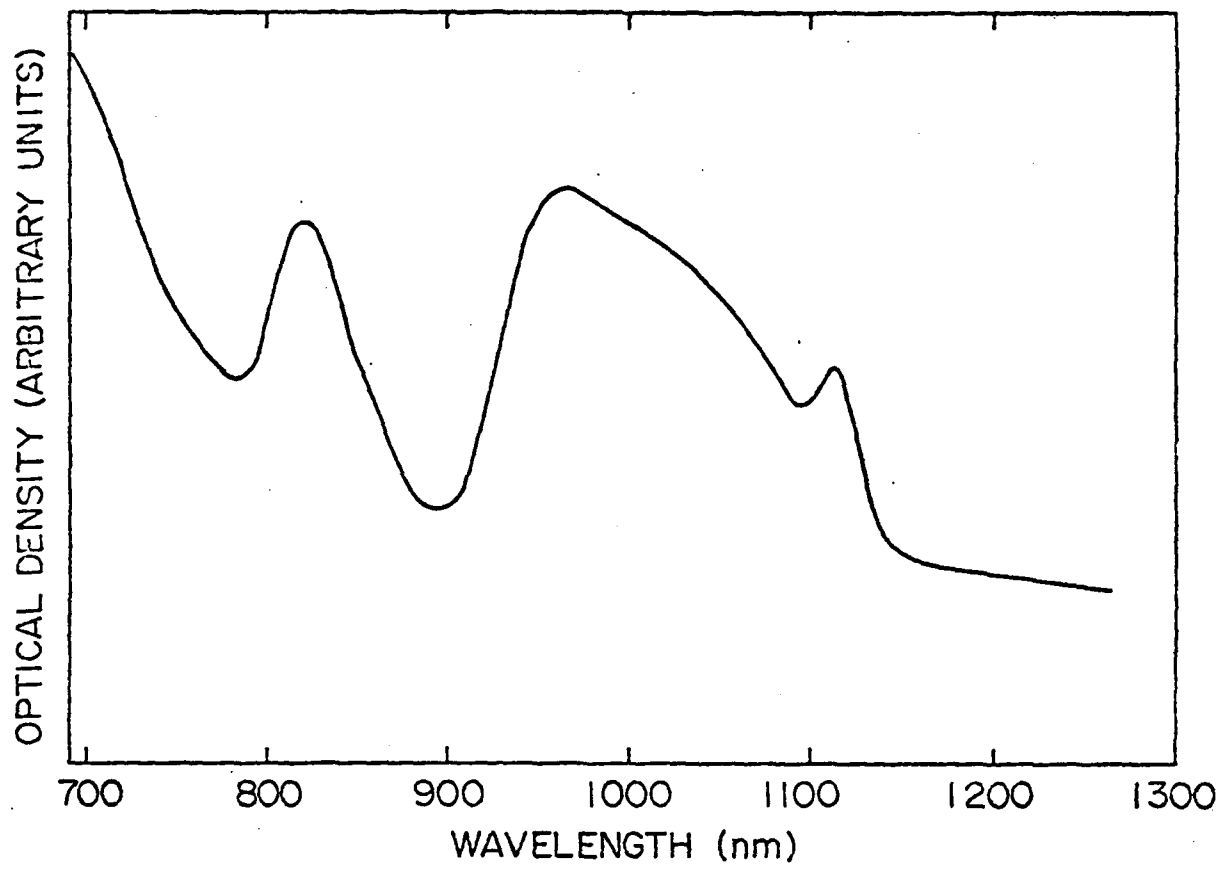

FIG. V.1(c)--Infra-red absorption spectra of pure CsI when exposed to UV-light along the (010) direction. (c) at LNT when sample was cooled the second time.

AD-A118 516 STANFORD UNIV CA CENTER FOR MATERIALS RESEARCH F/G 20/10
LONG RANGE MATERIALS RESEARCH. SUPPLEMENT 1. INVESTIGATION OF L--ETC(U)
JAN 77 A M SALAU, C W BATES N00014-75-C-1171
UNCLASSIFIED CMR-77-1-SUPPL-1 NL

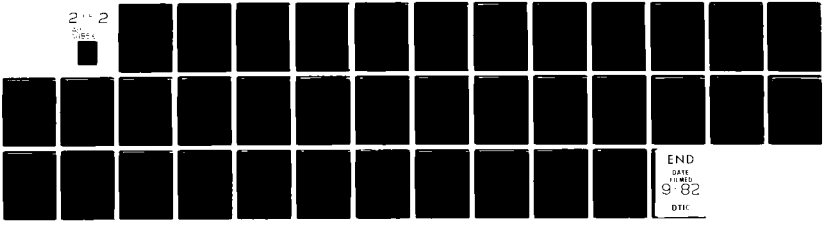

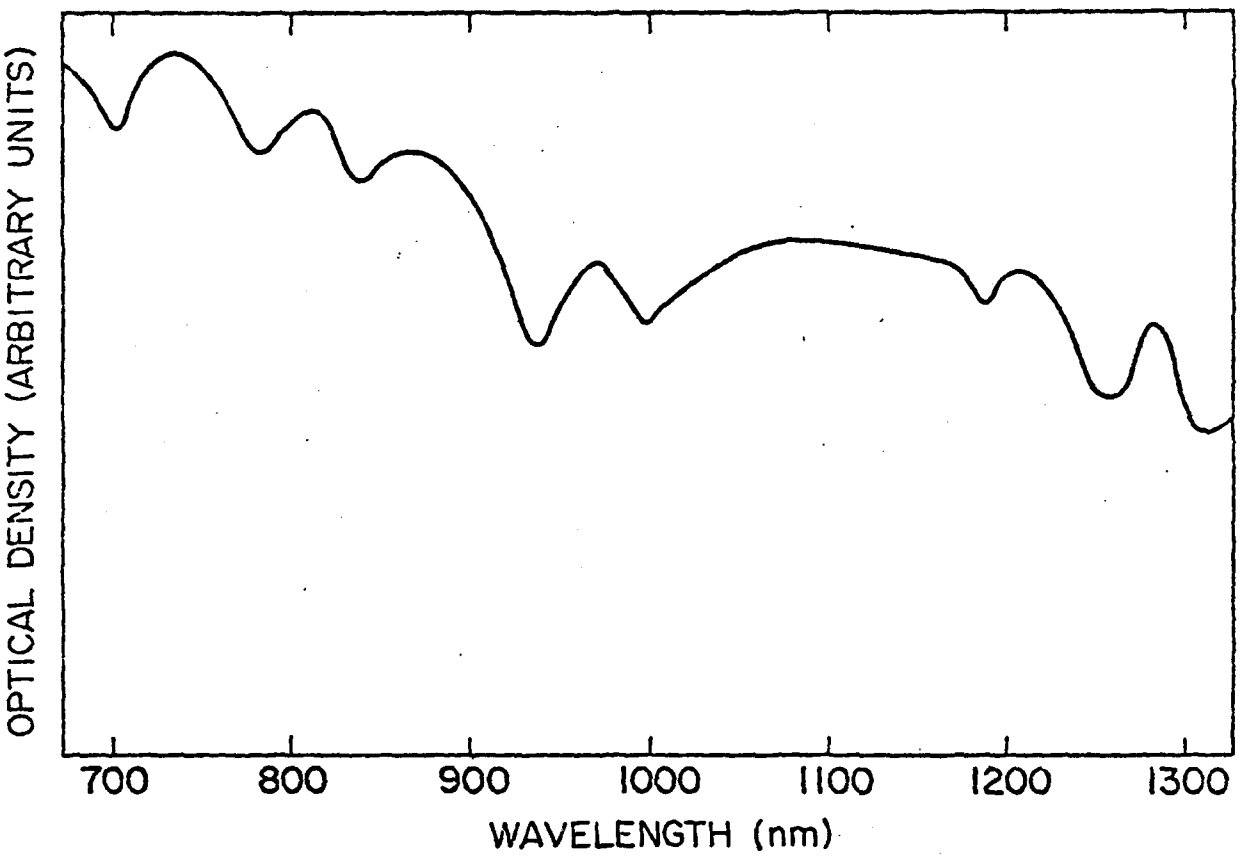

FIG. V.1(d)--Infra-red absorption spectra of pure CsI when exposed to UV-light along the (010) direction (d) at LNT when sample was cooled the second time but for longer irradiation time.

the 810 nm and the 740 nm infra-red absorption bands are the so-called F′- and F-centers in CsI respectively. Other authors observed these absorption bands in their colored and X-rayed CsI sample. But at RTAC, the absorption spectrum is structureless, except for the absorption at 830 nm.

Figure V.2(a) shows the infra-red absorption spectra of a CsI sample that was not exposed to non-ionizing ultra-violet radiation at RTBC but only LNT and RTAC. Between (1000-1200 nm) there is evidence of structures though considerably weaker than those observed at LNT if the sample were irradiated with UV-light at RTBC. There is a weak structure at 1150 nm and a broad band centered at 1050 nm . Also there is a bump at 830 nm. From Fig. V.2(b) we see that all the structures disappeared except the one at 830 nm at RTAC.

Figure V.3 shows the infra-red absorption spectra of a CsI sample that was irradiated at LNT for about 4 hours and the radiation cut-off before measurements were taken. It should be noted that the sample whether exposed to UV-radiation or not at RTBC makes no difference in the observed spectra at LNT and RTAC. The only evidence of structure is at about 1160 nm, no structure at 830 nm. But at RTAC Fig. V.3(b), the 830 nm band is the only structure just as for previous cases. Figure V.4 shows the infra-red absorption spectra of unirradiated pure CsI at LNT and RTAC.

Discussion:

From the empirical fit of the F-band by Dawson and Pooley, the F-band is supposed to lie in the energy range (1.65 - 1.70 eV) which in wavelength is between 730 and 750 nm which agrees with the positions

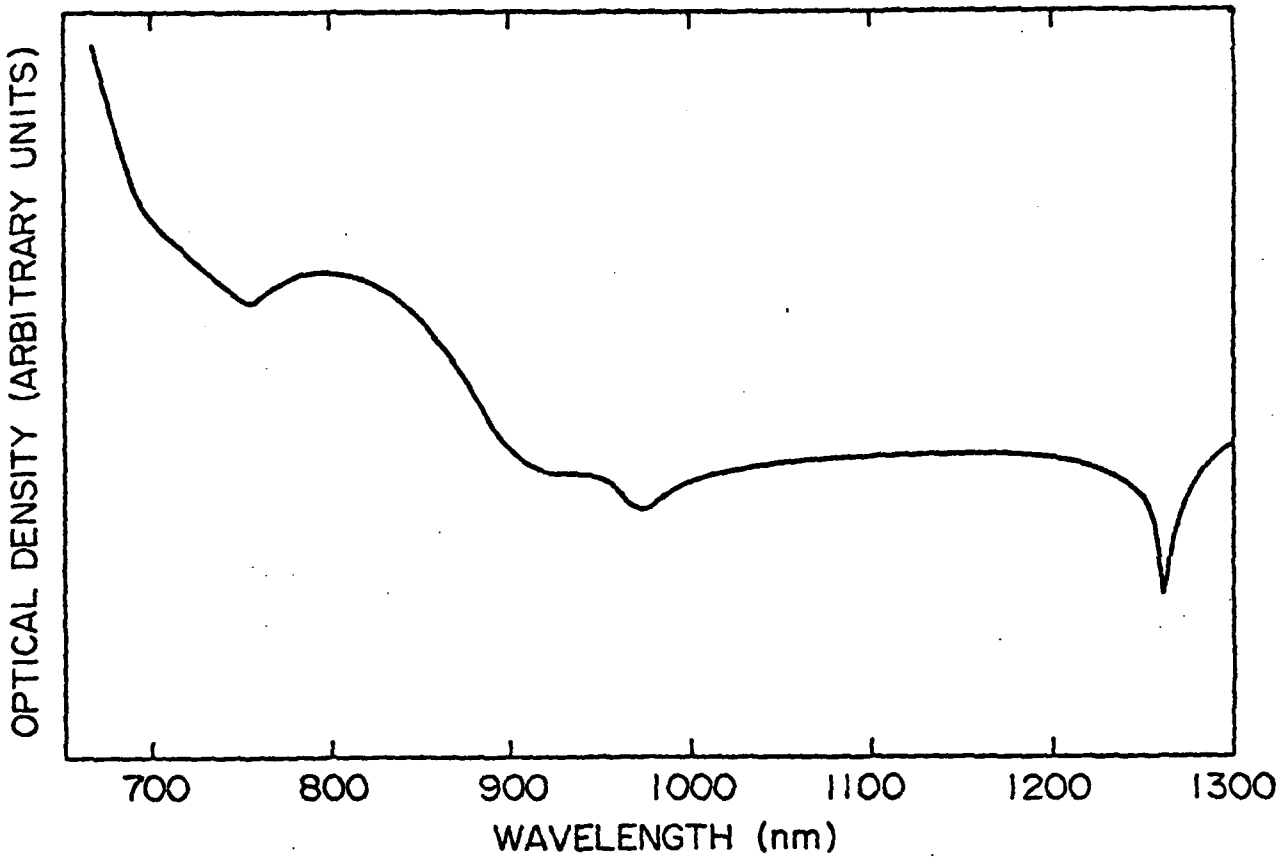

FIG. V.2--Infra-red absorption spectrum of pure CsI at LNT without irradiation at RTBC.

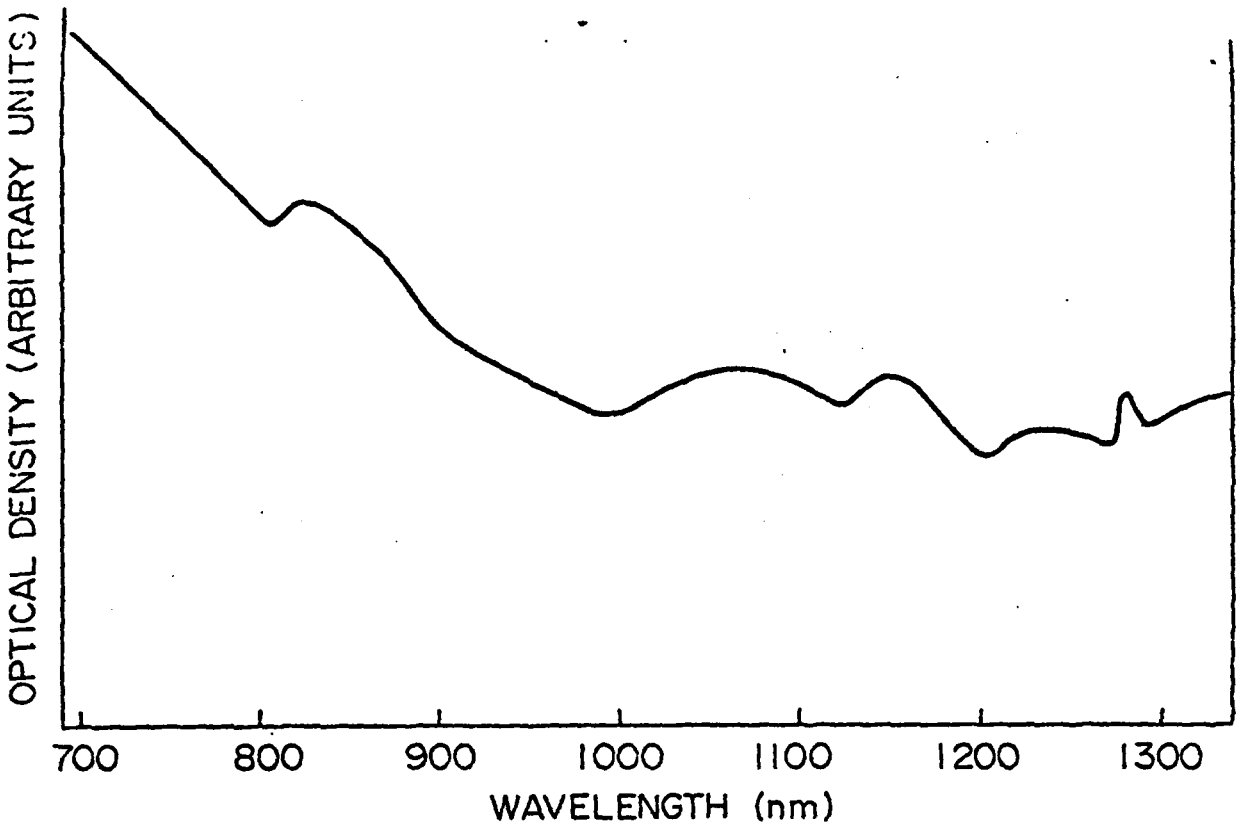

FIG. V.3--Infra-red absorption spectrum of CsI irradiated at LNT for 4 hours and irradiation cut-off during measurements.

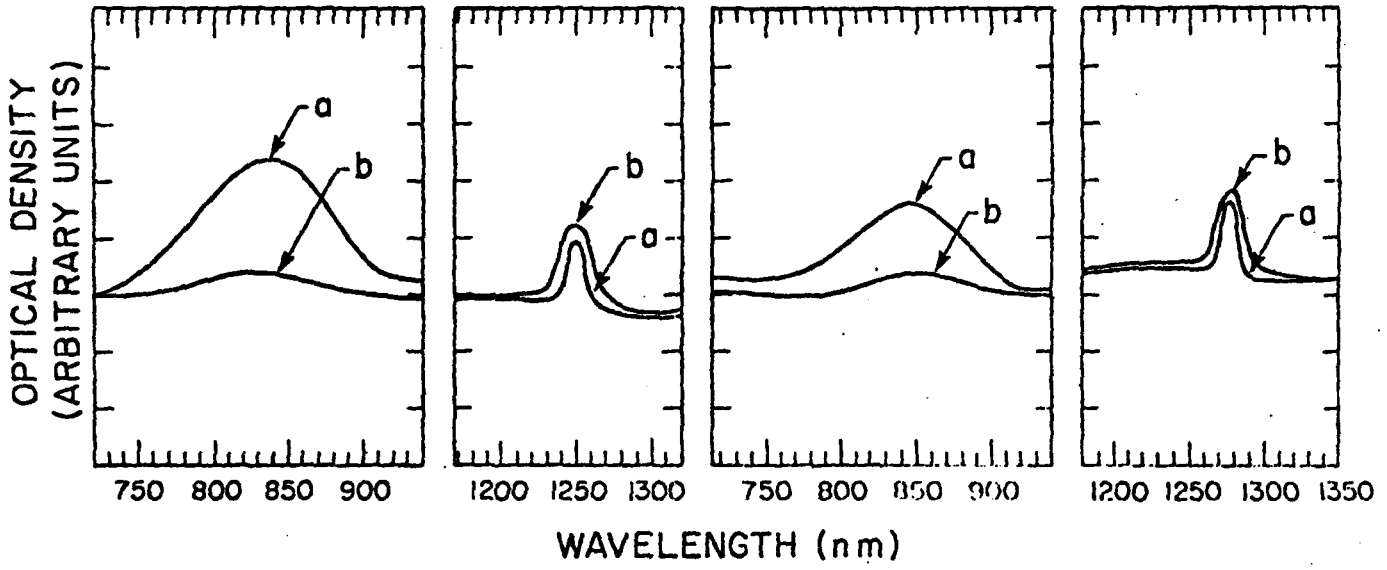

FIG. V.4--Absorption spectra of F- and M-bands in pure CsI
(a) at LNT curve a - before bleaching
(b) at RTAC curve b - after bleaching

(740 nm) of the F-band observed in CsI .[62,65] As mentioned earlier, other authors were only able to produce F-centers in CsI not by exposing the samples of CsI to ionizing radiations but by coloring using the method of electrolysis at high temperatures. We can thus probably assign the 740 nm band in Fig. V.1(d) to an F-center absorption band. But as we warm the sample up to room temperature this structure is lost probably because of optical bleaching. Thus, this shows that F-centers can be produced in CsI easily by exposing it to non-ionizing UV-radiation at RTBC, and then cooling to LNT (with irradiation on), warming up and then cooling again to LNT. After about 20-30 minutes one can take absorption measurements to detect the F-band. The absorption may be weak because of the small concentration produced by using non-ionizing UV-radiation. Probably successive cooling and warming can produce high concentration of F-centers.

The only prominent and well resolved band at LNT for a CsI sample that had been exposed to UV-radiation at RTBC is the 1100 nm band. We can not assign this band to the so-called M-band located at about 1185 nm in CsI because of the 85 nm shift and its temperature dependence. At room temperature the M-band in CsI shifts to about 1220 nm. On the other hand, the 1100 nm band completely bleaches at room temperature, that is to say this band is highly unstable thermally contrary to the behavior of the so-called M-band in CsI . This center at 1100 nm may be an excited state of the M-band as the K-band is to the F-center. It is not the R-center either because the R-center

is more thermally stable; that is warming to room temperature does not destroy R-centers. The 1100 nm band is probably an M^+-center.

Other absorption bands observed at LNT, especially the 820 nm band can be tentatively associated with the F'-band located at ~ 830 nm in CsI , though with a shift of 10 nm. This band bleaches on warming to room temperature as expected. We also observed the 1050 nm and 1200 nm bands observed by Avaian et al. in their colored (by electrolysis at 460°C) CsI crystals. It should be noted that except for the F- and F'-centers, other centers (M and R) have not been studied to any extent in CsI .

C. ELECTRON SPIN RESONANCE

Introduction:

Since the optical studies indicate that the basis for creating exciton trapping sites is primarily through the cycling of the temperature, it was decided to investigate the actual trapping sites themselves by combining optical techniques with electron spin resonance. If the trapping sites are indeed paramagnetic, then it should be possible to determine some of the important magnetic parameters and perhaps more fully characterize the sites themselves. In addition, we should, in principle, be able to observe any effect that the incident irradiation has with respect to a particular trapping site.

Results:

1. Pure CsI

Immediately after receipt, the pure Harshaw crystals were placed in the spectrometer and weak ESR signals were observed at room temperature. Upon annealing at 520°K for a four to five hour period, slowly returning the sample to room temperature in steps of 10 degrees every twenty minutes, and recording the ESR spectra under the same experimental conditions, all ESR signals disappeared. Signals from the unannealed crystals were tenatively assigned to defects produced by the cutting, grinding and polishing of the pure material by the supplier. As standard practice, it is suggested that all pure crystals be annealed, as described above, before any ESR studies are done to eliminate any complicating ESR structure.

As the pure crystal was slowly cooled to 80°K, an ESR signal appeared described by magnetic parameters indicating the presence of a defect believed to be that of an F center. The signal is characterized by a g value of 2.003 ± 0.001 and a peak-to-peak linewidth of approximately 100 Gauss. The signal intensity increased (the lineshape remained unchanged hence the peak-to-peak amplitude increased) as the temperature was lowered to 80°K and changed very little between 80°K and 20°K (due presumably to saturation) – the maximum amplitude occurring at ~ 60° - 70°K. The lineshape was essentially Gaussian and at 80°K showed initial saturation above roughly forty milliwatts incident power upon the cavity and seemed to retain its initial lineshape when saturated up to 200 nW. This saturation behavior is usually characteristic of lines that are inhomogeneously broadened.

Upon warming of the sample from 80°K to room temperature, the ESR signal continues to persist. See Fig. V.5. Only annealing at evaluated temperatures will successfully bleach the pure CsI crystal. Regardless of the number of bleachings and coolings the pattern is as follows:

RTBC - no EST signals.

80°K - ESR signals - F centers.

RTAC - ESR signals - F centers.

There appears to be no hyperfine structure on the ESR line attributed to the F-center and no obvious asymmetry of the F-center line itself.

Under conditions of rather high gain there is an indication of a wealth of ESR lines down in amplitude by one to two orders of magnitude relative to the F-center signals and which appears to be anisotropic in nature. Apparently, the responsible electrons are in rather shallow traps since warming to room temperature is sufficient for bleaching. However, we hesitate to make any further statement with respect to their origin with the S/N presently obtainable. As the pure CsI crystal is cooled in the presence of optical irradiation at both 217 nm and 235 nm, the amplitude of the ESR signal is relatively light insensitive – perhaps a 5% increase in the ESR signal is observed – and remains unchanged at a variety of other frequencies and optical intensities.

Since the technique of irradiating pure CsI samples during cooling produced a small increase (5%) of the ESR signal during the

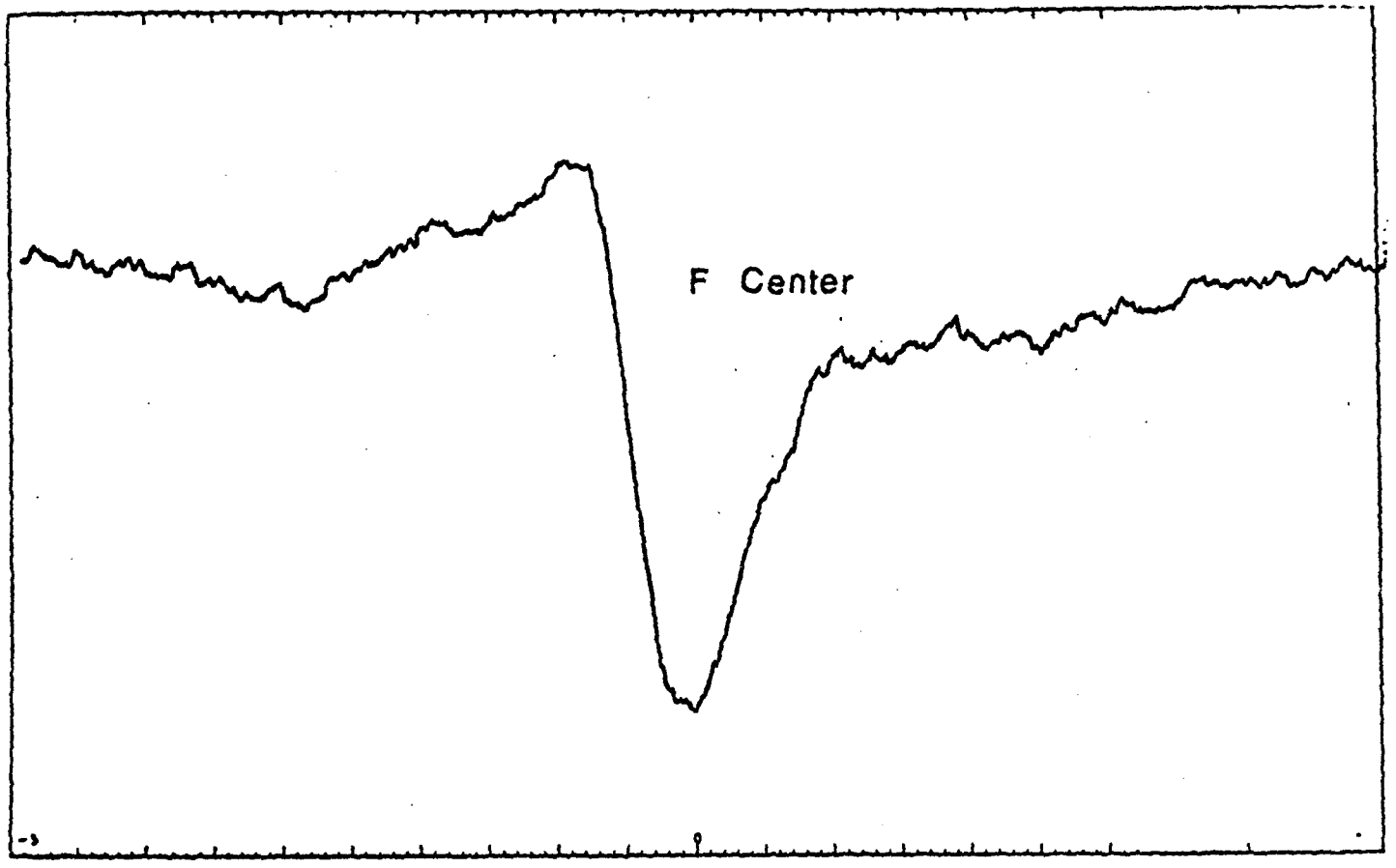

FIG. V.5--RTAC ESR signal of pure CsI
scan range = 1 kG, H_0 = 3230 G., Mod. Amp. = 20 G.,
mod. freq. = 100 kHz, ν_0 = 9.15 GHz, Response Time = 1 sec.
μ-wave pwr = 200 mW, Temp. = Room (after cooling)
Receiver Gain = 3.2×10^4 .

time of irradiation which was several minutes at best, it was decided to irradiate a sample for several hours with ultraviolet light at low temperatures and then observe the ESR signal. The results are shown in Fig. V.6 for a pure sample of CsI which had been irradiated by means of a high pressure Hg vapor lamp for 6 hours at a temperature of about 6°K. The ESR signal intensity has increased by almost an order of magnitude over the previous one for pure CsI. This result appears to confirm the proposition that not only can F-centers be produced by ultraviolet radiation, but also the wealth of orientation dependent ESR structure indicates the presence of an anisotropic V-center. It is still not possible at this time to analyze the anisotropic ESR spectrum and to assign a structural model designating the particular V-center involved. However comparing the disappearance of this V-center at 20°K and above with the disappearance at this temperature of the 300 nm emission band supposed to be due to radiative recombination of V_K-center plus a trapped electron (F-center) suggests the association of this V-center with the V_K-center.

2. Optical Grade CsI(Tℓ)

Upon annealing the optical grade thallium doped (0.1 mole percent) CsI crystal a large ESR signal was recorded at both 540°K and 297°K. At 540°K a rather symmetric ESR line was observed having a peak-to-peak linewidth of approximately 100 Gauss and a rather large g-vale of 2.06 ± .002. A narrow ESR line (δ = 20 Gauss) appeared at slightly higher field characterized by a g-value of 2.00 ± .02 with a hint of

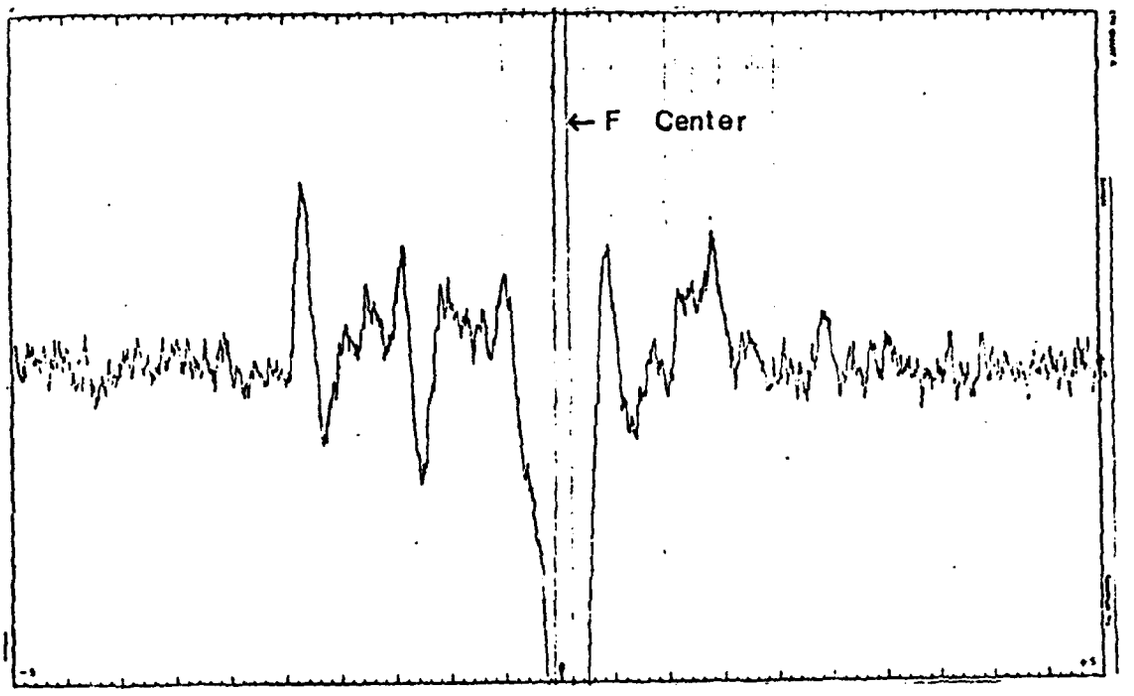

FIG. V.6--Pure CsI irradiated at 6°K with a Hg lamp for 6 hours and stored at LN temperature for three days. Second Derivative ESR spectrum. scan range = 1 kG, H_0 = 3588, Mod. Amp. = 32 G., at 100 kHz Mod. Freq. and 20 G Hz Mod. Freq., ν_0 = 9.58 GHz, Response Time = 3 sec., μ-wave pwr. = 80 mW, Temp = ~ 10°K, Receiver Gain = 2.5×10^2 at 100 kHz and 2.5×10^2 at 35 Hz.

structure. Upon cooling to room temperature, the latter line remained unchanged in position and decreased in amplitude by about a factor of 2 - 3 . All indications of structure disappeared.

On the other hand, the low field ESR line width remained constant, but the spectral center shifted downfield by roughly 100 Gauss giving a room temperature g-value of 2.090 ± .002. In addition to the field shift, structure appeared on the shoulders of the line while the amplitude decreased to roughly one-half its value at the higher temperature. The lineshape at this temperature was independent of crystal rotation. This sequence is shown in Fig. V.7 and is given in Table V.1.

Further cooling of the CsI(Tℓ) crystal to 80°K gives rise to a large ESR signal that can be easily decomposed into two lines - one is the "low field" ESR line observable at higher temperatures having a δ = 100 Gauss and a g value of 2.042 ± .002, while the second is a new ESR center having a g value of 2.205 ± .004 and a peak-to-peak linewidth of ~ 1 kG. The new lineshape is dependent upon crystal orientation and on temperature and has an overall intensity that is much greater than that of the δ = 100 G ESR line. Tentatively, an assignment of the g = 2.042 ± .002, δ = 100 G corresponding to that of an F-center and the g = 2.205 ± .002, δ ~ 1 kG, anisotropic, broad ESR line to that of a V-center (self-trapped hole) is made. See Figure V.8. Upon warming back to room temperature the ESR line corresponding to the V-center is significantly broaded, the linewidth increases by more than a factor of three and the signal intensity drops by something greater than an order of magnitude. The

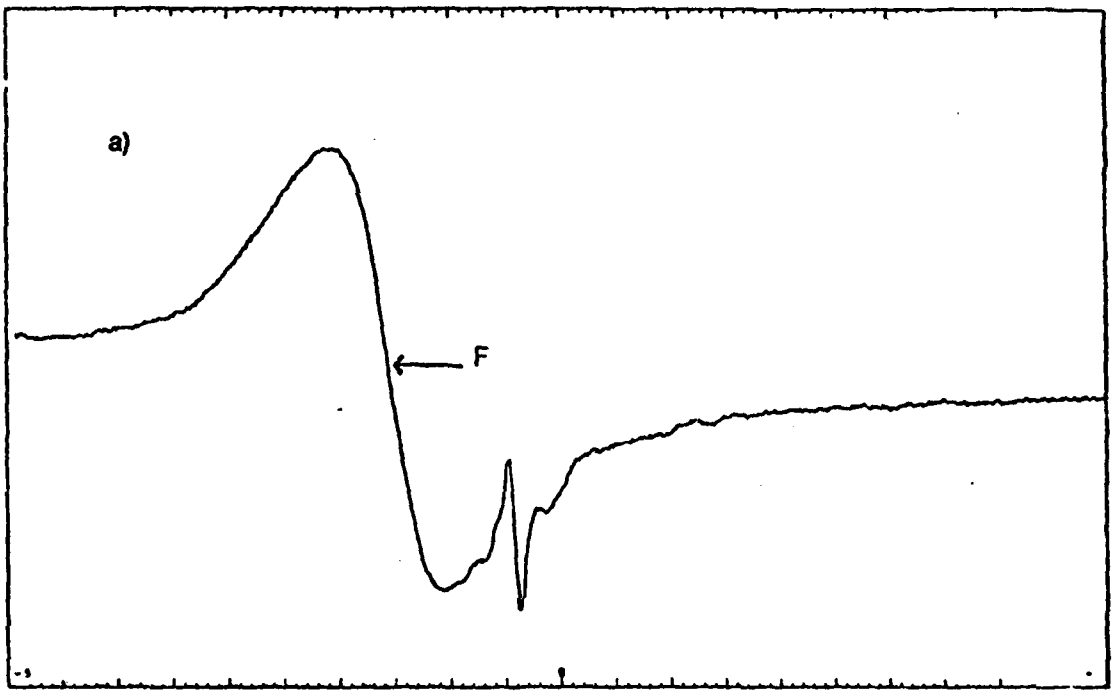

FIG. V.7(a)--ESR spectra of CsI(Tl) as a function of temperature

(a) Tl doped CsI annealed at 260°C for 10 hours. scan range = 1 kG, H_0 = 3321 G., Mod. Amp. = 20 G., mod. freq. = 100 kHz, ν_0 = 9.15 GHz, Response Time = 0.250 sec.
Receiver Gain = 6.3×10^3.

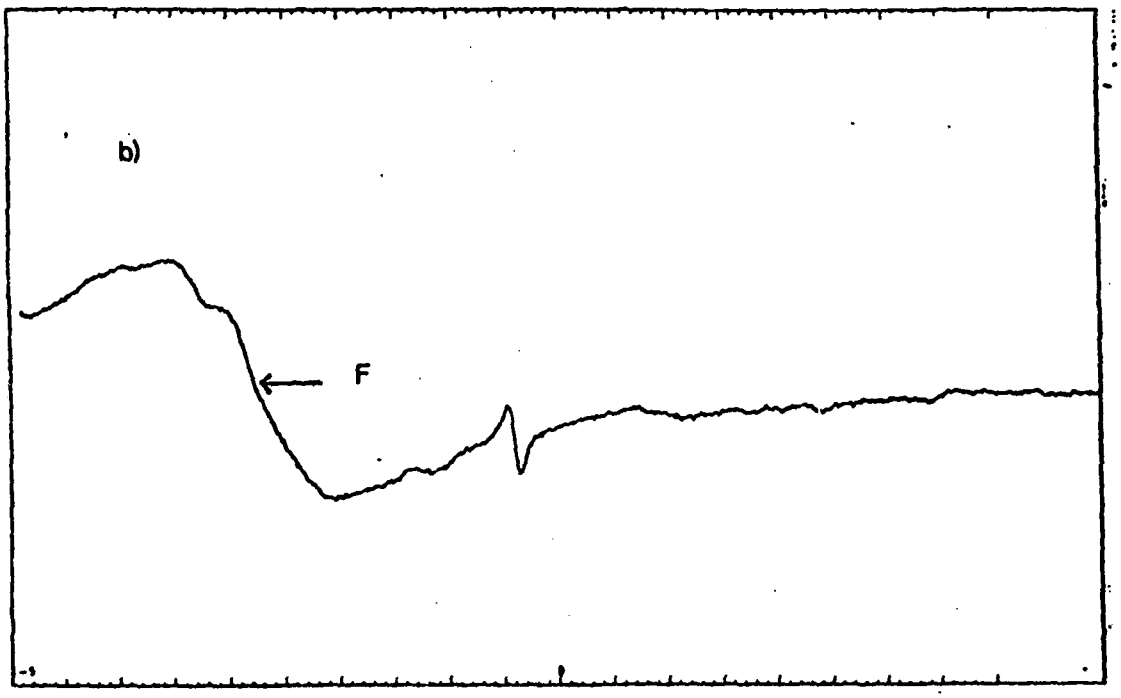

FIG. V.7(b)--ESR spectra of CsI(Tl) as a function of temperature.

(b) Tl doped CsI annealed for 10 hours at 260°C and brought to room temperature over a 5 hour period.
scan range = 1 kG, H_0 = 3321 G., Mod. Amp. = 20 G.,
mod. freq. = 100 kHz, ν_0 = 9.15 GHz, Response Time = 0.250 sec.,
μ-wave pwr. = 200 mW., Temp. = Room, Receiver Gain = 6.3×10^3.

TABLE V.1

The experimental sequence of events in recording the ESR spectra of CSI(Tℓ) at three different temperatures.

	540°K			297°K		
	Structure	g-value	δ(p-p)	Structure	g-value	δ(p-p)
low field line	No	2.06	100	Yes	2.09	100
hi field line	Yes	2.00	20	No	2.00	20

	80°K		
	Structure	g-value	δ(p-p)
Broad line	Yes	2.205	~1kG
Low field line	Yes	2.042	100G
Hi field line	disappeared		

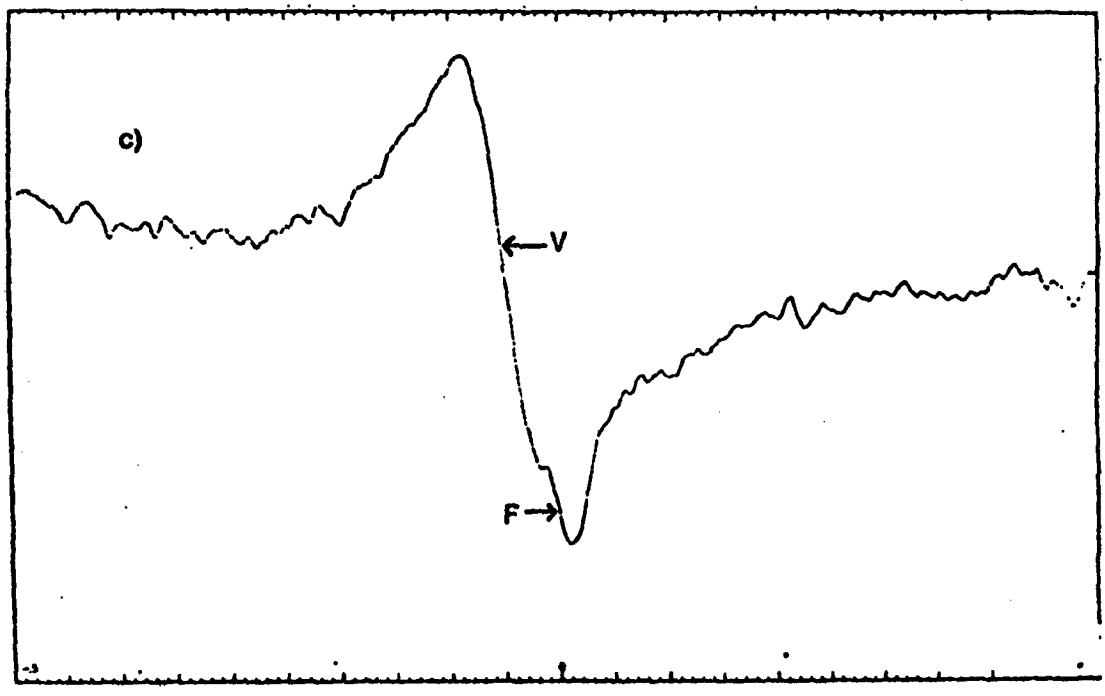

FIG. V.8--ESR spectra of CsI (Tl) as a function of temperature.
c) Tl doped CsI at -175°C.
scan range = 4 kG, H_0 = 3,200, Mod. Amp. = 10G.,
mod. freq. = 100 kHz, ν_0 = 9.15 GHz, Response Time = 1 sec.
μ-wave pwr. = 100 mW, Temp. = -175°C, Receiver Gain =
1.6×10^4 .

ESR line corresponding to the F-center persists in RTAC. As in the case of the pure crystal irradiation of the thallium doped crystal has little effect on the ESR signal.

To support the contention that the X-band observed in the optical spectrum was specifically related to a V_K center it was thought that perhaps this center might be observable in the ESR spectrum. Heretofore V_K centers have been studied extensively in alkali halide structures and in particular have been observed in CsI(Tℓ) to give an 11 = (2I + 1) line ESR spectrum arising from the molecular ion I_2^- (nuclear spin of iodine = I = S/2). However, to our knowledge, all V_K centers found in the literature have been produced in the presence of ionizing (X-ray) irradiation. It was hoped to observe the presence of such centers upon cooling the sample to 20°K in the presence of non-ionizing irradiation (UV at ~ 5 eV). Experimental ESR results do not show the presence of an eleven line V_K center spectrum at the necessary levels of concentration [2×10^{10} δ × (2I + 1) spins in the cavity = 2×10^{14}] spins in the volume (~ 0.1 cm^3) of CsI(Tℓ) crystal used in the experiment.*

ESR Analysis:

ESR studies on both pure and doped CsI crystals suggest the presence of an F center, i.e., an electron occupying an anionic vacancy,

*That is, if V_K centers were present at a concentration of 2×10^{15} spins/cm^3, thenwe would see an ESR spectrum having a S/N ratio of roughly 1:1. To see, in practical terms, a S/N ratio of 10:1, a spin concentration of ~ 2×10^{15} spins/cm^3 is necessary. With non-ionizing radiation we do not produce a high enough concentration of V_K centers to record an observable ESR signal.

produced by the inherent stress or strains that permeate the sample upon cooling to 80°K. Experimental evidence shows the presence of

i) a small g-shift from the free electron value of 2.0023,

ii) a Gaussian lineshape that saturates inhomogeneously,

iii) a peak-to-peak linewidth of ~ 100 G,

iv) sample is transparent before cooling and opaque at 80°K and RTAC, and substantiates the assignment as that of an F center arising from crystal stress or strain upon cooling. It is well known that F centers give a strong optical absorption in the visible region and this is attributed to the β-band absorption at 225 nm, near the first exciton absorption band. Irradiation of pure CsI at both the fundamental absorption edge (235 nm) and at 225 nm show photoluminescence when monitoring the optical absorption, emission and excitation spectra but affect the ESR spectra negligibly. This suggests that the trapping sites (F centers) are produced by the cooling of the crystal only and that the effect of the light is to excitonically populate the trapping sites. Upon warming, the deep traps continue to be stable allowing radiative exciton recombination with various crystal defects possibly leading to the observed luminescence.

A second type of center was found in the Tl:doped material, which was anisotropic in nature and exhibited a rather broad spectral width of the order of a kilogauss. Cooling the doped CsI crystal can cause a variety of defects and, in particular, a variety of V centers. For example, Känzig describes a self trapped hole, a hole trapped by a cation vacancy, an unpaired electron located on three halogen atoms, or formation of a molecule ion by an interstitial halogen atom. The

tentative assignment of this as a V center seems consistent with experimental data and substantiates the observed luminescence behavior by providing a radiative e^--hole recombination mechanism at sites created by the temperature cycling. Since the V center are anisotropic in nature, interesting optical data are likely to be obtained using polarized incident radiation and/or observing polarized luminescence.

However our polarized luminescence studies showed that the intrinsic luminescence observed in CsI is not polarized. This result is not surprising as we do not expect to observe polarization from such isotripic center, like the F-center[7] we produced by cooling and exposing CsI to non-ionizing ultraviolet radiation.

CHAPTER VI

A PROPOSED MODEL FOR THE LUMINESCENT MECHANISM IN PURE CsI

A. INTRODUCTION

The intrinsic luminescence which occurs at low temperatures in alkali halides especially those with the NaCl-structure has been attributed by Kabler and also Murray and Keller to the radiative recombination of a free electron with a self-trapped hole (V_K-center). However, the intrinsic luminescence in alkali halides with the CsCl-structure is not well understood. Consequently we undertook a combined study of the optical properties and electron spin resonance (ESR) of pure CsI (which is relatively strain and defect free) from liquid helium to room temperature to elucidate the fundamental mechanisms involved in the intrinsic luminescence of alkali halides with the CsCl-structure (taking CsI as a case study) for excitations extending from the long wavelength tail of the fundamental absorption through the excitonic region, i.e. (235 - 205 nm). The optical techniques through absorption, emission and excitation spectra give information on the electronic transitions occurring in the material and the ESR data reveal the nature of the trapping sites which, from previous studies, we expect to be paramagnetic.[48]

Our optical and ESR data on pure CsI (discussed in Chapters IV and V) suggest the need to re-examine the so-called "self-trapped exciton" model usually observed in alkali halides because our (a) ESR

spectrum showed two components F- and V_K-centers; (b) excitation spectra for the intrinsic luminescence are different from those measured by Lamatsch, et al;[19] (c) we observe RTAC luminescence, and (d) we observed a new absorption band in the infrared which is thermally more unstable than the so-called M and R bands. In this chapter we hope to present our proposed models on the observed intrinsic luminescence at low and room temperatures in CsI .

B. TRAPPED EXCITON MODEL (TEM)

Excitons produced during an optical absorption process in alkali halides can either be trapped at vacancies, electron or hole excess centers to produce "trapped excitons". Another form of trapping of excitons is that produced by the combination of a free electron with a self-trapped hole (V_K-center), the well known "self-trapped exciton" in alkali halides. The intrinsic luminescence observed at low temperatures has been explained by the self-trapped exciton model while impurity luminescence is explained by radiative recombination of trapped excitons in alkali halides. However, cooling and exposing CsI to non-ionizing radiations produced these two exciton traps to be discussed below.

Self-trapped exciton:

It is generally assumed that a self-trapped exciton has the configuration $(V_K + e)^*$ in alkali halides but our optical and ESR data on pure CsI which is relatively strain and defect free suggests a different configuration for the self-trapped exciton. This can be explained as follows:

When CsI is cooled to liquid helium temperatures excitonic excitations produce three emission bands at 300 nm, 350 nm and 430 nm. The intrinsic emission bands at 300 nm and 430 nm disappeared at 25°K and above for excitonic excitations. The disappearance of the 300 nm band at 25°K and above is consistent with other authors results.[19,41] These authors proposed that this intrinsic emission band at 300 nm is probably due to the radiative recombination of self-trapped excitons of the configuration $(V_K + e)^*$ – that is, V_K-center plus a free electron.[7,8] However, from our optical data the excitation spectrum for this emission band at 300 nm below 25°K peaks at 230 nm, a wavelength between the so-called β-(225 nm) and α-(235 nm) bands. Thus we feel that this emission band is due to radiative recombination of excitons in metastable states which decay non-radiatively at high temperatures. To support this contention we performed ESR measurements to determine the nature and the symmetry of these centers responsible for the 300 nm emission band. The results suggest the existence of two paramagnetic species F- and V_K-centers at low temperatures in pure CsI which has been cooled and exposed to non-ionizing ultraviolet radiations. It is interesting to note that the anisotropic center (tentatively associated with the V_K-center)[41] diminished in intensity considerably above 25°K, the temperature at which the 300 nm emission band disappeared. Thus combining optical data which shows that the excitation spectrum of the 300 nm emission peaks very close to the β-band (exciton-trapped at an F-center) and the disappearance of the so-called self-trapped hole (V_K-center) at

25°K the temperature at which the 300 nm band disappears, suggests that the self-trapped exciton responsible for the 300 nm intrinsic luminescence is probably of the configuration

$$V_K + F \rightarrow \square + 4.1 \text{ eV} \quad ,$$

that is, radiative recombination of V_K- and F-centers which results in the 300 nm emission plus creation of negative-ion vacancies which in turn, can act as electron or exciton traps. Therefore we feel that the intrinsic luminescence located at 300 nm in pure CsI is due to radiative recombination of self-trapped excitons probably of the configuration self-trapped hole (V_K-center) plus a trapped electron (F-center), i.e., (V_K + F) instead of the usual configuration self-trapped hole (V_K-center) plus a free electron, i.e., $(V_K + e)^*$ proposed by other authors.

Trapped Excitons

Following the model developed by Bassani and Inchauspe to locate the α- and β-absorption bands in alkali halides, we interpret the observed absorption bands at 237 nm and 225 nm shown in Fig. IV. as being due to trapped excitons. The calculations are done using the equations derived by Bassani and Inchauspe and discussed in Chapter II. The calculated α- and β-bands are located at 235 nm and 225 nm in CsI respectively. It is reassuring to note that the calculated and measured values of the α- and β-absorption bands in CsI are in close agreement.

The evolution of the emission spectra obtained by selective excitation in the two bands at 225 nm and 235 nm as a function of temperature of a bulk single crystal of pure CsI are shown in Figs. IV.11(a) and (b). The excitation spectra of the two emission bands at 320 nm and 430 nm are also shown in Fig. IV.11(c). The two emission spectra have excitation spectra peaking at 237 nm with a hump at about 227 nm which agrees fairly well with both calculated and measured values of the α- and β-absorption bands.

Therefore combining the optical and ESR data on pure CsI we propose that the so-called blue luminescence (430 nm) in CsI is due to the radiative recombination of excitons trapped at negative ion vacancies and F-centers.

So from the above discussion on the "trapped exciton" models, we believe that there are two competing luminescent centers that give rise to the observed intrinsic luminescence in pure CsI (and probably other alkali halides with the CsCl-structure) at low temperatures. However, when the sample warms back to room temperature, we observed luminescence which was not there at RTBC. This RTAC luminescence is discussed below.

RTAC Luminescence

Cooling and exposing CsI which is relatively pure and strain and defect free to non-ionizing UV-radiation at low temperatures, suggests from absorption studies and reinforced by theoretical calculations the creation of halogen-ion vacancies and F-centers which act as recombination sites or traps for free holes and electrons or

mobile excitons. Also our ESR data (discussed in Chapter V) supports this contention of creating F-centers as a result of cooling CsI to low temperatures. Thus we propose that the RTAC luminescence can tentatively be associated with vacancies (traps) or other lattice imperfections created by the motion and clustering of dislocations which exist in the crystal as a result of thermal contraction of the crystal during cooling. That the cooling acts as a plastic deformation can be explained as follows. It has been shown that the minimum external stress required to move a dislocation in simple cubic crystals is very small ($\sim 10^5$ dynes). This is three orders of magnitude less than the critical shear stress of 10^8 dynes induced by straining due to cooling in CsI.[54] Also it should be noted that the elastic limit observed in CsI is of the order of 10^7 dynes one order of magnitude less than that induced by cooling. Consequently we are led to the conclusion that cooling produces plastic deformation in CsI because (a) the stress produced by cooling as a result of thermal contractions makes the dislocation highly mobile which in turn is responsible for slip that produces, in many crystals, plastic deformation, (b) cooling induced stress exceeds the measured elastic limit and (c) RTAC photoluminescence measurements persists even after several days, though the peak position of the excitation spectrum shifts to longer wavelengths (250 nm) after about two weeks. Therefore, dislocation motion and clustering as a result of thermal contraction of the crystal due to cooling produces vacancies and other lattice imperfections that can act as traps for electrons and holes or mobile excitons. However, it

should be noted that using Smakula's equation[65]

$$N_f \approx 0.87 \times 10^{17} \frac{n}{(n^2 + 2)^2} \alpha_{max}(cm^{-1})\, W_{1/2}(eV) \sim 10^{15}$$

where

N = concentration of traps

n = refractive index of CsI $\sim \sqrt{\epsilon_\infty} \sim 1.73$

α_{max} = maximum absorption coefficient ~ 2.3 (Eq. 4.1)

$W_{1/2}(ev)$ = half-width maximum of absorption band at 840 nm $\sim$ 0.2 eV

and f = oscillator strength assumed to be unity;

the concentration of traps thus produced by cooling (without irradiation at low temperature) is very small ($\sim 10^{15}$ cm^{-3}) and we are able to detect absorption bands in the infra-red region in our crystal which was just cooled without exposure to non-ionizing UV-ratiation only at very high sensitivity. The absorption bands are located at 840 nm and 1280 which are shifted by 100 nm from the normal F and M-bands in CsI . The location of F- and M-bands 100 nm higher in wavelength than that previously observed does appear at this time to make the assignment of an F-center somewhat tentative in spite of the previous supporting data.

CHAPTER VII

CONCLUSION

RESULTS

The studies have increased our understanding of photoluminescent properties of CsI . Five major results have been obtained:

(a) The intrinsic luminescence observed in pure CsI (which is relatively strain and defect free) at low temperatures originates from two different centers: (1) self-trapped excitons (V_K + F) instead of the usual configuration (V_K + e), and (2) excitons bound to F-centers or negative ion-vacancies.

(b) We observed that straining by cooling produces plastic deformation in CsI which in turn leads to the creation of vacancies that act as electron-traps (F-center) that are still stable at room temperature and consequently give rise to the observed RTAC luminescence.

(c) Straining by cooling and exposing CsI to non-ionizing UV-radiation at low temperatures produces color centers F , F′ and M^+-bands. It is interesting to note that this is the first evidence of producing color centers in CsI using non-ionizing UV-radiation.

(d) We also observed that if pure CsI is plastically deformed (4% strain being typical), its optical properties are similar to those of sodium activated CsI . Also the emission and excitation peaks located at 440 nm and 240 nm respectively in the deformed CsI at RTBC, are identical with those of pure CsI at RTAC, which supports the contention that straining by cooling plastically deforms CsI .

(e) Electron spin resonance measurements suggest the nature and symmetry of the centers responsible for the observed intrinsic luminescence in CsI to be those of F- and V_K-centers.

APPENDIX A

We recall that the energy difference between the first exciton absorption band (E_f) and the trapped exciton absorption band (E_T) is composed of three parts: ΔE_1, the change in electrostatic energies; ΔE_2, the change in repulsive energies and ΔE_3, the change in polarization energies.

$$\text{i.e. } \Delta E = E_f - E_T = \Delta E_1 + \Delta E_2 + \Delta E_3 \quad .$$

From Eqs. (2.3) and (2.4), ΔE_1 can be easily obtained using elementary geometry (Fig. II.1) while ΔE_2 involves direct substitution and ΔE_3 involves terms of the form

$$A = \sum \left\{ \frac{1}{r_{ij}^4} + \frac{1}{r_{kj}^4} - 2 \cos \frac{(r_{ij} , r_{kj})}{r_{ij}^2 \; r_{kj}^2} \right\} .$$

This type of summation can be divided into two parts:

$$A_1 = \sum \left\{ \frac{1}{r_{ij}^4} + \frac{1}{r_{kj}^4} \right\}$$

and

$$A_2 = \sum \frac{\cos(r_{ij} , r_{kj})}{r_{ij}^2 \; r_{kj}^2} \quad .$$

A_1 : Summation of this type has been calculated by Jones and Ingham to be about 16 and 20 for the NaCl and CsCl-type alkali halides respectively.

A_2 : Considering the two dimensional model of the alkali halides (CsCl-type) shown in Fig. II.1 and for any ions i , j , k , we can express the cosine term as

$$\cos (r_{ij} , r_{kj}) = \frac{r_{ij}^2 + r_{kj}^2 - r_{ik}^2}{2\, r_{ij}\, r_{kj}}$$

using elementary trigonometry.

If the origin of the coordinate system coincides with site 1 of Fig. II.1, then the distance to any given ion of the space lattice can be expressed (in terms of interatomic spacing) as

$$r_{ij}^2 = r_0^2 (l^2 + m^2 + n^2)$$

and

$$r_{kj}^2 = r_0^2 [(l - z)^2 + m^2 + n^2]$$

where l , m , n are whole numbers (or coordinates of a point in the crystal) and $z = r_{ik}$, the distance between the i^{th} ion and the vacancy.

For our case, $z = 1$, that is r_{ij} is even when r_{kj} is odd and vice-versa. Now if

$$l^2 + m^2 + n^2 \equiv P$$

then

$$(l - 1)^2 + m^2 + n^2 \equiv P - 2l + 1 \ ,$$

and

$$\cos(r_{ij} , r_{kj}) = \frac{P + P - 2l + 1 - 1}{2[P(P - 2l + 1)]^{\frac{1}{2}}} \ .$$

Hence

$$A_2 \equiv \sum_{\ell,m,n} \frac{2(P - \ell)}{[P(P - 2\ell + 1)]^{3/2}} \cdot \text{(valid for even or odd P)}$$

This is usually written as

$$A_2 = \sum_{\ell} \sum_{m} \sum_{n} \frac{2(P - \ell)}{[P(P - 2\ell + 1)]^{3/2}} \cdot$$

even or odd P.

Also this type of summation has been done by Reitz and Gammel et al.

They obtained the values

$$\sum_{\substack{i \\ \text{pos ions}}}'' \frac{\cos(r_{2i}, r_{3i})}{r_{2i}^2 \, r_{3i}^2} - \sum_{\substack{i \\ \text{pos ions}}}'' \frac{\cos(r_{1i}, r_{3i})}{r_{1i}^2 \, r_{3i}^2} = 0.7015$$

and

$$\sum_{\substack{i \\ \text{neg ions}}}'' \frac{\cos(r_{2i}, r_{3i})}{r_{2i}^2 \, r_{3i}^2} - \sum_{\substack{i \\ \text{neg ions}}}'' \frac{\cos(r_{1i}, r_{3i})}{r_{1i}^2 \, r_{3i}^2} = 1.232 \cdot$$

The other constants involved in the calculation of the α and β-bands in CsI are tabulated below

anion-cation distance	r_0	3.95×10^{-8} cm
Madelung constant	α_M	1.76
Repulsion parameter	ρ	0.34×10^{-8} cm
Anion polarizability (I^-)	α_-	7.10×10^{-24} cm^3
Cation polarizability (C_s^+	α_+	2.42×10^{-24} cm^3

high frequency dielectric constant	ϵ_∞	3.03
static dielectric constant	ϵ_s	5.65
energy of first exciton peak	E_f	5.77 eV (215 nm)

Using the calculated values of B and C and above parameters in Eqs. (2.3 and (2.4), give

	ΔE_1	ΔE_2	ΔE_3	ΔE	E_{Tc}	E_{TO}
α-band	1.07 eV	-0.08 eV	-0.47 eV	0.52 eV	5.25 eV (236.2 nm)	5.23 eV (237 nm)
β-band	--	-0.08	0.34	0.26	5.51 (225 nm)	5.51 (225 nm)

REFERENCES

1. K. J. Teegarden, Phys. Rev. B 108, 660 (1957).
2. W. J. Van Scirer, Phys. Rev. 120, 1193 (1960).
3. M. Tomura and Y. Kaifu, J. Phys. Soc. Japan 15, 1295 (1960).
4. J. Ramaminti and K. J. Teegarden, Phys. Rev. 145, 698 (1966).
5. K. J. Teegarden and R. F. Weeks, Phys. Chem. Solids 10, 211 (1959).
6. R. F. Edgerton, Ph.D. Thesis, University of Rochester, New York (1962).
7. M. N. Kabler, Phys. Rev. 136, A1296 (1964); also Lamb and Compton, Phys. Rev. 106 (1957).
8. R. B. Murray and F. J. Keller, Phys. Rev. 137, A942 (1965).
9. T. G. Castner and W. Kanzig, Phys. Chem. Solids 3, 178 (1957).
10. R. F. Woods, Phys. Rev. Letters 15, 449 (1965); also R. F. Woods, Phys. Rev. 151, 629 (1966).
11. H. Rabin and J. H. Schulman, Phys. Rev. Letters 4, 6, 280 (1960). D. W. Lynch, A. D. Brothers, and D. A. Robinson, Phys. Rev. 139, 1A, A285 (1965).
12. C. W. Bates, Jr., Varian Associates Central Research Member #200 (June 1967); also Adv. Electronics and Electron Physics 28A, 451 (1969).
13. R. B. Murray, Int. Symposium on Lumin, Munich (1965).
14. M. Aegerter, et al., Int. Conference on Scintillators (Munchen), 292 (1965).
15. J. M. Donahue and K. Teegarden, J. Phys. Chem. Solids 29, 2141 (1968).

16. Z. L. Morgenstern, Optics and Spectroscopy 7, #2, 231 (1959); also 8, #5, 672 (1960).

17. S. Masunaga, I. Morita, and M. Ishiguro, J. Phys. Soc. Japan 21, #4, 638 (1966).

17. T. Towyama, I. Morita, and M. Ishiguro, J. Phys. Soc. Japan 25, #4, 1133 (1968); also
T. Towyama, Phys. Letters 31A, #4, 206 (1970).

19. H. Lamatsch, J. Rossel, and E. Saurer, Phys. Stat. Solid(b) 48, 311 (1971); also 49, 311 (1972).

20. D. Pooley, Solid State Comm. 3, 241 (1965); also
D. Pooley, Proc. Phys. Soc. (GB) 87, 245 (1966).

21 H. N. Hersh, J. Phys. Chem. Solids 27, 771 (1966), also
H. N. Hersh, J. Electrochem. Soc. 144C, (1971).

22. R. Pohl and R. Hilsch, Zeits f. Physik 59, 812 (1930).

23. J. E. Eby, K. Teegarden and D. Dutton, Phys. Rev. 116, 1099 (1959); also W. Martienssen, J. Phys. Chem. Solids 2, 257 (1957) and 8, 294 (1959).

24. K. J. Teegarden and G. Baldini, Phys. Rev. 155, #3, 896 (1967).

25. R. Know and N. Ichauspé, Phys. Rev. 116, 1093 (1959).

26. R. S. Knox, Theory of Excitons, S.S.P. Supplement 5 edited by Turnbull and Seitz.

27. A. W. Overhauser, Phys. Rev. 101, 1702 (1956).

28. Taft and Phillips, Phys. Rev. 106, 671 (1957); also J. Chem Solids 3, 1 (1957).

29. C. J. Delbecq, P. Pringsheim, and P. Yuster, J. Chem. Phys. 19, #5, 574 (1951).

30. C. Klick and D. Patterson, Phys. Rev. 130, #6, 2169 (1963).

31. Bassani and Ichauspé, Phys. Rev. 105, #3, 819 (1957).

32. Mott and Gurney, Electronic Processes in Ionic Crystals, Dover, New York (1964).

33. J. E. Jones and A. E. Ingham, Proc. Roy. Soc. (London), A107, 636 (1925); also
E. S. Rittner, R. A. Hunter, and F. K. Du Pre, J. Chem. Phys. 17, 198, 204 (1949); and Reitz et al., 19, 894 (1951).

34. A. A. Tsertsvadze, Sov. Phys. S.S. 3, #2, 241, 370 (1961); 3, #7, 1428 (1962).

35. H. B. Rosenstock, Phys. Rev. 131, #3, 1111 (1963).

36. G. A. Rozman, Sov. Phys. S.S. 7, #7, 1555 (1966).

37. N. I. Ivanova and A. P. Zhukovskii, Opt. and Spectros. 12, 56 (1962).

38. A. Panova and Shiran, Opt. and Spectros. 32, 55;108 (1972).

39. Ya. A. Valbis, Opt. and Spectroscopy 21, 106;957 (1972).

40. I. Parfianovich, et al., J. Lumin. 1,2, 657 (1970).

41. J. P. Pellaux, T. Sidler, A. Nouailhat, and M. A. Aegerter, Sol. St. Comm. 13, 479; 970 (1973).

42. Yu. I, Bolko, et al., Sov. Phys. S.S. 13, #10 (1971).

43. P. R. Moran, Phys. Rev. 137, #3a, A1016 (1965).

44. O. L. Hsu, Ph.D. Thesis, Stanford University, Stanford, Ca.

45. K. J. Teegarden, Phys. Rev. 105, 1222 (1957).

46. R. Weeks, Ph.D. Thesis, University of Rochester, New York (1958).

47. C. A. Hutchison, Phys. Rev. 75, 1769 (1949).

48. F. Huges and J. G. Allard, Phys. Rev. 125, 173 (1962).

49. A. M. Portis, Phys. Rev. 104, 584 (1956).

50. W. B. Fowler and D.L. Dexter, Phys. Rev. 128, 2154 (1962).

51. C. Klick and J. Schulman, Advances in Research and Applications V. S.S.P. Edited by F. Seitz and D. Turnbull

52. M. Lax, J. Chem. Phys. 20, 1752 (1952).

53. D. L. Dexter, Advances in Research and Applications VI. S.S.P. Edited by F. Seitz and D. Turnbull

54. C. Kittel, Introduction to Solid State Physics, 4th Ed., Wiley, New York (1974).

55. F. J. Keller and F. W. Patten, Solid State Comm. 7, 1603 (1969).

56. D. Leniart, Instrument Division, Varian Associates, Palo Alto, Ca

57. S. S. Ballard, L. S. Combes, and K. A. McCarthy, J. Opt. Soc. Ame. 43, 975 (1953).

58. J. Vallin. O. Beckman, and K. Salama, J. Appl. Phys. 35, #4 (1964).

59. A.L.N. Stevels and A.D.M. Schrama-de-Pauw, Phillips Res. Repts. 29, 340 (1974).

60. R. Englman,and B. Barnett, J. Lumin. 3, 37 (1970).

61. E. Goldstein, Sitz. Berliner Acad. Wiss. 937 (1894).

62. D. Lynch and D. Robinson, Phys. Rev. 174, 1050 (1968); also D. Lynch, et al., Phys. Rev. 139A, 285 (1965).

63. H. Rabin and J. Schulman, Phys. Rev. 125, 1584 (1962).

64. P. Avakin and A. Smakula, Phys. Rev. 120, 2007 (1960).

65. Schulman and Compton, Color Centers in Solids, Pergamon Press (1962).

66. Dawson and Pooley, Phys. Stat. Solidi, 35, #1, 95 (1969).

67. W. B. Fowler, Physics of Color Centers, Academic Press (1968).